Title
Role of Glial Cells in Diesel Exhaust Particulate Extract-Induced Neurotoxicity in the Larval Zebrafish Brain

Author
Murata, Hiromi

Publication Date
2021

Peer reviewed|Thesis/dissertation

UNIVERSITY OF CALIFORNIA

Los Angeles

Role of Glial Cells in Diesel Exhaust Particulate Extract-Induced Neurotoxicity in the Larval Zebrafish Brain

A thesis submitted in partial satisfaction of the

requirements for the degree Doctor of Philosophy

in Molecular Toxicology

by

Hiromi Murata

2021

ABSTRACT OF THE DISSERTATION

Role of Glial Cells in Diesel Exhaust Particulate Extract-Induced Neurotoxicity in the Larval Zebrafish Brain

by

Hiromi Murata

Doctor of Philosophy in Molecular Toxicology

University of California, Los Angeles, 2021

Professor Jeff Bronstein, Chair

Parkinson's Disease (PD) is the second most common neurodegenerative disease. Its pathological hallmarks include loss of dopaminergic neurons in the substantia nigra, aggregation of alpha-synuclein (α-syn) leading to the formation of Lewy bodies, and neuroinflammation. Epidemiological studies have reported positive associations between exposure to air pollution (AP) and incidence of PD. This research investigates the mechanisms behind responses of microglia and astroglia to the extract of a major component of AP, diesel exhaust particulates (DEPe), in zebrafish (*Danio rerio*, ZF). DEPe exposure led to significant injury of dopaminergic neurons in the ZF, and resulted in structural and functional activation of microglia. Elimination of microglia using a morpholino oligonucleotide did not significantly attenuate the DEPe-

induced neuron injury, suggesting that microglia may not play a direct role in acute DEPe-induced neuron loss in our ZF model, and that their response is possibly heterogeneous in nature. Microglia were also activated with transgenic overexpression of human α-syn (hα-syn), and were significantly higher in number in the forebrain compared to hα-syn non-expressors. When the ZF overexpressing hα-syn were treated with DEPe, we observed significant neuronal injury, sustained microglial activation, and slightly decreased microglia-neuron interactions compared to control treatment, suggesting that DEPe exposure may affect microglia-neuron interactions, but the microglial response is complex. Single-cell RNA sequencing of larval ZF heads revealed 27 distinct clusters of cells. 55 differentially expressed genes (DEG) were identified in the microglial cluster with DEPe exposure. The DEG suggested that many microglia were activated and inflammatory, but were also mounting an anti-inflammatory and possibly neuroprotective response. 43 DEG were identified in the astroglial cluster. While some upregulated genes were related to astroglial activation and proliferation, other markers of a reactive state in astroglia were lowered, indicating a heterogeneous response. This was supported by IPA Comparison Analysis of pathways most changed with DEPe exposure in microglia and astroglia. Subcluster analysis identified gene expression profiles that suggest the presence of various states of the microglia and astroglia. Ultimately, these studies begin to reveal mechanisms that occur in microglia and astroglia in the context of DEPe exposure that may alter risk of PD development.

The dissertation of Hiromi Murata is approved:

David Krantz

Beate Ritz

Michael Sofroniew

Jeff Bronstein, Committee Chair

University of California, Los Angeles

2021

Table of Contents

List of Figures and Tables

Chapter 1

Hiromi Murata Vita

Education

University of California, Berkeley Aug. 2011 – May 2015
B.S. in Chemical Biology, Minor in Molecular Toxicology

Research Experience

Research Assistant, Research Adviser: Dr. Kent Daane Jun. 2014 – Aug. 2015
Dept. of Env. Science, Policy & Management University of California, Berkeley

Undergraduate Research Assistant, Research Adviser: Dr. Neil Tsutsui Sept. 2013 – Aug. 2014
Dept. of Env. Science, Policy & Management University of California, Berkeley

Undergraduate Research Assistant, Research Adviser: Dr. Isao Kubo Jul. 2013 – Dec. 2014
Dept. of Nutritional Science & Toxicology University of California, Berkeley

Publications

- ***Murata, H.**, et al. Single-cell Characterization of the Role of Microglial and Astroglial Cells in Diesel Exhaust Extract Neurotoxicity. In preparation.*
- ***Murata, H**., Barnhill, L.M., Bronstein, J.M. Air Pollution and the Risk of Parkinson's Disease. Submitted for publication.*
- Jami, S.M., **Murata, H.**, Barnhill, L.M., Li, S., Bronstein, J.M. Diesel Exhaust Exposure Alters the Expression of Networks Implicated in Neurodegeneration in Zebrafish Brains. *Cell Biol Toxicol.* 2021.
- Barnhill, L.M., Khuansuwan, S., Juarez, D., **Murata, H.**, Araujo, J.A., Bronstein, J.M. Diesel exhaust extract exposure induces neuronal toxicity by disrupting autophagy. *Toxicol. Sci.* 2020.
- Barnhill, L.M., **Murata, H.**, Bronstein, J.M. Studying the Pathophysiology of Parkinson's Disease Using Zebrafish. *Biomedicines.* 2020.
- Barnhill, L.M., Khuansuwan, S., **Murata, H.**, Araujo, J., and Bronstein, J.M. Air Pollution and Risk of Parkinson's Disease: Mechanistic Studies. *J. Mov. Disord*. 2017.

Awards

- Molecular Toxicology NIEHS T32 Pre-Doctoral Training Grant (2017-2020)
- Cal Alumni Association Leadership Scholarship (2011-2015)

Posters and Presentations

- "Single Cell Analysis of the Role of Glial Cells in Diesel Exhaust Particulate Extract (DEPe) - Induced Neurotoxicity", UCLA Neurodegenerative Diseases Symposium, Los Angeles, CA, April 29, 2021
- "Role of Microglia in Diesel Exhaust Particulate Extract-Induced Neurotoxicity and Clearance of α-Synuclein Aggregates in the Larval Zebrafish Brain", Society of Toxicology 59th Annual Meeting, Anaheim, CA, March 16, 2020 (*meeting cancelled due to COVID-19*)
- "Using the Transgenic Zebrafish Model to Compare Mechanisms of Action of Two Environmental Toxicants with Opposite Correlations to PD Development, DEPe and CSE", Society of Toxicology 58th Annual Meeting, Baltimore, MD, March 12, 2019

- "Utility of zebrafish in the study of air pollution induced neuroinflammation", SoCal Zebrafish Meeting, Pasadena, CA, September 14, 2018
- "Roles of Microglia in Diesel Exhaust Particulate Extract-Induced Neuron Loss and Clearance of α-Synuclein Aggregates in the Larval Zebrafish Brain", Society of Toxicology 57th Annual Meeting, San Antonio, TX, March 13, 2018
- "Toxicity Assay of Cinnamic Acid and Methyl Cinnamic Acid on Beet Armyworm Midgut Cells", College of Natural Resources Poster Session 2014, Berkeley, CA, April 25, 2014

Introduction

Parkinson's disease (PD) is the 2nd most common neurodegenerative disease after Alzheimer's (Elbaz, Carcaillon, Kab, & Moisan, 2016). A majority of PD patients are aged 60 and above, as PD tends to be a disease that develops slowly and progressively over decades. As the population of developed countries increases in average age due to overall improvements in general medical technology, there will most likely be an increasing number of PD patients in the near future.

There are various neuropathological hallmarks of PD. The first hallmark is the gradual loss of DA neurons in the substantia nigra pars compacta, and other regions of the nervous system. This loss of DA neurons leads to the impairment of motor control (Mazzoni, Shabbott, & Cortes, 2012). Secondly, there is an accumulation of a presynaptic protein, α-syn, which leads to the formation of toxic aggregates called Lewy bodies within the neurons and in the cytosol (Stefanis, 2012). These aggregates are called Lewy neurites when the aggregates are on axons. Thirdly, neuroinflammation has been observed in the brains of patients with PD, as well as in animal models of the disease (Q. Wang, Liu, & Zhou, 2015). Hence, neuroinflammation is increasingly recognized as a major pathological hallmark and topic of interest in PD research.

Neuroinflammation, Glial Cells, and PD

Neuroinflammation is increasingly implicated in PD as contributing to its progressive nature, but its role is not very well understood. This is because although inflammation is usually a protective reaction to an acute insult, such as an infection or environmental exposure. In the case of PD and other neurodegenerative diseases, excessive inflammation has been hypothesized to damage neurons and contribute to the development and progression of the disease. In mice

treated with the inflammation-inducer lipopolysaccharide (LPS), dopaminergic neurons were selectively reduced (Qin et al., 2007). Certain single nucleotide polymorphisms in the human leukocyte antigen (HLA) genes HLA-DR and HLA-DQ increase risk of PD (Hamza et al., 2010). T-cells in PD patients have been seen to recognize α-syn as antigens (Sulzer et al., 2017). Finally, a meta-analysis of 11 studies that studied non-steroidal anti-inflammatory drug (NSAID) use and incidence of PD found that ibuprofen users have a slightly reduced risk of developing PD (Samii, Etminan, Wiens, & Jafari, 2009).This link between inflammation and PD will be interesting to study in the context of diesel exhaust particulate extract exposure, as we keep in mind that neuroinflammation may be beneficial for the CNS by promoting quick responses to toxin exposure, leading to repair and regrowth of tissue, but may also be toxic to neurons due to the microglial release of inflammatory and neurotoxic factors.

One of the first responders to injury and infection in the CNS are microglia, the macrophages of the brain. Previous work has begun to describe possible roles that microglia play in the pathogenesis of PD. Pathologic studies have shown that activated microglia exist in the substantia nigra of the brains of patients with PD (H. M. Gao & Hong, 2008). However, the determination of whether microglial activation is one of the triggers of the disease, or is a consequence of other pathological events that occur in the CNS, is something that is continuing to be investigated in this field. Positron emission tomography (PET) studies have shown that microgliosis occurs early in PD and is sustained (Gerhard et al., 2006), and activated microglia have been observed in various animal models of PD (Czlonkowska, Kohutnicka, Kurkowska-Jastrzebska, & Czlonkowski, 1996), (Hoenen et al., 2016), (Sanchez-Guajardo, Febbraro, Kirik, & Romero-Ramos, 2010). Clearly, they are present throughout the progression of PD, and this

research aims to identify and describe further the roles that microglia play in responding to air pollution (AP) exposure and possibly leading to the development of this disease.

Astrocytes are the most abundant cell type in the CNS, and outnumber neurons by fivefold, due to their various functions. Although the exact mechanism of astrocytes' role in the development of PD is not fully understood, there are various studies that have linked astrocytes and the pathogenesis of PD. Astrocytes have been seen to take up DA neuronal debris in a rat DA neuronal injury model - astrocytes were seen to contain tyrosine hydroxylase and dopamine transporter (DAT), which are both expressed in DA neurons (Morales, Sanchez, Rodriguez-Sabate, & Rodriguez, 2017). Astrocytes have also been seen in vitro and in vivo to take up α-syn and in response release proinflammatory cytokines and chemokines (H. J. Lee et al., 2010). Also, areas of neurodegeneration in PD patients have shown high levels of GFAP, a protein found in activated astrocytes (Barcia, 2013). Clearly, astrocytes are present and might contribute to the pathogenesis of PD, but their exact role, and role in the context of AP exposure, is not well-understood.

When considering the roles that these cells of interest play in the development of PD, regardless of if the context is environmental, such as AP exposure, or simply a more well-established genetic model of the disease, it is important to keep in mind that these cells are not a homogeneous population at any given time in the CNS. There exist various states of these cells that require careful, contextual characterization, as that will help inform our understanding of the mechanisms by which our exposures of interest contribute to the development of PD. This work aims to do this through various methods, both *in vitro* and *in vivo*.

Causes of PD

Only about 10-15% of cases of PD are directly due to a genetic mutation. Some mutations implicated in PD are autosomal dominant, such as mutations in the genes *snca, lrrk2,* and *vps35* (Klein & Westenberger, 2012). The *snca* gene has been studied extensively, with five autosomal dominant mutations having been identified as linked to the development of PD (Siddiqui, Pervaiz, & Abbasi, 2016). These mutations tend to lead to increased SNCA protein oligomerization, and ultimately neurotoxicity. Some mutations involved in PD are autosomal recessive, such as those in *Park2* and *Park7.* For example, the *Park7* gene encodes for DJ-1 protein, crucial for lipid raft assembly in astrocytes. With less DJ-1 protein production, the ability of the astrocytes to maintain homeostasis of the cerebrospinal fluid is affected, leading to accumulation of neurotransmitters such as glutamate, ultimately leading to neuronal excitotoxicity (Booth, Hirst, & Wade-Martins, 2017).

Environmental exposures have been increasingly studied in the context of PD development. One chemical family that has been extensively studied with regards to its link to PD are pesticides. Pesticides such as rotenone, benomyl (Fitzmaurice et al., 2013), paraquat (Tanner et al., 2011), maneb, and ziram (Lulla et al., 2016) have been linked to the development of PD (Paul et al., 2018), (A. Wang, Cockburn, Ly, Bronstein, & Ritz, 2014). Rotenone, a lipophilic insecticide and piscicide, is one of the most well-studied pesticides with links to PD. It is commonly used in rats to prepare rotenone-induced PD for research purposes. Rotenone acts by inhibiting Complex I of the electron transport chain, resulting in progressive neurodegeneration of dopaminergic and non-dopaminergic neurons, alpha-synuclein accumulation, and oxidative damage in the CNS. Interestingly, these rotenone-treated animals develop PD-like symptoms, such as bradykinesia, postural instability, and/or rigidity (Cannon et

al., 2009). Benomyl is a benzimidazole fungicide that has been linked to the development of PD through its inhibitory effects on aldehyde dehydrogenase (ALDH). This occurs through the metabolism of benomyl into compounds such as butyl isocyanate, which inhibits ALDH, along with downstream metabolites such as S-methyl N-butylthiocarbamate (MBT) which is converted by CYP enzymes to MBT-sulfoxide, which is also a potent ALDH inhibitor. This leads to the toxic accumulation of aldehydes such as DOPAL, and dopaminergic neuron loss. In addition, at higher concentrations, benomyl has been observed to inhibit 26S UPS activity (Fitzmaurice et al., 2013). Paraquat is another well-recognized pesticide of which the mechanism of toxicity is still being investigated. It is currently understood that exposure to paraquat results in the formation of reactive oxygen species (ROS) and lipid peroxidation, which has been observed to damage the nervous system, GI system, lungs, and liver (L. Gao, Yuan, Xu, & Liu, 2020). It has been observed to reduce dopaminergic neuron count and lead to behavorial changes associated with PD (Tanner et al., 2011). Finally, exposure to the dithiocarbamate fungicide ziram has been associated with a 300% increased risk of developing PD (A. Wang et al., 2011). Currently, it is understood that ziram is toxic to dopaminergic neurons through the inhibition of E1 ligase in the ubiquitin proteasome system which is implicated in the accumulation of α-syn (Chou et al., 2008).

The above examples outline some very interesting potential mechanisms by which environmental exposures influence the development of PD, including inhibition of the proteasome, inhibition of ALDH, increase in ROS, and inhibition of Complex I of the electron transport chain. These changes affect dopaminergic neuron health and protein degradation, which directly influences α-syn accumulation, and are useful framework to keep in mind as we

attempt to uncover mechanisms by which air pollution and its major components may be involved in the development of PD.

AP and PD Epidemiology

According to data available in 2017, 92% of the world's population lived in areas that exceeded the WHO guideline for PM2.5 (Health Effects Institute, 2019), a major toxic component in AP. AP is a newer focus for research on environmental exposures that may be related to PD, and is not as well understood as other chemical exposures, such as pesticides. However, it is vital to study the link between AP exposure and development of PD, as the median age of the global population increases and AP remains the world's leading environmental cause of mortality (Health Effects Institute, 2019). The following studies are examples of the links that evidence the necessity of this research.

There are several epidemiological studies that link exposure to AP with neurodegeneration. One study of 1,696 PD patients in Denmark, with population controls matched by year of birth and sex, used the residential addresses of all participants to determine their distance from major roadways. The study found that exposure to ambient AP from traffic was linked with a 9% higher risk of developing PD per interquartile increase in the NO_2 exposures that they measured, which represented traffic-related AP (Ritz et al., 2016), with the largest odds ratio observed in participants that have lived in cities. Another study followed 110,000 people in Canada and found that exposure to ambient manganese in the air was associated with advanced age of PD onset (Finkelstein & Jerrett, 2007). Also, a nationwide population-based case controlled study done in Taiwan found that exposure to nitric oxides and carbon monoxide in the air from traffic was positively associated with PD incidence (P. C. Lee et

al., 2016). There are many other studies that link the exposure to AP with PD epidemiologically. There are also studies that do not conclusively link exposure to AP with development of PD, such as the Nurse's Health Study. This study followed a cohort of female nurses and studied whether exposure to airborne metals was associated with an increased risk of developing PD. They found limited evidence of association between adulthood ambient metal exposure and development of PD (Palacios et al., 2014). Clearly, it is crucial to determine the exact mechanisms of toxicity of components of AP, in order to understand how exposures can lead to PD, and what can be done to prevent its development.

Diesel Exhaust, a Major Component of AP

One major component of AP is Diesel Exhaust (DE). Inhabitants of populated cities and those with various automobile-related occupations are exposed to DE on a regular basis, yet the molecular mechanisms of action of DE toxicity have only recently been explored. DE itself is a heterogeneous mixture, with various components of varying molecular sizes and classifications. There are particles of carbon of varying sizes, such as graphitized carbon, and larger 60-100nm soot particles. There also exist metal and metal-oxide particles that are around 10nm, various polycyclic aromatic hydrocarbons (PAHs), and toxic and nontoxic inorganic gases, such as nitrogen, carbon monoxide, and nitrogen monoxide (Steiner, Bisig, Petri-Fink, & Rothen-Rutishauser, 2016).

DE toxicity has been studied in animal models and has shown links to various disease hallmarks of PD such as DA neuron loss, α-syn accumulation, and neuroinflammation. In one study, rats exposed to various densities of DE exhibited accumulation of a-syn in the midbrain at the highest exposure dose, suggesting DE exposure may be associated with early PD-like

pathology (Levesque, Surace, McDonald, & Block, 2011). The midbrain also exhibited increased TNFa and IL-1B levels with DE exposure. In a similar study, rats exposed to DE exhibited generalized neuroinflammation through increased levels of whole-brain IL-6 protein, nitrated proteins, and IBA-1 protein. In addition, TNFα, IL-1β, IL-6, and the IBA-1 microglial marker protein levels were increased in most regions tested, with the highest response observed in the midbrain. When Diesel Exhaust Particles (DEP) were administered intratracheally, there was increased microglial IBA-1 staining in the substantia nigra, along with elevated TNFa in the whole brain and serum after 6 hours (Levesque, Taetzsch, et al., 2011). Specifically in the zebrafish model, DEPe exposure has been observed to injure various neuronal populations, including dopaminergic, and lead to abnormal swimming behavior. In addition, the accumulation of one form of zebrafish synuclein in this model appeared to be correlated with the dysfunction of neuronal autophagic flux. Treatment with nilotinib, an inducer of autophagic degradation, was neuroprotective (Barnhill et al., 2020).

Clearly, the scientific community has begun to describe and understand ways in which DEPe/DE exposure may alter mechanisms in the brain that are relevant to PD development. The research described in this study focuses on two glial cell types of interest, using the ZF as a model organism, aims to not only uncover neuroinflammation-related mechanisms that may be induced by DEPe exposure, but also characterize possible sub-states of the microglia and astroglial cells induced by this exposure.

The Utility of Zebrafish

ZF, or *Danio rerio*, like mice and rats, are used very commonly in basic science research, as well as in industry. The use of ZF in laboratory research comes with various benefits. Firstly,

they are very easily and inexpensively maintained in large systems of circulating water and numerous tanks, housing various transgenic lines at once. They are also extremely prolific breeders, with each pair of breeding ZF producing between 100-300 eggs per day, once per week, with the simple break of daylight as their trigger. They develop extremely quickly, compared to mice and rats, and the entire process is visible through their transparent bodies. This makes ZF embryos extremely useful in fluorescence and confocal imaging and developmental studies, which are noninvasive compared to other studies. More than 70% of human genes have a ZF orthologue (Howe et al., 2013), and the entire ZF genome has been sequenced, making them an extremely useful model organism.

In the context of studying an environmental toxin such as diesel exhaust particulate extract (DEPe), and determining the mechanisms of action of toxicity, ZF are a useful model. Pathways of interest can be efficiently studied in numerous ways *in vivo* (expression of transgenic fluorophores and other reporter genes, live imaging and immunohistochemistry, behavioral assays, feeding experiments, etc.) in a timely fashion, and toxicity screens can be performed very efficiently. Although not identical to their human counterparts, ZF microglia and astroglia are well-described at the single cell level (Oosterhof et al., 2017), (Lange et al., 2020), (Mazzolini et al., 2020), and have many conserved functions and developmental timelines that are identical to microglia and astrocytes in humans, making ZF useful models to study specific pathways in neurodegenerative disorders (Peri & Nusslein-Volhard, 2008), (Saleem & Kannan, 2018), (Barnhill et al., 2020). Most neurodegenerative diseases take decades to develop. Therefore, researchers often model specific pathways of interest that are linked to the development of these neurodegenerative diseases, rather than attempting to model the entire time-course of the disease. The ZF is a very useful model organism for efficiently modeling

these specific Adverse Outcome Pathways (AOP) in a vertebrate *in vivo* system, particularly in the context of environmental exposures. At first glance, the exposure route in water of zebrafish embryos, and the inhalation of DE by humans may seem rather disparate. However, accumulated levels of a class of toxins enriched in DE, xenobiotic polycyclic aromatic hydrocarbons (PAH), have been quantified in human organs including the brain, through a dispersive liquid-liquid microextraction procedure followed by GC-MS analysis (Pastor-Belda et al., 2019). 5 of the 13 PAHs quantified in the study were detected in our DEPe as well, through GC-MS analysis performed by the Wisconsin State Laboratory of Hygeine. The mean concentration of those 5 PAHs quantified in the study were between 0.1 to 0.7 ng/g, which were rather comparable to their levels in our DEPe treatment, which was 0.3 to 2.2 ng/g. Although these PAHs are not a large proportion of the entirety of the makeup of our DEPe, the above data shows that the levels of some of the quantifiable, well-described PAH components in our DEPe treatment are biologically relevant. By studying conserved processes and cell functions through modeling these specific AOP, we can identify how AP affects human health in efficient and biologically relevant ways.

Research Direction

This study identifies specific pathways and mechanisms that are involved in the microglial and astroglial response to DEPe exposure, and their implications in the development of PD. The three Chapters in this work approach these findings in a sequential manner, with Chapter 1 focusing on the microglial response to DEPe exposure *in vivo*, in the context of one of the main disease hallmarks of PD, the loss of dopaminergic neurons. This is modeled in the chapter through the use of a transgenic line, *Vmat2:GFP*, that fluorescently labels

monoaminergic neurons, and *mpeg1:mCherry*, which transgenically labels macrophages, including microglia. We characterized the response to DEPe exposure by quantifying neuronal injury and microglial activation. In Chapter 2, we focused on the role of microglia in the context of another major disease hallmark of PD, the accumulation of hα-syn. We characterized microglial activation and neuronal loss with and without the presence of DEPe to begin to describe the microglial response to these perturbations. In Chapter 3, we identify specific genes and pathways that are most affected by DEPe exposure in our two cell types of interest through differential gene expression (DEG) analysis and IPA Comparison Analysis. We use Gene Set Enrichment Analysis to initially characterize the microglial and astroglial clusters as a whole, but then perform subcluster analysis and interpretation of subcluster marker genes to begin to characterize the cells as being in various states. This work is critical to understand how AP exposure, which is an unavoidable and very ubiquitous environmental exposure, may affect the functioning of major glial cell types in the brain, and ultimately lead to the development of PD and other neurodegenerative diseases.

Dissertation: Chapter 1

Role of Microglia in Neuronal Injury Observed with Diesel Exhaust Particulate Extract Exposure

Introduction:

The presence of activated microglia in the PD brain is being increasingly accepted and investigated. In 1988, HLA-DR positive reactive microglia were observed in the substantia nigra of post-mortem PD brains (McGeer, Itagaki, Boyes, & McGeer, 1988). As the development of PD continues, the presence of activated microglia have been observed in various parts of the brain (Imamura et al., 2003). In an MPTP-induced animal model of PD, the infiltration of T-cells and the upregulation of the expression of MHCs has been observed as well (Kurkowska-Jastrzebska, Wronska, Kohutnicka, Czlonkowski, & Czlonkowska, 1999). Various studies have performed positron emission tomography (PET) to identify and quantify activated microglial cells in PD patients, and have observed significantly higher levels of activated microglia in various areas of the brain, such as the substantia nigra, midbrain and cortices (Ouchi et al., 2005), (Gerhard et al., 2006), (Iannaccone et al., 2013). Clearly, microglial activation is occurring in the PD brain, and it is important to understand its role in the development of PD, and equally so in the context of environmental exposures.

Although not the most abundant glial cell type in the CNS, microglia have been well studied in mammalian model organisms in the context of a variety of neurodegenerative diseases (Hansen, Hanson, & Sheng, 2018), (Butovsky & Weiner, 2018), making it an important cell type to study in the context of PD. In addition, the zebrafish has been successfully used to study microglial dynamics and responses (Oosterhof et al., 2017), (Mazzolini et al., 2020), (Hamilton, Astell, Velikova, & Sieger, 2016). Therefore, we decided to study the microglial response to

DEPe exposure to begin to understand the mechanisms of action by which DEPe may injure neurons, and on a greater scale, identify possible mechanisms that link exposure to AP to the development of PD. We hypothesized that DEPe exposure activates microglia structurally and functionally, and that knocking down microglial expression will influence neuronal survival with DEPe exposure. We tested this by quantifying microglial structural change, which is well-associated with activation state, as well as quantifying of its functional change through live-imaging acidified lysosomes. We quantified neuronal injury using a transgenic line that labels aminergic neurons.

Methods:

Zebrafish husbandry and fish lines used

Zebrafish (*Danio rerio*) were raised at 28.5C on a 14-hour light, 10-hour dark cycle. The lines used were AB (wild-type), *Vmat2:GFP*, *mpeg1:mCherry*, *HuC:Gal4*, *UAS:asyn:T2A:eGFP*. All zebrafish lines were used in accordance with the UCLA Animal Research Council (ARC) and Division of Laboratory Animal Medicine (DLAM) guidelines.

Zebrafish DEPe treatment

Diesel exhaust particulate extract (DEPe) used in this study was prepared from SRM #1975 from the National Institute of Standards and Technology (NIST), a dichloromethane extract of diesel particulate matter. The dichloromethane was evaporated using a controlled flow of nitrogen gas in a fume hood, and the remaining material was weighed and resuspended in dimethyl sulfoxide (DMSO) to a stock concentration of 25mg/ml. Comprehensive list of components analyzed by mass spectrometry are available in Supplementary Materials. Embryos for treatment were

manually dechorionated at 24hpf using Dumont #5 Fine Forceps. Each treatment consisted of 20 embryos in a final volume of 10mL E3 buffer in Corning Costar 6-well Plates. The final concentration of DEPe in the treatment well was 20ug/ml. Final DMSO vehicle concentration was 0.1% in both treatments. Embryos were treated until 3-5 days post-fertilization (dpf), depending on the experimental setup. They were euthanized through the addition of 1ml of 5mg/ml tricaine methanesulfonate to each well.

pU1 morpholino injection

Pu.1 morpholino oligonucleotide solution or scramble morpholino solution (0.4mM), was injected into homozygous *mpeg1:mCherry* embryos at the 1-4 cell stage. The injections were performed under a stereomicroscope with approx. 3nL of injection mixture injected per embryo. Injected embryos were placed in a 10mm plastic Petri dish and incubated at 28 degrees C in egg water. Embryos were treated at 24hpf with DMSO or DEPe as described above.

Zebrafish imaging process

After euthanization at 3dpf using tricaine methanesulfonate, the larvae were fixed in 4% PFA for 4 hours at 25C. They were washed with 1X DPBS and permeabilized in a solution of 10 ug/mL Proteinase K for 5 minutes. The Proteinase K was washed off with ddH2O for 5 minutes. The larvae were placed in a blocking solution of 5% BSA + 5% goat serum for 1 hour. Primary antibody was applied in 2% blocking solution overnight at 4C. The antibody was washed off over 8 washes, 15 minutes per wash, and the secondary antibody was applied in 2% blocking solution. After washing off the secondary antibody, the sample was placed in 50% glycerol for 30 minutes, and cleared in 100% glycerol until time of dissection. The labeled larvae in 100%

glycerol were dissected using Dumont #5 Fine Forceps. The brains were carefully removed and mounted in 100% glycerol for imaging on Leica SPE (Leica Microsystems Inc, Buffalo Grove, IL). Aminergic neurons in the telencephalon, diencephalon, and microglia were all imaged in Z-stacks of 2um. The fluorescence quantifications were performed using the Corrected Total Cell Fluorescence (CTCF) method (Hammond, 2014). Student's T-test, One-way ANOVA, and post-hoc tests, described in each Figure legend, were performed using Graphpad Prism 9.

Zebrafish image analysis using FIJI/ImageJ

FIJI/ImageJ were used to quantify aminergic neuron counts in telencephalon, diencephalon, and islet cell scans. Z-projection was applied to the image, the projected images were blinded, and neuron counts were performed using the Multi-point Tool.

For quantification of microglial activation, the images were blinded, Z-projection was applied to each image, converted to grayscale (16-bit), brightness/contrast adjustments were uniformly applied to eliminate background signal, images were made binary, skeletonized, and Simple Neurite Tracer was used while observing the original Z-projected image to select microglial branches and run Analyze Skeleton. The maximum branch length, or the quantification of the length of the longest branch coming off of the central node, and the average path length, or the quantification of the average length from the end of one branch to the end of another, was quantified (Morrison & Filosa, 2013).

RNA extraction, cDNA preparation, and rtPCR

For analysis of changes in expression of inflammatory cytokines, 24hpf WT embryos were treated with DMSO or DEPe as described above. At 5dpf, the larvae were euthanized and RNA

extraction was performed using TRIzol reagent (Invitrogen) according to product protocols. cDNA was prepared using iScript cDNA Synthesis Kit (Bio-Rad). rtPCR reaction was conducted using SsoAdvanced Universal SYBR Green Supermix. Cycle number data was analyzed to represent fold change values using the 2^-ddcT method.

Gene	Primer (F and R)
Elf-1a	F: CTT CTC AGG CTG ACT GTG C R: CCG CTA GCA TTA CCC TCC
il-1b	F: GCC TGT GTG TTT GGG AAT CT R: TGA TAA ACC AAC CGG GAC A
tnf-a	F: GCG CTT TTC TGA ATC CTA CG R: TGC CCA GTC TGT CTC CTT CT
il-8	F: AGC TTG AGA GGT CTG GCT GTA GA R: GCG TCG GCT TTC TGT TTC A

Primers used in rtPCR analysis of pro-inflammatory cytokine expression.

Results:

5day DEPe exposure injures monoaminergic neurons

In Vmat2:GFP neurons treated with DMSO or DEPe from 1dpf to 5dpf (Fig. 1E, 1F), the neurons in the telencephalon were significantly more injured with DEPe treatment compared to DMSO (Fig. 1A, 1C). There was a significant 20% loss of neurons in the telencephalon by count and 37% loss by fluorescence quantification. The loss of neurons in the diencephalon was 10% by count and 16% by fluorescence quantification, which were not significant (Fig. 1B, D).

Figure 1: Aminergic neuron count and fluorescence quantification in the telencephalon and diencephalon at 5dpf in *Vmat2:GFP* larvae with DEPe exposure

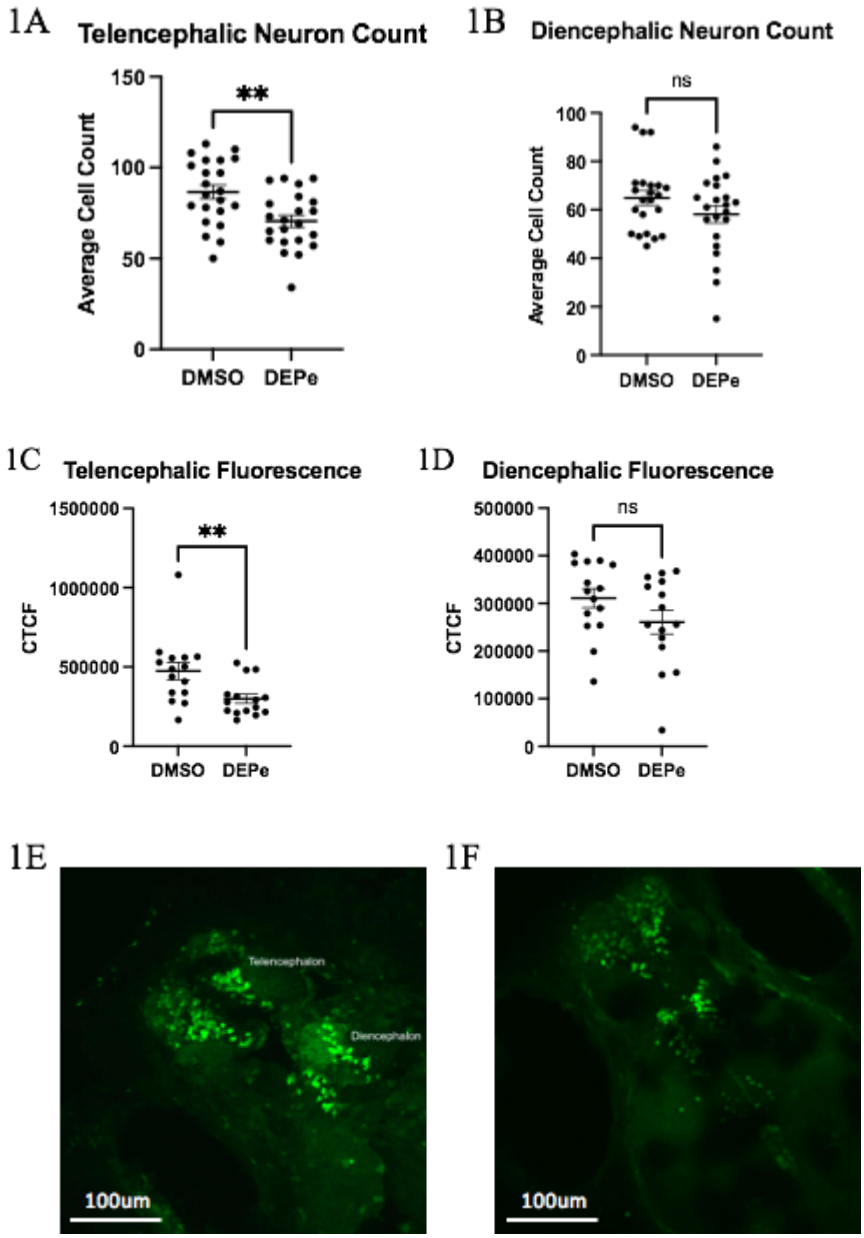

Figure 1: *Vmat2:GFP* embryos were treated with 20ug/mL DEPe or DMSO control until 5dpf and aminergic neuron injury was quantified. 1A: There was a significant loss of telencephalic neuron count with DEPe exposure. 1B: There was no significant change in diencephalic neuron count with DEPe exposure. 1C: There was a significant loss of telencephalic fluorescence with DEPe exposure. 1D: There was no significant loss of diencephalic fluorescence with DEPe exposure. 1E: Dorsal view of 5dpf DMSO-treated *vmat2:GFP* ZF brain. 1F: 5dpf DEPe-treated *vmat2:GFP* ZF brain. Student's T-test, ** = $p<0.01$, n = 22, 15. All error bars represent standard error of the mean.

Microglia are structurally and functionally activated with 5day exposure to DEPe

Microglial activation was quantified in two ways: structural and functional activation. Microglia are known to retract their processes and decrease their branching complexity when they are activated. Utilizing the Skeletonization and Simple Neurite Tracer functions on FIJI, we quantified the changes in microglial structure of every skeletonized microglial cell in the scans of DEPe treated and DMSO treated brains. We observed a significant 22% decrease in maximum branch length of microglia in DEPe treated brains compared to DMSO treated brains (Fig. 2A). There was a significant 74% decrease in the number of branches and 86% decrease in number of junctions with DEPe treatment (Fig. 2B, 2C) which represent a decrease in branching complexity of the microglia with treatment. These quantifications of microglial process lengths and branching patterns indicate that structurally, the microglia appear to exist in a more activated state with exposure to DEPe (Fig. 2D, 2E).

Microglia have also been observed to acidify lysosomes when activated (Majumdar et al., 2007). We live-imaged the acidification of lysosomes in the microglia using lysotracker dye (Fig. 2G, 2H). We quantified the number of microglia per brain that colocalize with lysotracker labeling, and found a significant increase of these microglia with DEPe exposure compared to DMSO, from an average of 1.1 to 4.7 microglia per brain at time of imaging (Fig. 2F). The percentage of microglia in the brain with lysotracker colocalization was also calculated, and significantly increased from 4.5% of the microglia in the brain to 24% of microglia with DEPe exposure. Therefore, DEPe exposure led to significantly higher counts of acidic lysosomes, which reflect a functional activation of microglia. These pieces of evidence - structural and functional quantification of activation - suggest that microglia in the 5dpf ZF brain with DEPe exposure are activated.

Figure 2: Microglial structural and functional activation in the telencephalon and diencephalon at 5dpf in *mpeg1:mCherry* larvae with DEPe exposure

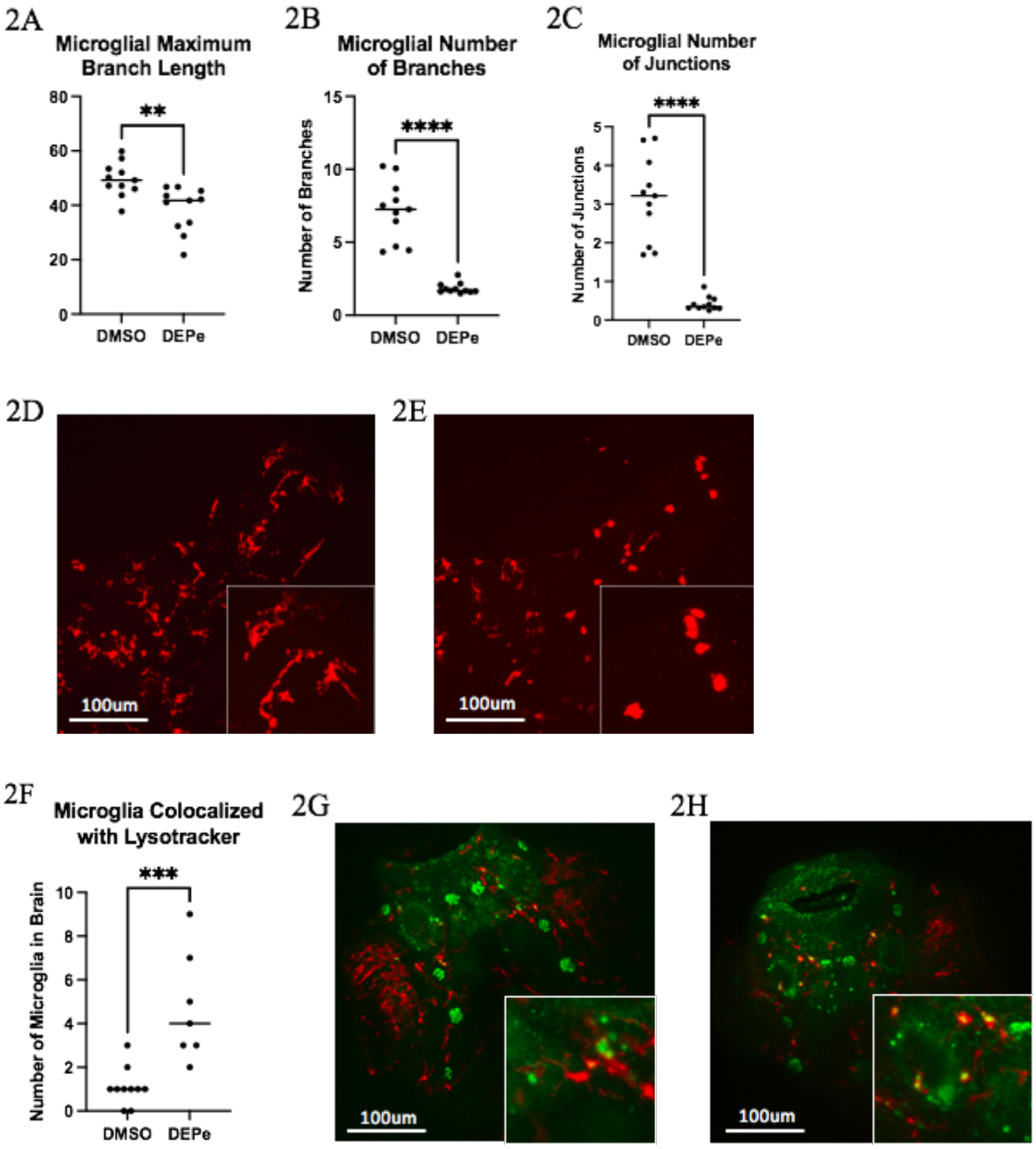

Figure 2: Quantification of 5dpf ZF microglial activation with DEPe exposure compared to DMSO control. 2A-2C quantified using Skeletonization and Simple Neurite Tracer on FIJI, Student's T-test, ** = $p<0.01$, **** = $p<0.0001$, n = 11, 11. 2A: The average maximum branch length in a microglial cell was significantly shorter with DEPe exposure. 2B: There were significantly fewer numbers of branches in the DEPe treated microglia compared to DMSO

control. 2C: There were significantly fewer junctions in the DEPe treated microglia compared to DMSO control. 2D: Dorsal view of DMSO-treated 5dpf *mpeg1:mCherry* ZF brain. 2E: DEPe-treated 5dpf *mpeg1:mCherry* ZF brain. 2F: Significantly more microglial cells colocalized with lysotracker-labeling in DEPe treated 5dpf *mpeg1:mCherry* larvae compared to DMSO. 2G-2H: Live view of DMSO-treated (2G), and DEPe-treated (2H) 5dpf *mpeg1:mCherry* ZF brain also treated with Lysotracker Green. Student's T-test, *** = $p<0.001$, n = 10, 7.

Systemic and head-specific expression of pro-inflammatory cytokines with DEPe exposure

We quantified systemic (whole-body) and head-specific changes in expression of inflammatory cytokines using rtPCR. Out of the 3 pro-inflammatory cytokine expressions quantified, we found that il-1B expression was significantly increased with DEPe exposure compared to DMSO exposure systemically (Fig. 3A). The other pro-inflammatory cytokines (TNFa and IL-8) did not exhibit significant changes in their expression with DEPe treatment. Clearly, DEPe treatment induces not only an inflammatory response in the form of microglial activation, but the response is also evident systemically through increased expression of IL-1B. Due to our disease of interest being in the brain, we also performed the same expression experiment on RNA collected from the heads of DMSO or DEPe treated ZF larvae. There were no significant changes in the fold change, or expression, of the three pro-inflammatory cytokine genes with DEPe treatment in the heads (Fig. 3B). This result may be due to the rtPCR assay being unable to reflect the cell-level changes in expression that are occurring in the microglia, which make up only 30 or so cells in the brain. In addition, it is very possible that the microglia are mounting a heterogeneous response to DEPe exposure, and this measurement may not accurately reflect the intricacies of how they are responding to this exposure.

Figure 3: Whole-body and head-only expression of pro-inflammatory cytokines at 5dpf with DEPe exposure

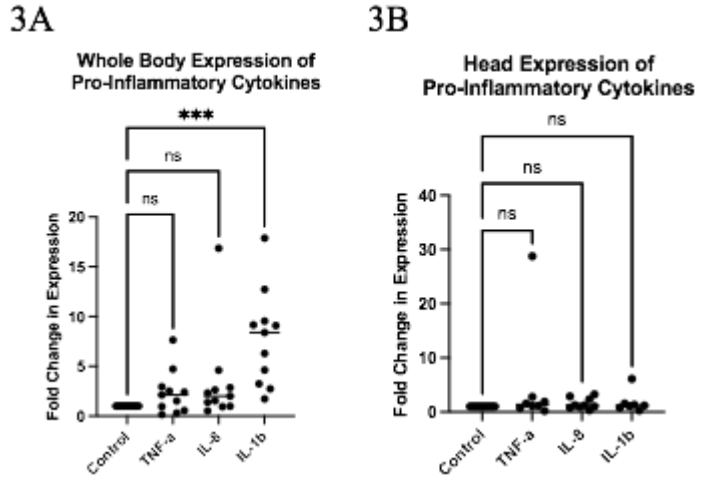

Figure 3: Quantification of changes in expression of pro-inflammatory cytokines with DEPe exposure. 3A: Whole-body expression of pro-inflammatory cytokines with DEPe exposure, IL-1b expression was significantly upregulated compared to DMSO. 3B: Head-only expression of pro-inflammatory cytokines with DEPe exposure, there were no significant changes. One-way ANOVA with Dunnett's test, *** = $p<0.001$, n = 5 samples, each sample prepared from RNA from ~20 larvae. All error bars represent standard error of the mean.

When knocking down microglial expression using morpholinos, injury to aminergic neurons at 3day DEPe treatment was not significantly attenuated

Next, we determined if these activated microglia play a direct role in the injury to neurons that occurs with DEPe exposure. We knocked down microglial expression in the larval ZF, temporarily, using morpholino oligonucleotide for Pu.1 injected at the 1-4-cell stage (Fig. 4A, B, C). This led to a complete loss of microglia for up to 3 days (72 hpf). Because the microglial expression begins to return after 3dpf, the DEPe treatment was performed from 1dpf as usual, to 3dpf. A scramble morpholino was utilized as a control for the effects of microinjection on the embryo. The telencephalic neuron count with DEPe treatment was

significantly lower in the scramble and pU1 injected larvae compared to the uninjected larvae. However, there was no significant difference in the neuron counts between the two injection paradigms with DEPe treatment (Fig. 4D). There were no significant differences in neuron count with DEPe observed in the diencephalon, even with injection (Fig. 4E).

Figure 4: Morpholino-induced knockout of microglial expression and effect on aminergic neuron count in 3dpf *mpeg1:mCherry* larvae with DEPe exposure

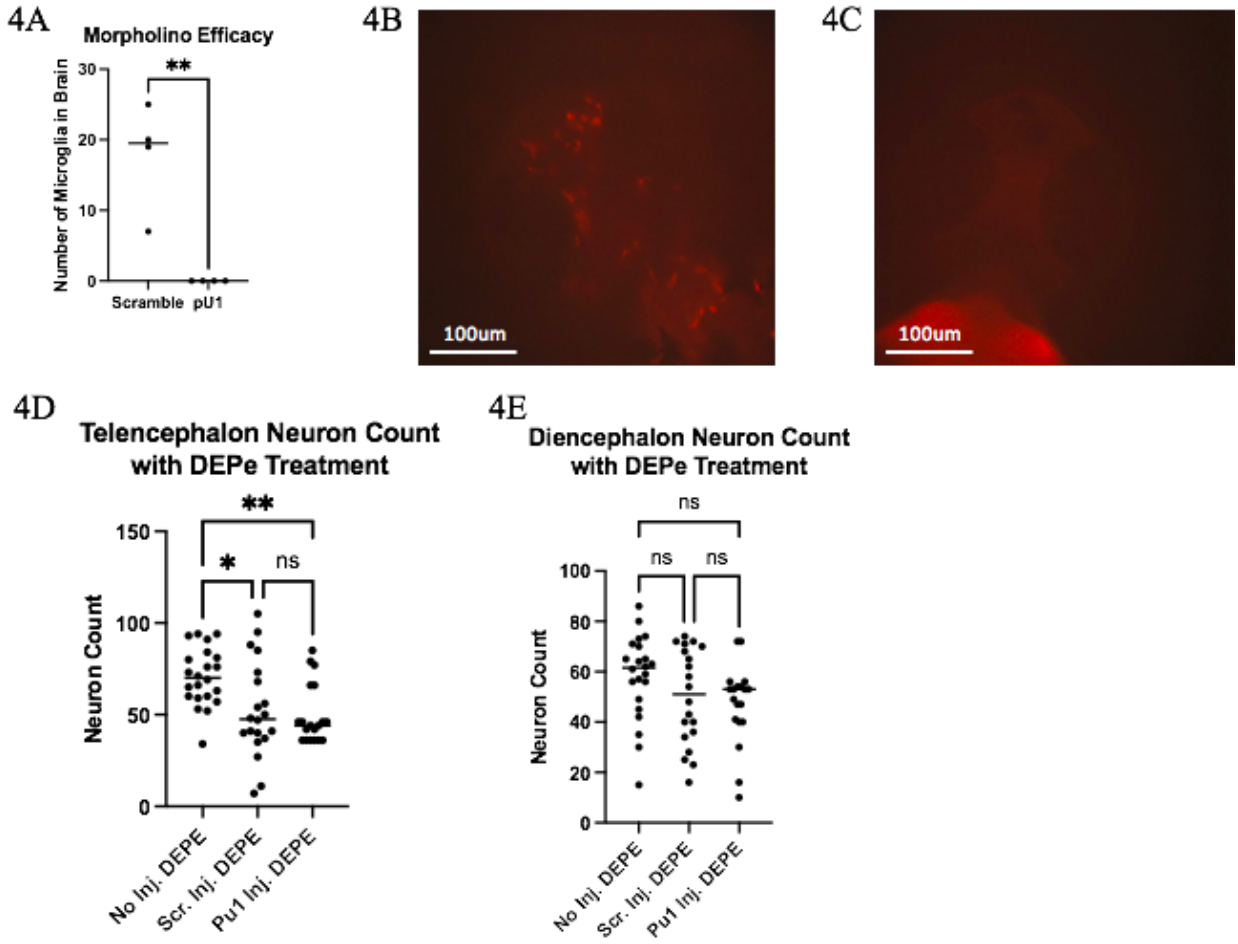

Figure 4: Efficacy of *pU1* MO-induced microglial knockdown and its effects on neuron counts with DEPe exposure. 4A: Injection of *pU1* MO consistently and completely knocked down microglial expression compared to scramble control MO injection. 4B, 4C: Dorsal view of live 2dpf *mpeg1:mCherry* embryo injected with scramble MO (4B), *pU1* morpholino (4C). 4D: Number of surviving neurons after DEPe exposure until 3dpf. Significant loss in the

telencephalon was observed with both scramble and *pU1* MO injection and DEPe exposure, but there was no significant difference in survival between the two injected groups. 4E: There was no significant change in neuron counts with DEPe exposure across any conditions tested in the diencephalon. One-way ANOVA with Sidak's multiple comparisons test, * = $p<0.05$, ** = $p<0.01$, n = 20-22 embryos per condition. All error bars represent standard error of the mean.

Discussion:

We demonstrated that DEPe exposure is toxic to aminergic neurons and simultaneously induces structural and functional activation of microglial cells. Our findings are well-supported by what is already known regarding the toxicity of diesel-related toxicants in experimental settings. Previously published data from our group has shown that a different DEPe mixture is toxic to neurons as well, including aminergic neurons (Barnhill et al., 2020). Furthermore, our observed structural and functional microglial activation with DEPe exposure *in vivo* is in line with previously observed response of microglia in culture to diesel exhaust particle (DEP) and the extracts containing adsorbed compounds from DEP exposure, that are not necessarily identical to the DEPe used in this study in terms of source and makeup (Levesque et al., 2013).

In addition, our observed lack of changes in expression of pro-inflammatory cytokines in the head samples can be explained by the small number of microglia in the brain compared to all other cell types, but is also supported by previous observations that show that DEP treatment does not cause microglia to produce cytokines *in vitro* (Levesque, Taetzsch, et al., 2011), (Block et al., 2004). It is very possible that the microglial response to DEPe exposure is much more complex than something that can be described with a simple screening of a few candidate genes, and multiple microglial responses are occurring at any one time. Despite differences in the exact formulation of the DEPe utilized in these studies, there are clear patterns in how microglia respond to DEPe exposure and our *in vivo* work strengthens this knowledge.

Knocking down microglial expression using the pU1 oligonucleotide microinjection did not affect the survival of neurons with DEPe exposure. This can be explained in multiple ways. Firstly, because of the short-term nature of the knockdown and the experimental setup, only the effects of the knockdown on the acute toxicity of DEPe were assessed. There may exist longer-

term effects of microglial knockdown on neuronal survival with DEPe exposure, but due to experimental design, they were not detected. In addition, it is important to keep in mind that these experiments are not attempting to fully duplicate what occurs in human exposures that lead to the development of PD over decades. Instead, in our larval ZF work, we are utilizing the concept of Adverse Outcome Pathways (AOP), which represents and readily communicates what may occur in certain disease processes. By taking the results from experiments that utilize the AOP framework, we can interpret and communicate results that explain mechanisms of interest. In this particular model, knocking down microglial expression attempted to address the question of whether or not microglia are directly involved in neuronal toxicity in the context of this specific exposure, but no changes were observed. In order to continue to answer this question, more intricate experimental techniques are necessary, such as identifying how microglia may have different responses to DEPe exposure at this time point, and performing this study long-term to describe the effects of the lack of microglia over time.

We also recognize that microglial knockdown through the microinjection of the pU1 morpholino oligonucleotide resulted in Vmat2 neuron toxicity, which may have influenced our results. This is because the microinjection, performed on the embryo at the 1-4 cell stage, disturbs the developmental process of the embryo, and tends to result in embryos that are not as robust and healthy as those that are uninjected. This was accounted for in the analysis by using a scramble morpholino as a control for the effects of the injection, and making the key comparison of the effect of microglial knockdown between the two injected groups. One way this may be addressed is to use a comparatively less disruptive technique to knock down microglial expression, such as the use of a transgenic line or treatment. We thoroughly explored these avenues. We attempted to prepare *irf8*-/- embryos from heterozygous *irf8*+/- larvae, obtained

from the Talbot Lab at Stanford University, which is a line that has a knockout of *irf8*, a gene critical for macrophage development, including microglia (Shiau, Kaufman, Meireles, & Talbot, 2015). However, the embryos had very poor survival with the homogeneous knockout, and we were unable to successfully identify *irf8*-/- larvae through fin clip genotyping and maintain a line of these double knockout adults for future use. In addition, we tested pexidartinib (PLX3397), which is commonly used in mammalian models to knock down microglial expression (Merry et al., 2020), (Elmore et al., 2014). This did not have any effect on microglial expression in our larvae, and pexidartinib has not been shown to successfully knock down zebrafish microglia in the literature. Therefore, our injection technique, which exhibited an extremely thorough and easy knockdown of microglia, was our choice.

We are interested in further investigating and characterizing the inevitably heterogeneous nature of the microglial population in the 5dpf larval zebrafish, and how they are distinguished from each other in terms of function and gene expression. We believe that there may be different microglia that exist in different functional states, and this is not necessarily something that can be elucidated from these initial studies. Analyzing gene expression changes at single cell resolution will be informative and allow us to further characterize not only their response to DEPe exposure and identify pathways that are activated with this exposure, but also begin to identify multiple states that may exist in activated microglia in addition to homeostatic ones.

Dissertation: Chapter 2

Microglial α-syn Processing in Response to Diesel Exhaust Particulate Extract Exposure

Introduction:

Our initial characterization of the response of microglial cells in our model to DEPe exposure indicated they are likely activated, but their presence does not seem to affect acute neuronal injury resulting from the DEPe exposure, as observed in a microglial knockdown experiment. In order to further investigate the mechanisms by which DEPe exposure may be linked to the development of PD, continuing with our focus on microglia as the main cell type of interest, we introduced the element of α-syn, a protein that is very well-established in the pathology of PD to accumulate and form toxic Lewy bodies. By combining the presence of human α-syn (hα-syn) with the environmental exposure of interest, DEPe, we sought to explore another major mechanism related to the development of PD: the impact of microglia on α-syn pathology, and how DEPe exposure may influence it.

The toxic aggregation of α-syn and subsequent formation of Lewy bodies and Lewy neurites is a very well-established pathology in PD. However, as mentioned in the previous Chapter and also applicable here, the timing and extent to which microglia may contribute to α-syn pathology and lead to adverse effects, and the timing and extent to which α-syn may induce microglial activation, is still being established. In some studies, microglia have been established to behave in a protective manner in the presence of abnormal levels of α-syn. In one study, microglia have been observed to actively clear and degrade α-syn via selective autophagy, or synucleinphagy, and prevent neurodegeneration, through engulfing neuron-derived α-syn and directing them into autophagosomes for degradation (I. Choi et al., 2020). However, in other

studies, the microglial response to the presence of α-syn appears to be more directly neurotoxic and less protective. One study found that microglial exosomes facilitate α-syn transmission *in vitro* and *in vivo* in PFF-induced α-syn aggregation models upon inspection of the exosomes produced by the microglia that induced protein aggregation and death in recipient neurons (Guo et al., 2020). In addition, we must consider when these seemingly opposing responses may be occurring, whether that may be simultaneously, and that the microglial response at any given time is dynamic in different parts of the brain, or along a time course, with one response occurring early on in disease development, and the other occurring later on.

In addition, microglial activation itself is a major observation in PD patients' brains (Imamura et al., 2003), (Croisier, Moran, Dexter, Pearce, & Graeber, 2005), (Doorn et al., 2014), (Ferreira & Romero-Ramos, 2018). Microglial activation has been observed to occur early (Stokholm et al., 2017), (Ouchi et al., 2005) and last for years (Gerhard et al., 2006). It is also very likely that not all microglia exist in the same activation and functional state at any given moment.

These were some of the known microglial responses and behaviors that have been observed in the context of PD development, and are outcomes that we attempted to describe in this Chapter, *in vivo,* in the hα-syn-expressing zebrafish model. Because α-syn plays such a large role in the pathology of this disease, we were interested in investigating its interactions with our glial cell type of interest, microglia, in our transgenic model, and in addition, understanding how exposure to DEPe may perturb these processes.

Methods:

Transgenic lines used

The cross of *HuC:Gal4 (+/+) x UAS:asyn:T2A:eGFP (+/-), mpeg1:mCherry (+/+)* was performed for every biological replicate. The HuC:Gal4(+/+) fish express the Gal4 transcription factor under the neuron-specific HuC promoter, and in the resulting embryos from the cross, the Gal4 transcription factor binds to the upstream activating sequence (UAS). This leads to the expression of the genes of interest, which are the hα-syn and eGFP, which sandwich a T2A self-cleaving peptide. Upon translation, the hα-syn and eGFP become translated separately in a 1:1 ratio, due to the T2A sequence containing a sequence that induces ribosomal skipping during translation. Therefore, the hα-syn and eGFP proteins are formed and originate in the same cells. Additionally, the *UAS:asyn:T2A:eGFP (+/-), mpeg1:mCherry (+/+)* contributed mCherry expression in all resulting embryos from the above cross, allowing for visualization of microglia by imaging the mCherry fluorophore. At 24hpf, the cardiac GFP expression was assessed as a visual marker of the hα-syn expression genotype. The embryos were then split into two groups, those expressing hα-syn and the non-expressers. If DEPe treatment was performed in the hα-syn expressors, the protocol was identical to that of Chapter 1, with the 24hpf starting timepoint and 5dpf ending timepoint of treatment. At 5dpf, the larvae were euthanized using tricaine methanesulfonate, and were fixed and antibody labeled against mCherry and hα-syn.

Microglial quantification

The forebrain was determined to be the most anterior protrusion of the brain, separated from the optic tectum by the boundary formed by the lateral widening of the brain at the optic tectum. The transgenically expressed mCherry fluorophore of the microglia in the region was antibody

labeled as described in Chapter 1, in order to maximize the detection of the presence of the microglia and not risk bleaching of the fluorophore, imaged using the Leica SPE confocal microscope (Leica Microsystems Inc., Buffalo Grove, IL), and quantified by using the Z-projected images on ImageJ of each sample and counting individual microglia.

Neuronal quantification

The hα-syn-containing neurons were quantified by counting the cells positive for hα-syn in the forebrain region. The HuC neurons were quantified by counting all cells that contained GFP in the forebrain. The forebrain was selected as the area of analysis due to the high concentration of hα-syn expression across samples (around 43% of fluorescence when antibody labeled), easy identification and localization, microglial migration to the region, and the presence of aminergic neurons. They were quantified in the same way as the Vmat2 neurons, through Z-projection of 2um stacks collected using confocal microscopy via Leica SPE (Leica Microsystems Inc., Buffalo Grove, IL), and quantification using ImageJ's counting tool.

Student's T-test was performed using Graphpad Prism 9. * = $p<0.05$, ** = $p<0.01$, *** = $p<0.001$. All error bars represent standard error of the mean.

Quantification of interaction between microglia and hα-syn-containing neurons

Z-projected images and the original TIF files containing every image representing 2um slices of 5dpf brains from *HuC:Gal4 (+/+) x UAS:asyn:T2A:eGFP (+/-), mpeg1:mCherry (+/+)* larvae that were screened for hα-syn expression, treated with DMSO or DEPe, were analyzed using ImageJ. Any neuron that had a visible α-syn cluster inside of it was considered eligible for interaction. The number of microglia performing an interaction were counted in each image, by

first viewing the overall Z-projected image to identify potential areas containing cells that may be interacting or overlapping, then using narrower, more precise projections from the TIF files to confirm the overlaps were indeed on the same plane and are true interactions.

Results:

Microglia are structurally and functionally activated with overexpression of hα-syn in the ZF brain

We first determined if microglia are structurally and functionally activated in the 5dpf ZF brains that transgenically overexpress hα-syn. Skeletonization and Simple Neurite Tracer analysis revealed that the maximum branch length of the skeletonized microglia were significantly shorter for the microglia in the brains overexpressing hα-syn compared to the microglia in brains not overexpressing hα-syn (Fig. 5A, 5H, 5I). Interestingly, the number of branches and number of junctions were not significantly altered with the overexpression of hα-syn, even though they were significantly smaller with DEPe treatment, shown in Chapter 1.

Microglia move to the forebrain with overexpression of hα-syn in the ZF brain

We next determined if there were any significant changes in the number of microglia that reside in certain regions of the brain that are relevant to aminergic neurons with overexpression of hα-syn. We separated the brain into two regions, the forebrain and the optic tectum, to determine how the distribution of microglia changed. There was a significant increase in the number of microglia present at 5dpf in the hα-syn-overexpressing forebrains (16 microglia on average) compared to non-hα-syn-overexpressing brains (10 microglia on average) (Fig. 5B).

However, the number of microglia were comparable in the optic tectum. In addition, the total number of microglia in the non-expressors (48 microglia on average) were comparable to the number of microglia in the hα-syn expressors (52 microglia on average). Therefore, the increase in the number of microglia in the forebrain region with hα-syn overexpression may be due to generation of microglia in that region or the movement of microglia specifically to that region from its source of generation.

Figure 5: Microglial activation quantification and microglial movement quantification in the 5dpf *HuC:Gal4 (+/+) x UAS:asyn:T2A:eGFP (+/-), mpeg1:mCherry (+/+)* brain.

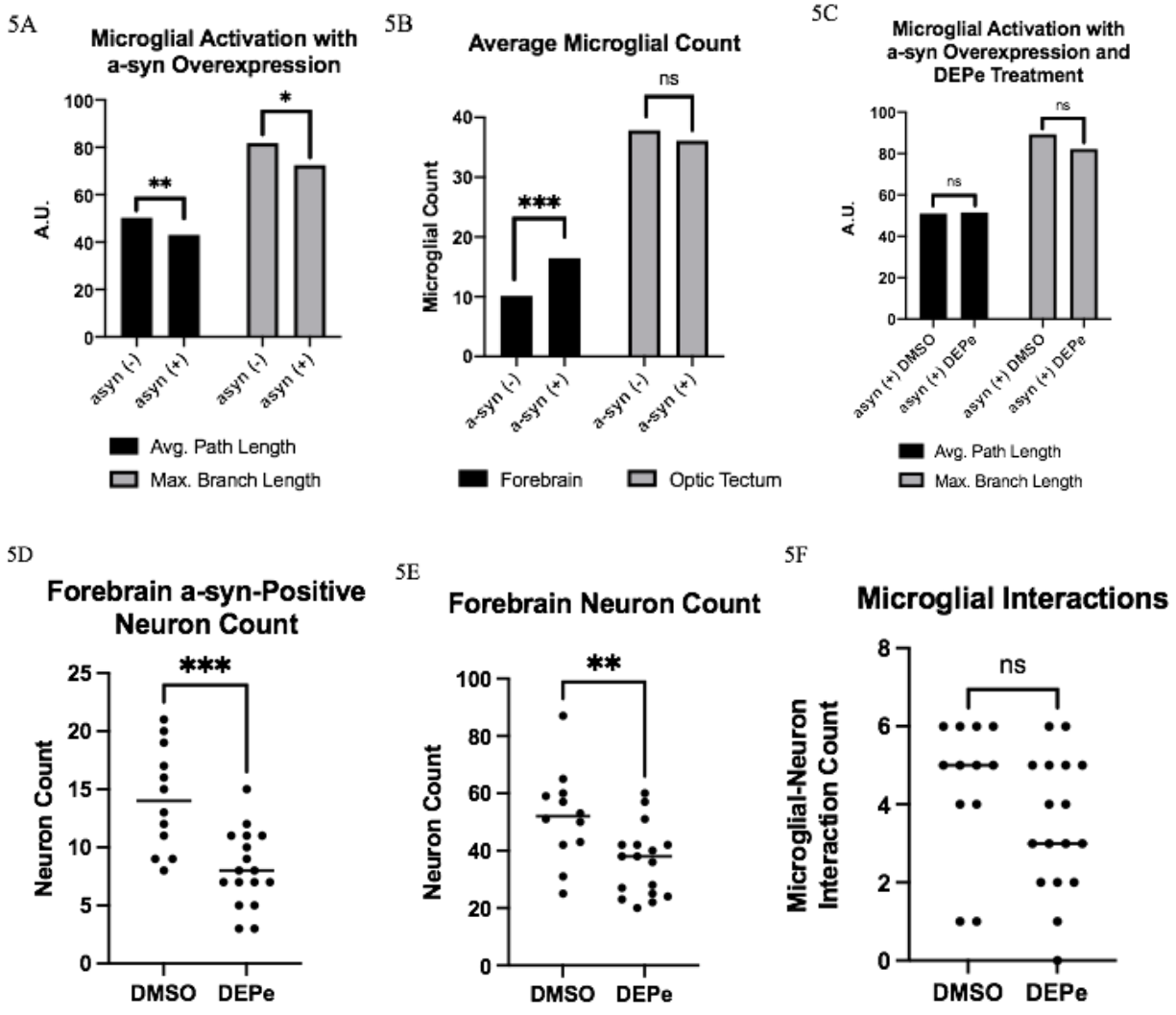

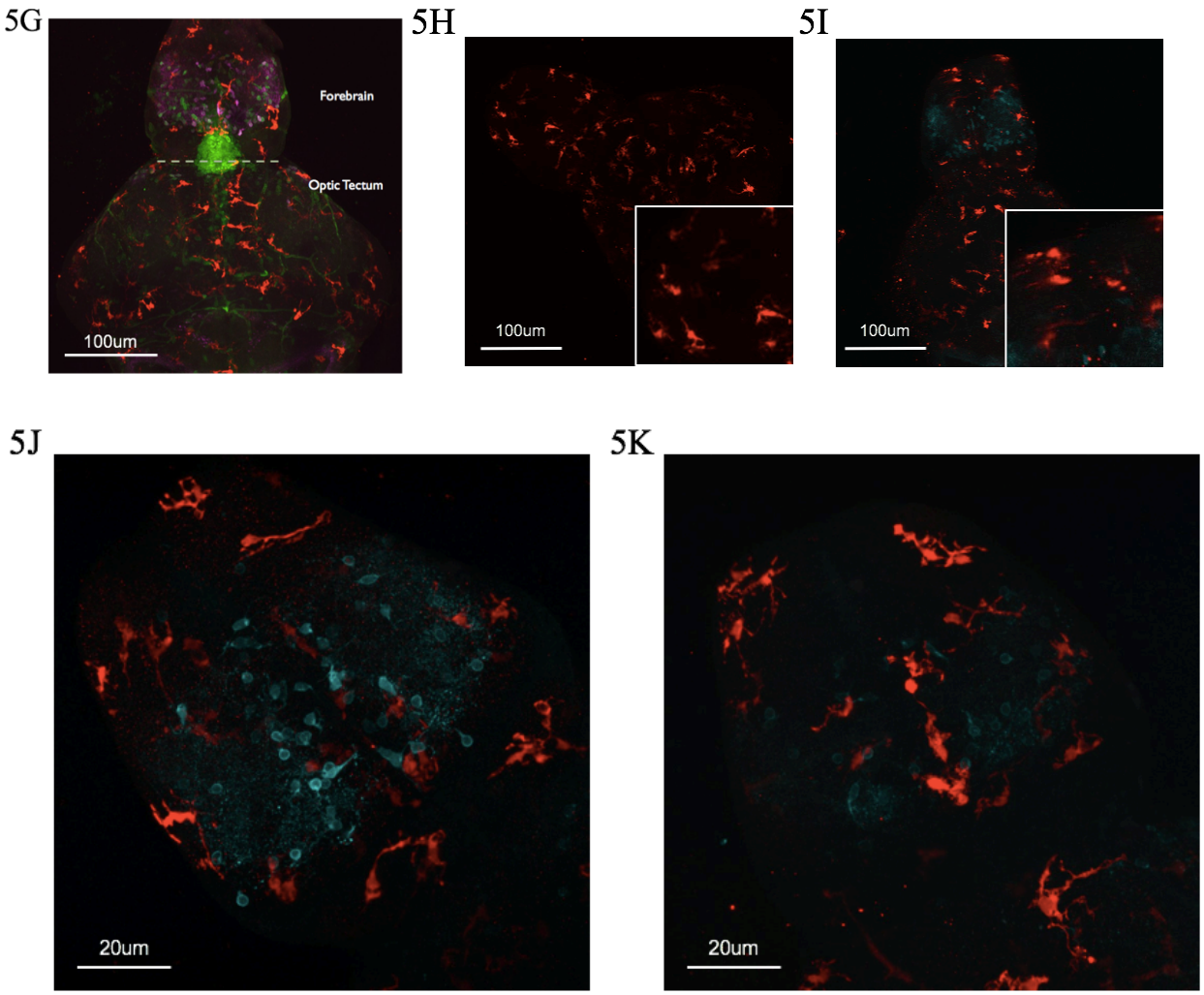

Figure 5: Microglial quantification in the 5dpf *HuC:Gal4 (+/+) x UAS:asyn:T2A:eGFP (+/-), mpeg1:mCherry (+/+)* brain. 5A: Average Path Length and Maximum Branch Length of microglia were significantly shorter in 5dpf larvae overexpressing hα-syn compared to controls, n=12, 14. 5B: The number of microglia were significantly higher in the forebrain with overexpression of hα-syn at 5dpf, but the number of microglia in the optic tectum were unchanged, n=7, 9. 5C: With DEPe treatment, microglia in 5dpf brains that overexpress hα-syn did not become any more activated, n=12, 17. 5D, 5E: With DEPe treatment, there was a significant decrease in the number of neurons that visibly contained hα-syn (5D), and there was also a significant decrease in the number of all visible GFP-containing neurons, regardless of alpha synuclein expression (5E), n=12, 17. 5F: There was no significant change in the number of microglia that interacted with an alpha synuclein containing neuron, n=12, 17. 5G: Sample image showing the dorsal view of 5dpf *HuC:Gal4 (+/+) x UAS:asyn:T2A:eGFP (+/-), mpeg1:mCherry (+/+)* brain distribution of hα-syn expression (magenta), eGFP, and mCherry-labeled microglia in the ZF brain. A large percentage (43%) of hα-syn expression, quantified by fluorescence, occurs in the forebrain. 5H: Dorsal view of mCherry-expressing microglia in control larva, lacking hα-syn expression. 5I: Dorsal view of mCherry-expressing microglia and hα-syn (cyan). 5J: Dorsal view of forebrain of DMSO-treated hα-syn expressing larvae at 5dpf. 5K: Dorsal view

of forebrain of DEPe-treated hα-syn expressing larvae at 5dpf. Student's T-test, * = $p<0.05$, ** = $p<0.01$, *** = $p<0.001$. All error bars represent standard error of the mean.

DEPe exposure significantly injures HuC neurons, and also those that overexpress hα-syn

We next studied if the presence of overexpressed hα-syn has an effect on the toxicity of DEPe on aminergic neurons and the extent of their injury. We analyzed the neurons visible in the forebrain. The transgenic line used for hα-syn overexpression drives overexpression under the *HuC* promoter, and not *Vmat2*, so the population of neurons quantified here are different to those in the previous chapter. However, by focusing on the forebrain region, we can consistently quantify populations that are of interest to us, as they are known to include aminergic neurons. We saw that treating hα-syn overexpressing embryos from 24hpf to 5dpf led to significant injury of visible neurons in the forebrain (Fig. 5E). There was also significant injury to just the aminergic neurons that contain visible hα-syn clusters (Fig. 5D, 5J, 5K).

Microglial activation is sustained with DEPe exposure in hα-syn brains

Microglia were structurally activated with overexpression of hα-syn, but we also wanted to determine if microglia would be activated with DEPe exposure in hα-syn overexpressing brains. So, we wanted to answer the question: will microglia exhibit an even more activated morphology with DEPe exposure, on top of already being activated in the presence of overexpressed hα-syn? We determined through the Skeletonization and Simple Neurite Tracer analysis that the microglia in forebrains of hα-syn overexpressing larvae that are treated with DEPe are not significantly different in terms of structural activation than microglia in the forebrains of untreated, hα-syn overexpressing larvae (Fig. 5C). They have a similar level of structural activation, which shows that they are indeed activated in the context of DEPe

exposure, but the activation is no more intense than in the environment of overexpression of hα-syn.

Microglial-hα-syn neuronal interactions were unchanged with DEPe exposure

In hα-syn overexpressing brains, we consistently observed microglia interact with neurons that contain visible hα-syn. We were extremely interested in determining if there DEPe exposure had an effect on the number of microglia that interacted with these neurons that visibly overexpress hα-syn. Any neuron that had a visible α-syn cluster inside of it was considered eligible for interaction. On average, 4.5 microglia were performing interactions with neurons in the forebrain of embryos untreated with DEPe. With DEPe treatment, the number of microglia interacting with neurons decreased to 3.47, and this was not a significant decrease ($p=0.13$) (Fig. 5F, 5J, 5K).

Discussion:

α-syn accumulation, leading to the development of Lewy Bodies, is a major disease hallmark of PD. However, it is important to keep in mind that the presence of Lewy Bodies in the substantia nigra is not a requirement for neuronal death, and that neuronal apoptosis occurs without the presence of Lewy Bodies (Tompkins & Hill, 1997). Keeping this in mind, and considering the complexity of the brain environment, we can easily assume that there are various other factors that influence neuronal death, such as the presence of microglial cells and their responses to pathologies involved in PD. In this chapter, we began to characterize how microglial cells respond to the presence of overexpressed hα-syn in our ZF model, and most importantly, how exposure to DEPe, a representative of a major component of AP, influences these microglial responses.

As expected, microglia were significantly more structurally activated with the overexpression of hα-syn in this ZF model compared to non-expressors. In addition, curiously, the microglia exhibited motility towards the most anterior region of the larval brain, the forebrain. The total numbers of microglia in the brain were comparable with and without the overexpression of hα-syn, so it is also possible, as described in Results, that the microglia were generated more readily in that region as well, and this requires further investigation to make a distinction as to which explanation applies.

The forebrain was selected as the site for further analysis of microglial-neuron interactions for various reasons. Firstly, there was a very high concentration of of hα-syn expression across samples (around 43% of fluorescence when antibody labeled) in the forebrain, which allowed it to be reliable region to study. Secondly, the forebrain is easily identified when performing 5dpf ZF larval brain dissections and imaging which leads to consistency in the

technique used to obtain results. Thirdly, we observed the significant increase in microglial counts in the forebrain region with hα-syn overexpression, which made us interested in characterizing the interactions in that region in particular. Finally, there is a reliable presence of aminergic neurons in the forebrain, as it contains the telencephalon and diencephalon (Cheng, Jesuthasan, & Penney, 2014), which were the two regions that were quantified for neuronal loss in Chapter 1 and contain many dopaminergic neurons (Kastenhuber, Kratochwil, Ryu, Schweitzer, & Driever, 2010). Therefore, the significant neuronal injury quantified in the forebrain region with DEPe exposure was expected. On the other hand, the sustained microglial activation in the forebrain region with DEPe exposure in the presence of overexpressed hα-syn was interesting, because it introduced some possible limitations of our model. The microglia may not be any more activated with DEPe exposure, but there also may be an upper limit on the ability of the experiment to detect any further changes in microglial activation state that is occurring.

The results from the interaction experiment in the final portion of this Chapter showed that DEPe exposure did not change the number of microglia interacting with hα-syn-containing neurons. However, we also established that DEPe exposure significantly injures hα-syn-containing neurons. Therefore, with DEPe exposure, there are significantly fewer neurons available for the microglia to interact with. Even with these decreased neuron counts due to DEPe treatment, the number of microglia interacting with hα-syn-containing neurons was not significantly different. This led us to the conclusion that the ability of microglia to interact with hα-syn-containing neurons is not directly influenced by DEPe exposure. This aligns with our results from Chapter 1, where microglial knockdown did not affect neuronal counts after DEPe exposure. Perhaps, due to the acute nature of this model, we are not fully describing the response

of microglia to DEPe exposure, and are only seeing a snapshot of a more complex, long-term microglial response.

Although knocking down the microglial presence in the region didn't directly attenuate neuronal death quantified by the change in telencephalon and diencephalon neuron counts as reported in Chapter 1, there are many ways that microglia have an influence on their brain environment, such as activation due to the presence of hα-syn (Zhang et al., 2007), release of cytokines (Smith, Das, Ray, & Banik, 2012), and involvement in reactive oxygen species production (Simpson & Oliver, 2020). It is very possible that these well-accepted microglial behaviors are able to persist and lead to neuronal death through other avenues, and that microglia themselves do not have to directly act upon neurons. In addition, it is very important to remember that microglia are not a homogeneous population, and that different states of microglia exist in the brain at any given time (von Maydell & Jorfi, 2019), with some microglia behaving in a more protective manner than other microglia.

Perhaps the knockdown of microglia, and the fact that no significant difference in microglial-neuronal interactions were quantified in this Chapter, can be explained by the oversimplification of the population of microglia we have been studying. Clearly, microglia are readily responding to these experimental perturbations, whether it is hα-syn in our ZF model or exposure to DEPe in the previous Chapter. In order to more accurately characterize the microglia and begin to identify pathways that are directly related to DEPe exposure, more sensitive and strategic analysis at single-cell resolution is necessary.

Dissertation: Chapter 3

Single-cell Characterization of Microglial and Astroglial Response to Diesel Exhaust Particulate Extract Exposure

Introduction:

Microglia are visible in the developing larval zebrafish brain at around 2.5 dpf, and originate from the rostral blood island (RBI), which is embryonic hematopoietic tissue. They mainly colonize the optic tectum of the midbrain in a circulation-independent manner, and some are visible in the forebrain and hindbrain. Most of the microglia enter the brain from the ventral periphery, and a small proportion enter the brain through the bilateral periphery between the eyes (J. Xu, Wang, Wu, Jin, & Wen, 2016). Zebrafish microglia have been observed to have functions such as expression of pro-inflammatory cytokines in response to injury, induction of neuronal regeneration, and clearing myelin debris (Var & Byrd-Jacobs, 2020). Microglia in the zebrafish have been described through gene expression profiling at various timepoints during the embryonic stage, and core microglial genes that are conserved in humans have been identified to characterize each time point (Mazzolini et al., 2020). Therefore, studying microglial responses to DEPe exposure using this model is relevant and informative in elucidating possible mechanisms of action that link AP exposure to the development of PD.

Zebrafish do not have a cell type identical to mammalian astrocytes, but they do have radial glial cells that have many similarities with mammalian astrocytes. These cells are generally bipolar in shape, rather than star-like, and behave as neural progenitors throughout the life of the fish. They play a homeostatic role at the brain barriers and neural circuits (Jurisch-Yaksi, Yaksi, & Kizil, 2020). The radial glial cells do not fully differentiate into astrocytes in the

way that astrocytes do in mammals, and they retain their radial glial nature throughout life. Even in adult zebrafish, radial glial cells play an important role in responding to neuronal loss by increasing neural stem cell proliferation and neurogenesis. They have been proposed to be the homolog of mammalian astrocytes based on a number of their characteristics including the presence of glutamate transporter EAAT2 orthologs in the zebrafish retinal glia (Niklaus et al., 2017), expression of connexin43 by radial glial networks (Chatterjee et al., 2005), and exhibiting synchronous activity during distinct neuronal states (Diaz Verdugo et al., 2019), similar to mammalian astrocytes. Also, these cells in the zebrafish hindbrain have been observed to be activated by norepinephrine, which is in line with the reactive nature of mammalian astrocytes (Mu et al., 2019). In addition, aquaporin-4 is expressed in the endfeet of mammalian astrocytes, and is also expressed in zebrafish radial glial cells, although not in the endfeet region (Grupp, Wolburg, & Mack, 2010). Due to this evidence of many similarities between radial glial cells in the zebrafish larvae and astrocytes, and to recognize there still exist some key differences, radial glial cells in the zebrafish will be referred to as astroglia in this work. Single-cell transcriptomic analyses have begun to characterize zebrafish astroglia, and the studies have revealed different types of neural progenitor cells with distinct transcriptional profiles, which evidence the heterogeneity of these cells in the zebrafish brain, even at the embryonic stage (Lange et al., 2020). Therefore, continuing this work to not only characterize the astroglial cells at single-cell resolution, but to also determine cell-type-specific responses to DEPe exposure, will be informative in furthering our understanding of the adverse outcome pathways involved in DEPe toxicity. In addition, our work aims to point the field in directions that future research can take in the context of targets for therapeutics for neurodegenerative disease.

Methods:

Zebrafish microinjection with pGFAP-GFP

pGFAP-GFP plasmid was injected into homozygous *mpeg1:mCherry* embryos at the 1-4 cell stage (Lam, Marz, & Strahle, 2009). The embryos were treated at 24hpf with DMSO or DEPe as described below.

5-day DEPe Treatment of ZF Embryos

Embryos for treatment were manually dechorionated at 24hpf using Dumont #5 Fine Forceps. Each treatment consisted of 20 embryos in a final volume of 10mL E3 buffer in Corning Costar 6-well Plates. The final concentration of DEPe in the treatment well was 25ug/ml. Final DMSO vehicle concentration was 0.1% in both treatments. Embryos were treated until 5dpf. They were euthanized through the addition of 1ml of 5mg/ml tricaine methanesulfonate to each well.

ZF Head Cell Dissociation and Preparation for 10X Genomics scRNA-seq

The DMSO and DEPe treated larvae were anesthetized with tricaine methanesulfonate. The heads and eyes were removed with Dumont #5 Fine Forceps. The isolated heads were placed in 1ml cold Ringer's Solution on ice in 1.5-ml microcentrifuge tubes. 15 heads were collected per experimental condition (DMSO, DEPe). The collected head tissue was gently pelleted for 20 seconds. The Ringer's Solution was removed, and the pellet was washed with 1X DPBS. The last DPBS wash was removed and 500ul room-temperature Accumax Cell Dissociation Solution was added to each microcentrifuge tube. The tubes were immediately placed in a 37C water bath. Every 10 minutes, the cell pellet was moved through the tip of a fire-polished glass pasteur pipette 20 times. After a total of 40 minutes in the water bath, and the tissue appeared to be 80-

90% dissociated, the tubes were removed from the water bath and placed on ice. 500ul of 1X DPBS was added to each tube to slow down dissociation. The 1ml sample was filtered through a 40um mini cell strainer (pluriSelect) into a sterile, round-bottom, 14mL (17 x 100mm) Falcon collection tube (Becton Dickinson). The microcentrifuge tube used for dissociation was rinsed with 0.5mL 1X DPBS, and was filtered through the same 40um strainer into the collection tube. The cells were pelleted at 1100 rpm for 10 minutes at room temperature. The supernatant was removed, and the pellet was resuspended in 70ul of 1xPBS + 0.04% BSA. This sample preparation protocol was performed 3 times to prepare 3 biological replicates per condition (45 heads total per condition).

10X Genomics scRNA-seq Run Parameters

10X Genomics scRNA-seq runs were performed at the UCLA Technology Center for Genomics and Bioinformatics (TCGB). 10,000 cells were targeted per run with 50,000 reads per cell on the NextSeq 500 High Output, with the read length of 1x75.

Bioinformatic Analysis of scRNA-seq Data

Bioinformatic analysis was performed on a 64-bit MacBook Air (Apple) running Mac OS X 10.13.6 with 4 GB of RAM. Reads generated from the NextSeq 500 High Output were first transferred to the UCLA Hoffman2 Cluster using Globus. All work on Hoffman2 was performed using Terminal. CellRanger mkref was run to prepare a zebrafish reference genome for alignment, using Danio_rerio.GRCz11.101.chr.gtf and Danio_rerio.GRCz11.dna.primary_assembly.fa, available from Ensembl. Firstly, the GTF files were filtered using cellranger mkgtf. Then, cellranger mkref was run. The sequences for GFP

and mCherry were added to the reference genome. Cellranger count was run for each GEM well, a total of 3 DMSO and 3 DEPe. Cellranger aggr was run to aggregate the 3 DMSO and 3 DEPe count data.

On RStudio Desktop, “Seurat”, “dplyr”, “ggplot2”, and “patchwork” packages were loaded. The filtered_gene_bc_matrices files from cellranger aggr were loaded to RStudio, and “Read10X” and “CreateSeuratObject” were used to create Seurat objects for each treatment condition. For each object, cells that had less than 500 detected genes were filtered out. “NormalizeData” was used to normalize the feature expression measurements for each cell, and “FindVariableFeatures” was used to find variable features for each Seurat object. Then, “FindIntegrationAnchors” was used to identify integration anchors using the Seurat objects as input, with the dimensionality of 1:20 as determined by “ElbowPlot”. These integration anchors were passed on to “IntegrateData”, which resulted in a Seurat object that contained the integrated, batch-corrected matrix of all cells for downstream joint analysis. A linear “scaling” transformation was applied using “ScaleData” to a variance of 1 and a mean of 0. Next, we performed principal component analysis on the highly variable genes in the scaled data using “RunPCA”. “FindNeighbors”, “FindClusters”, and “RunUMAP” were run to cluster cells. “DimPlot” was used to visualize the clustered cells.

“FindConservedMarkers” was used to identify canonical cell type marker genes conserved across conditions for each cluster. The cell identity of each cluster was determined through the identification of 3-5 cluster markers that fit the criteria: (1) gene must be highly expressed in a large proportion (25% or more) of the cells in that cluster, (2) gene must be lowly expressed in other clusters, (3) Avg. fold change of gene > 1.5, (4) Adjusted p-value < 0.01. Differentially expressed genes with DEPe treatment in the astroglial and microglial cluster were determined by

first creating a column in “meta.data” to hold the cell type identification and stimulation information, and switching the “current.ident” to that column. Then, “FindMarkers” was used to find the genes that are different between the DMSO and DEPe treated cells of that type.

Subcluster Analysis

The microglial and astroglial cell clusters were subsetted from the scRNA-seq data. For each subsetted cluster, the data was scaled, and was followed by “RunPCA,” “RunUMAP”, “FindNeighbors”, and “FindClusters”. Then, “FindMarkers” was used to identify differentially expressed genes most unique to each subcluster. These genes were converted to the human ortholog if available, and run through 4 pathway databases: "KEGG_2019_Mouse", "BioCarta_2016", "Reactome_2016", and "GO_Biological_Process_2018". The top 10 most significantly enriched pathways by adjusted P-value were reported and interpreted.

Gene Set Enrichment Analysis and IPA Pathway Comparison Analysis

Gene lists from the astroglial and microglial clusters were uploaded to the online tool Metascape for gene set enrichment analysis (GSEA), to functionally profile the gene sets. The lists were uploaded as *D. rerio*, and analyzed as *H. sapiens*. The enriched ontology clusters were identified and interpreted. Pathway analysis of the gene lists with corresponding expression values from the astroglial and microglial clusters was done using Ingenuity Pathways Analysis (IPA) software (QIAGEN Inc., https://www.qiagenbioinformatics.com/products/ingenuity-pathway-analysis), (Kramer, Green, Pollard, & Tugendreich, 2014). The ZF gene symbols were first converted to their human orthologs through bioDBnet: dbOrtho (Mudunuri, Che, Yi, & Stephens, 2009). The lists of converted human Entrez gene IDs and the corresponding expression values were

uploaded to IPA. The gene expression cutoff of 1.3 fold and p-value of 0.05 were set. The uploaded gene and expression data that met the cutoff parameters were compared to the gene expression data and consequently the pathway activation data in the IPA knowledge base, and the pathways most significant to the uploaded data were outputted. An overlap p-value was calculated using Fisher's exact test, which represents the probability that the enrichment, or overlap, of the genes in the filtered, uploaded dataset with the genes in a particular pathway in the IPA knowledge base is due to chance alone. For Comparison Analysis, pathways that had a Z-score > 2 and p-value < 0.05 were selected for interpretation. A Z-score with a magnitude of > 2 represents a significantly up- or down-regulated pathway, and was thus used as the cutoff for pathways to be included in Comparison Analysis. Resulting pathway lists and directionality were interpreted and reported.

RNAscope V2 Labeling

Zebrafish embryos were treated with DEPe at 24hpf, as described above. 5dpf larvae were euthanized with tricaine methanesulfonate and fixed using 4% PFA O/N at 4C in 1.5ml microcentrifuge tubes. The larvae were washed in 1ml 0.1% Tween 20 in DPBS (PBST) at RT, for 10 mins, 3 times. The PBST was removed and a series of MeOH washes were performed, with 1ml volumes 25%, 50%, 75%, and 100% methanol, each being rocked for 10 mins at RT. After the 100% MeOH wash, the larvae were able to be stored at -20C for up to 2 months. The 100% MeOH was removed and larvae were incubated in 0.2M HCl in 100% MeOH for 30 min, rocking at RT. The 0.2M HCl solution was removed, and the rehydration step was performed, where a series of washes starting with 1ml 75% MeOH, followed by 50% and 25% were performed for 10 mins at RT each. After the 25% MeOH wash, 1ml of 1% BSA was added and

the tubes were once again rocked at RT for 10 mins. As much of the 1% BSA was removed as possible without drying out the larvae, and 300ul of Protease Plus (Advanced Cell Diagnostics, Inc., Newark, CA) was added to each tube and the larvae were incubated at 40C for 60min. During the wait, the probes were brought to 40C for 10mins, and then were brought back to room temperature. Then, the C1-C3 probes (Advanced Cell Diagnostics, Inc., Newark, CA) were diluted appropriately, where the C1 probes were kept at 1X, and the C2 and C3 probes, which were at 50X working concentration, were diluted by the C1 probe or by Probe Diluent (Advanced Cell Diagnostics, Inc., Newark, CA) if only C2 or C3 probes were being diluted. Then, 50ul of the probe mixtures were applied to the tubes, and the tubes were kept at 40C overnight. After the overnight incubation, the probes were removed, and the larvae were washed with 1X Wash Buffer (Advanced Cell Diagnostics, Inc., Newark, CA) 2 times for 10min at RT, rocking. Then, the Wash Buffer was removed, and 2 drops of V2 Amp1 (Advanced Cell Diagnostics, Inc., Newark, CA) were applied to each tube, and the tubes were incubated at 40C for 30min. Then, the Amp1 was removed from each tube, and the larvae were washed with 1X Wash Buffer 2 times for 10min at RT, rocking. Then, the Wash Buffer was removed, and 2 drops of V2 Amp2 were applied to each tube, and the tubes were incubated at 40C for 30min. Then, the Amp2 was removed from each tube, and the larvae were washed with 1X Wash Buffer 2 times for 10min at RT, rocking. Then, the Wash Buffer was removed, and 2 drops of V2 Amp3 were applied to each tube, and the tubes were incubated at 40C for 15min. Then, the Amp3 was removed from each tube, and the larvae were washed with 1X Wash Buffer 2 times for 10min at RT, rocking. Then, the Wash Buffer was removed. The Opal Dyes 520 (Akoya Biosciences, Marlborough, MA, Cat.# FP1487001KT) and 570 (Akoya Biosciences, Marlborough, MA, Cat.# FP1488001KT) were diluted 1:300 using TSA Buffer (Advanced Cell Diagnostics, Inc., Newark,

CA), and were kept in the dark at 2-8C. 2 drops of HRP-C1 (Advanced Cell Diagnostics, Inc., Newark, CA) were applied to each tube, and the tubes were incubated at 40C for 15min. Then, the HRP-C1 was removed, and the larvae were washed with 1X Wash Buffer 2 times for 10min at RT, rocking. Then, 50ul of the diluted Opal Dye that the C1 was to be labeled with was applied to each tube, and the tubes were incubated at 40C for 30 min, protected from light. Then, the Opal Dye was removed, and the larvae were washed with 1X Wash Buffer 2 times for 10min at RT, rocking. Then, 2 drops of HRP Blocker were added and the larvae were incubated at 40C for 15 mins. Then, the HRP Blocker was removed and the larvae were washed with 1X Wash Buffer 2 times for 10min at RT, rocking. The steps starting with the application of HRP-C# were repeated for each Channel that was to be labeled in the sample. After the last washing step after the final HRP Blocker, 2% stock methyl green solution (prepared using ddH2O from powder, Sigma-Aldrich, SKU M8884-5G) was diluted 1:5000 using 0.1% Tween 20 in DPBS, and 1ml of the methyl green working solution was applied to each tube. The larvae were incubated overnight, rocking, at 4C. The methyl green solution was removed and the larvae were washed with Wash Buffer for 10 mins at RT, rocking. The larvae were then cleared in 50% glycerol for 30 mins. Larvae were dissected in 100% glycerol using Dumont #5 Fine Forceps to remove the brain from the rest of the body. The brains were mounted in 100% glycerol on microscope slides, and the brains were imaged at 40X using oil using a Leica SPE (Leica Microsystems Inc, Buffalo Grove, IL).

Results:

Overall Clustering Results

A total of 80,075 cells were analyzed. 39948 of those cells were from DMSO-treated heads, with an average of 19331 reads per cell. 40757 cells were from DEPe-treated heads, with an average of 18812 mean reads per cell. After filtering out low-quality samples, a graph-based clustering method was used to group the cells into clusters (T. Stuart et al., 2019). 27 transcriptionally distinct clusters were identified in the DMSO and DEPe treated cells (Fig. 6A). The clusters were represented by cells from all biological replicates, both DMSO and DEPe-treated (Fig 6B). The cell types of each cluster were identified through marker identification parameters outlined in Materials. As seen by the size of the dots and saturation of the color of the dots in Fig. 6C, which shows selected marker genes on the X-axis and cell types separated by DMSO or DEPe treatment on the Y-axis, the marker genes of a particular cell type were highly representative of that cell type regardless of treatment. This shows that the marker gene works well in both conditions to identify the cell type (Table 1).

Figure 6: Clustering diagram of all cells analyzed in scRNA-seq

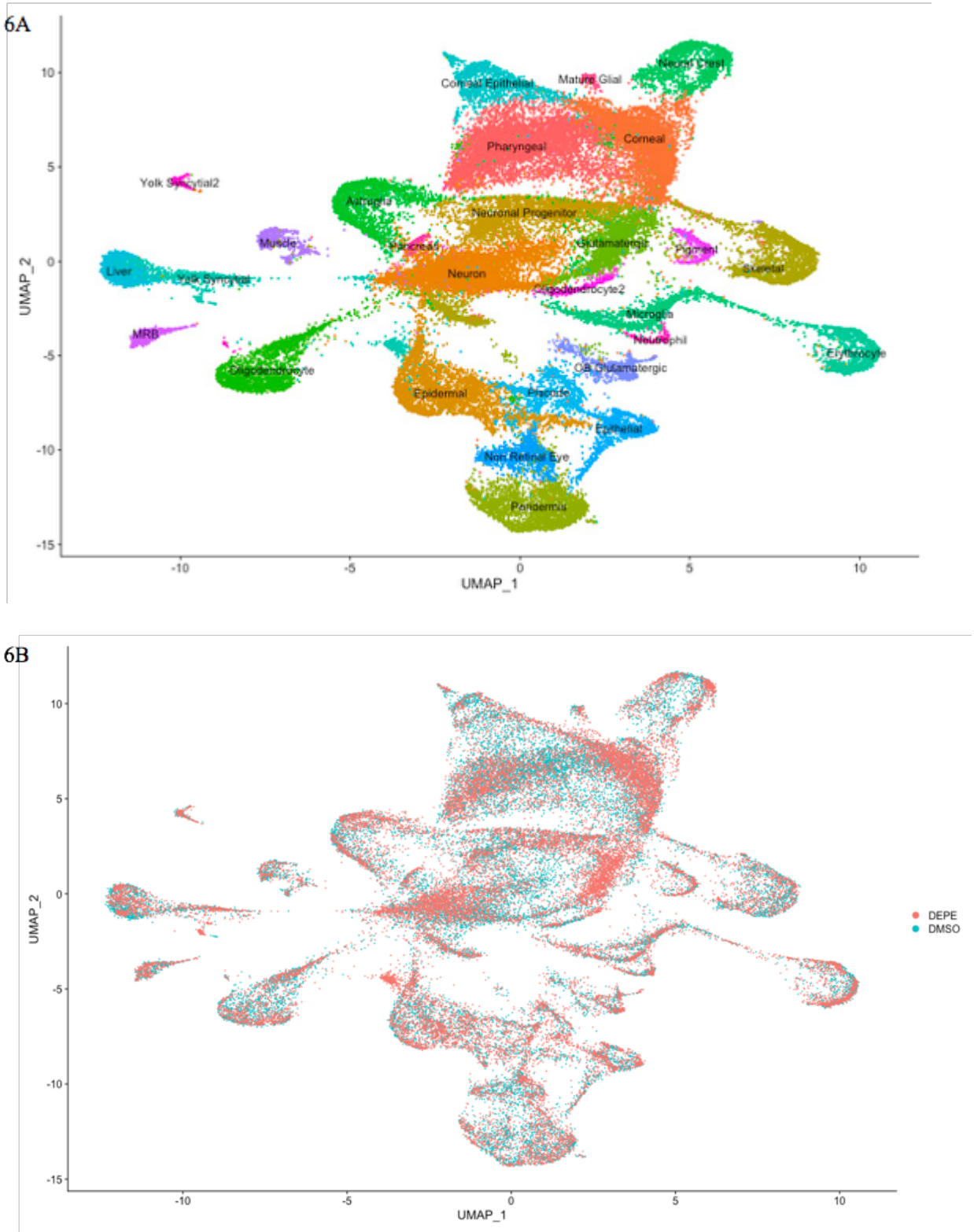

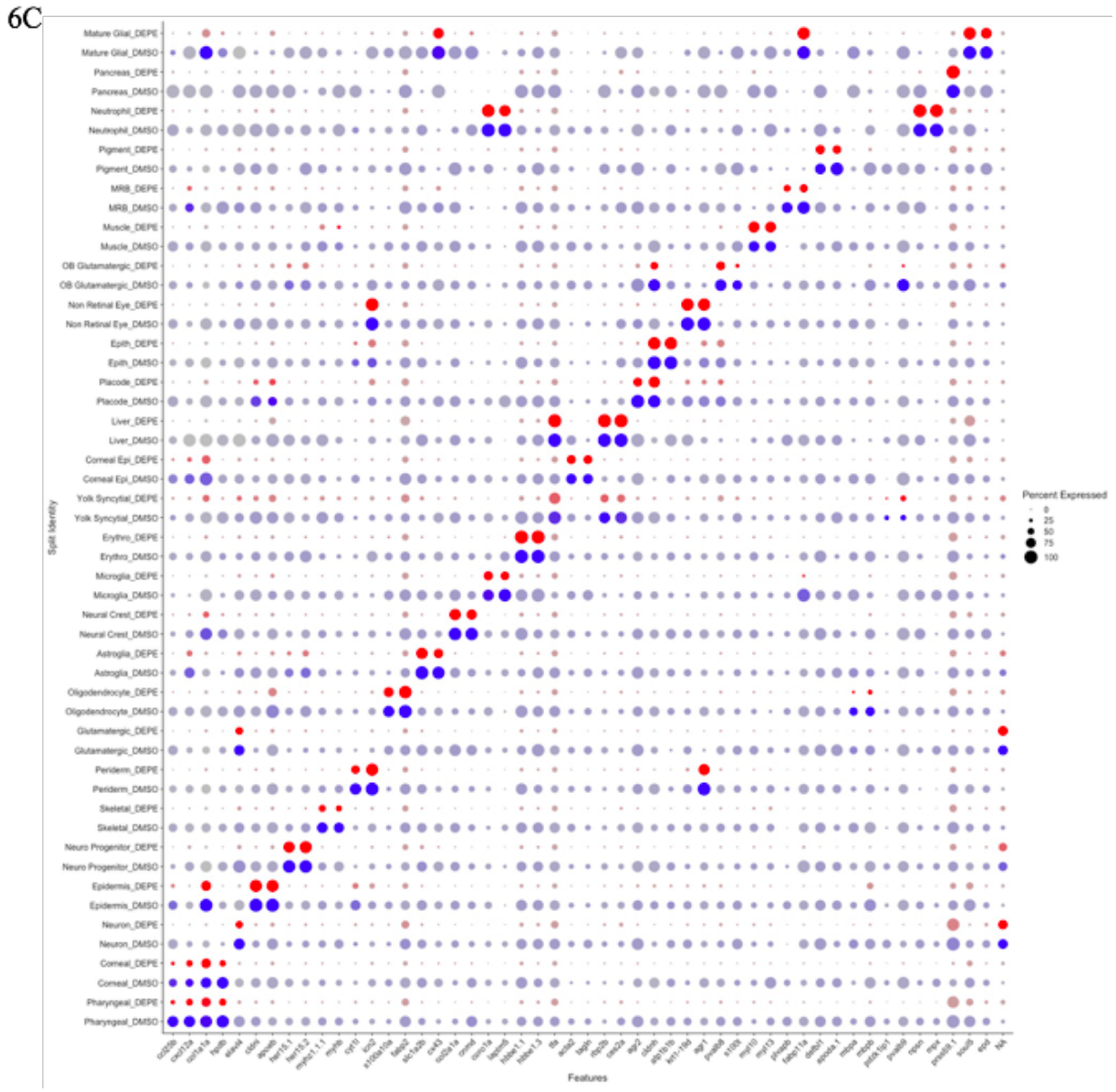

Figure 6: scRNA-seq and unbiased clustering analysis reveals various cell types in the 5dpf wild-type zebrafish head, with markers conserved across the DMSO and DEPe treatment conditions. 6A: Clustering diagram, also known as a UMAP plot, where each dot represents a cell, distances represent similarity, and inter-cluster distances also represent similarity of cell types (unlike tSNE), labeled by cell ID. 6B: UMAP plot, but the cells are labeled by treatment type. 6C: Chart showing selected markers (x-axis) of each cell type (y-axis), with the size of the dot representing the percent of cells in that cluster that express that gene, and the saturation of blue/red representing the p-value of the expression of that marker gene. Represents the relatively high, unique, and consistent expression of marker gene across DMSO and DEPe treatments for each cell type.

Table 1: Cell type marker list

	Cell Type	Markers	Cell Count
0	Pharyngeal arch	ccl25b, cxcl12a, ms4a17a.9	6140
1	Cornea	hpdb, ogna, thbs4b, col1a1a	5323
2	Neuron	tubb5, stmn1b , elavl4	5103
3	Epidermis	cldni, apoeb, pfn	3155
4	Neural progenitor	her15.2, her4.1, her4.2, her15.1	2751
5	Skeletal muscle	myhz1.1.1, myhb, tnni2a.1	2460
6	Keratin	cyt1l, icn2	2455
7	Glutamatergic neuron	elav14, nrn1a, stmn2a, adcyap1b	2394
8	Oligodendrocyte	rbp2a, s100a10a	2302
9	Astroglia	slc1a2b, gfap, s100b	2055
10	Chondrocyte	col2a1a, matn1, col9a2, col9a1a	1582
11	Microglia	cc134b.1, mfap4, mpeg1.1	1455
12	Erythrocyte	hbae3, hbbe1.1, hbbe1.3	1366
13	Yolk syncytial layer	tfa, serpina1l	1330
14	Smooth muscle	acta2, tagln, myl9a	1321
15	Liver	rbp2b, ces2a	1182
16	Placode	agr2, muc5.1, cldnh	1068

17	Epithelium	s100a11, cldnh, atp1b1b	1037
18	Eye (non-retina)	krt1-19d, krt92, agr1	1016
19	OB, glutamatergic	pvalb5, pvalb8, s100t, s100z	703
20	Muscle	myl10, myl13, myl4	631
21	Myeloid rostral blood	cdh5, gpr182, sox7, fabp11a, plvapb	582
22	Pigment	defbl1, apoda.1, gpnmb	502
23	Oligodendrocyte	mbpa, cd59, mbpb	364
24	Yolk Syncytial Layer	pvalb9, ifi30, selenop	264
25	Neutrophil	lyz, npsn, srgn, mpx	260
26	Pancreas	prss1, prss59.1, ctrb1, apoda.2	174
27	Mature glial cell	epd, ggctb, soul5	159

Table 1: Cluster identities and markers used to inform cell type identification. Cell count indicates the number of cells of that cell type in all cells from 90 total analyzed heads (45 heads collected from DMSO, 45 total heads collected from DEPe, consisting of 3 biological replicates of each).

Microglial Cluster Description and DEG Analysis

The microglial cluster (Cluster 11) was identified using the genes: *ccl34b.1, mfap4*, and *mpeg1.1* (Fig. 7A) (Svahn et al., 2013), (Raj et al., 2018). The mCherry fluorophore expression of the transgenic larvae used in this study was also assessed. However, the expression of mCherry was ultimately not relied upon as a marker of microglia, due to its less microglia-specific nature compared to the other marker genes, and its relatively very low level of

expression compared to reliable marker genes of microglia. Other known mammalian microglial markers, such as *laptm5*, were also highly upregulated in the cluster, but did not meet the parameters of marker selection in this particular model. Gene set enrichment analysis (GSEA) of the genes identified in the microglial cluster, conserved across treatment conditions, identified processes such as cell activation involved in immune response, nervous system development, metabolism of RNA, actin cytoskeleton organization, and regulation of cell adhesion to be most highly enriched in all microglial cells (Fig. 7B). These highly upregulated pathways are representative of well-known functions of microglia, as microglia are involved in the immune response, play important roles of phagocytosis and release of factors during brain development (Lenz & Nelson, 2018), metabolize RNA, and are often found to alter their structure during various states of activation.

With DEPe treatment, there were 55 significantly altered DEG in the microglial cells (Fig. 7C, Table 2). Some of the altered genes, such as *g0s2*, which has been observed in human microglia to be increased more than 3-fold in the presence of amyloid-beta (Walker, Link, Lue, Dalsing-Hernandez, & Boyes, 2006), *ccr9a*, which is a known marker of neurotoxic microglia that release high levels of TNFa (Li et al., 2006), and *apoeb*, upregulated in the pro-inflammatory, activated state of microglia (Walker, 2020) associated with Alzheimer's Disease, were highly upregulated, suggesting that there are microglial populations that are activated and potentially neurotoxic. Other significantly changed genes, such as the highly upregulated *il13*, which is known to be anti-inflammatory (Shin et al., 2004), (Miao et al., 2020), and the highly downregulated *cd74a*, a marker of activated microglia (Hwang et al., 2017), represent the possibility of the presence of microglia that are responding to DEPe exposure in a more protective, anti-inflammatory manner. In addition, the most highly upregulated DEG in microglia

with DEPe exposure was *grn2,* or granulin 2. Although there is no direct human ortholog of granulin 2, this gene is a paralog of the granulin gene in mammals, and encodes a shorter protein, similar to the product of proteolytic progranulin cleavage in mammals (Zambusi, Pelin Burhan, Di Giaimo, Schmid, & Ninkovic, 2020). Interestingly, in frontotemporal dementia, there are mutations in the progranulin gene, and there are generally lower progranulin levels leading to loss of progranulin function. Generally, healthy microglia have been observed to highly express progranulin, and therefore have high levels of granulin (Goedert & Spillantini, 2006). Therefore, the significantly high expression of *grn2* with DEPe exposure by microglia may be a compensatory or protective response. The intricate ways in which these DEG occur in the microglia with DEPe exposure suggest that these cells may be responding in a heterogeneous manner, and there are likely multiple activated states in which the microglia exist.

Table 2: Genes that are differentially expressed in microglial cells with DEPe exposure.

	Fold Change		**Fold Change**
grn2	5.574380555	**CABZ01058647.1**	1.347354042
icn	2.362166957	**si:dkey-21e2.16**	1.34449382
scinla	1.894250982	**srgn**	1.335552148
si:ch211-14a17.10	1.893145062	**CABZ01021592.1**	1.333724761
pvalb5	1.874865643	**si:dkey-21e2.14**	1.331168596
g0s2	1.815755982	**si:dkey-21e2.10**	1.329789289
il13	1.781904257	**fabp1b.1**	1.327708335

thy1	1.637391784	**BX322787.1**	1.327291235
apoc1	1.608713353	**tfa**	1.323033492
si:dkey-21e2.3.1	1.578870472	**apoa1b**	1.321287447
hbbe1.1	1.548410468	**mylpfa**	1.312756467
si:ch211-207n23.2	1.540890506	**actc1b**	1.309014809
apoeb	1.527787026	**ccl20a.3**	1.308253707
il17a/f2	1.509928653	**krt5**	1.306298023
si:dkey-247k7.2	1.483516228	**ccr9a**	1.298837197
myhz1.1	1.472410126	**elavl4**	1.293876822
cst14b.2	1.464081817	**atp2a1**	1.29314754
si:dkey-21e2.15	1.451568216	**si:ch73-359m17.9**	1.291737356
si:ch211-212d10.1	1.436802272	**si:dkey-21e2.8**	1.291196361
hbbe2	1.422749262	**nkl.1**	0.777343688
FP236331.1	1.419917825	**lgals3bpb**	0.776339154
s100a11	1.419093518	**pgam1a**	0.771836684
ifi30	1.40363528	**si:ch211-161c3.6**	0.76424604
agr2	1.394821988	**cxcr4b**	0.73150926
si:ch73-359m17.7	1.388832686	**cd74a**	0.728394705
cpa5	1.375196459	**fthl28**	0.685357349

pdia2	1.357693902	**star**	0.400666768
and2	1.347875299		

Table 2: Differentially expressed genes in the microglial cells with DEPe exposure.

Figure 7: Microglial cluster marker expression data, GSEA and DGE analysis results

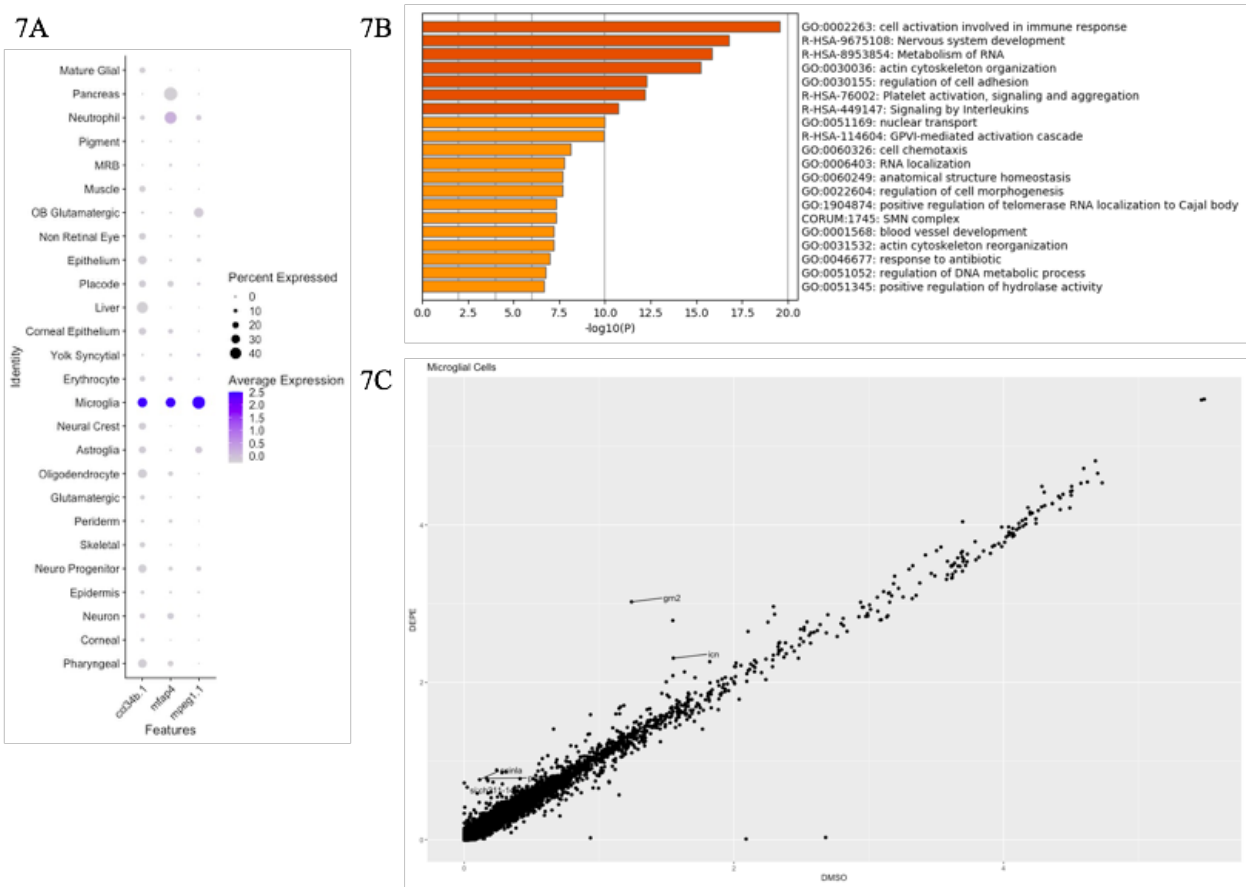

Figure 7: Microglia were identified with highly upregulated marker genes, gene set enrichment analysis revealed most enriched biological processes, and differentially expressed genes were identified. 7A: The microglial markers ccl34b.1, mfap4, and mpeg1.1 were highly and uniquely expressed in the microglial cells compared to other cell clusters. 7B: Gene set enrichment analysis gives us an overall look at the most enriched biological processes given the gene expression data from the microglial cluster. The top enriched biological processes, such as cell activation involved in immune response, nervous system development, metabolism of RNA, and actin cytoskeleton reorganization are known functions of activated microglia. 7C: Scatter plot featuring and labeling some of the most differentially expressed genes in microglia that exhibit a dramatic response to DEPe exposure.

Astroglial Cluster Description and DEG Analysis

The astroglial cluster (Cluster 9) was identified using the markers: *slc1a2b, gfap, s100b* (Fig. 8A). The expression of eGFP under the gfap promoter using the plasmid injection at the successfully led to the expression of eGFP fluorophore in many cells, but similar to the expression of mCherry, it was ultimately not utilized as a marker gene in the identification of astroglial cells. This was due to the fact that the *gfap* gene was already being used as a reliable endogenous marker, and the eGFP expression was relatively low, and due to the injection paradigm, mosaic. Other known astrocyte markers, such as *fabp7a* and *cx43*, were also highly upregulated in the cluster, but did not meet the parameters of marker selection. The 5 most enriched pathways in the astroglial cluster by Metascape enrichment analysis, regardless of treatment type (DMSO vs. DEPe) were eukaryotic translation elongation, brain development, cell projection morphogenesis, developmental growth, and response to growth factor (Fig. 8B). These enriched biological processes are logical to describe the processes astroglial cells in the zebrafish embryo are involved in, as they have been observed to be involved in neural development (Jurisch-Yaksi et al., 2020), have cellular processes, and respond to growth factors in response to injuries (Lyons & Talbot, 2014).

With DEPe treatment, there were 43 identified DEG in the astroglial cluster (Table 3, Fig. 8C). In a similar fashion to the microglial DEG, the astroglial DEG represented a very complex and heterogeneous response to DEPe exposure. *Col10a1a* was a highly upregulated gene (1.71-fold), and it has been observed to be elevated after brain injury and is a known astrocytic activator (Neo & Tang, 2017). In addition, *igfbp1a* was also highly upregulated (1.35-fold), and its overexpression in astrocytes has been observed to impair brain development and reduce glial cell proliferation in response to injury (Ni, Rajkumar, Nagy, & Murphy, 1997).

Although the astroglial cells as a whole cannot be characterized from just these two changes, the changes themselves parallel what has been observed in activated astroglia responding to injury. Interestingly, *fabp7b*, which when upregulated has been observed to promote a pro-inflammatory response in astrocytes harmful for motor neuron survival (Killoy, Harlan, Pehar, & Vargas, 2020) was a significantly downregulated (0.69-fold) DEG with DEPe exposure. In addition, we observed a significant upregulation (1.39-fold) of *hpgd*, a gene that has been established to be lowered in expression in astrocytes treated with LPS (Madeddu et al., 2015). These changes suggest that not all gene expression changes with DEPe exposure reflect previously seen changes in astroglia that have been characterized as activated, and that a complex response necessitating subcluster-level interpretation is occurring.

Table 3. Genes that are differentially expressed in astroglial cells with DEPe exposure.

	Fold Change		**Fold Change**
gh1	4.50204708	**sncga**	0.735563579
BX908782.2	2.599339567	**prss59.2**	0.73396921
rho	2.128039429	**prss59.1**	0.725296821
col10a1a	1.71809239	**ela3l**	0.719098309
si:ch211-133n4.6	1.703578434	**atp1a1b**	0.714574585
apoeb	1.488017504	**slc6a1b**	0.713426329
si:ch73-335l21.4	1.452278351	**prss1**	0.709208868

and2	1.395610983	**si:dkey-183j2.10**	0.705624043
hpgd	1.38786806	**slc3a2a**	0.705433127
igfbp1a	1.348486969	**slc7a10b**	0.696050057
sst1.1	1.330654731	**fabp7b**	0.694348419
pnocb	1.327086317	**urp2**	0.68897906
foxj1a	1.324569631	**apoda.2**	0.687316908
pde6ha	1.320080606	**prss35**	0.687249623
icn	1.304306132	**slc6a11b**	0.677916266
rlbp1a	1.296437477	**sept8b**	0.673571585
serpina1	0.775775116	**ela2l**	0.669694862
cyt1l	0.77576635	**mbpa**	0.669310568
aldocb	0.774160703	**cpa5**	0.658313051
gpd1b	0.76518863	**ela2**	0.631246022
zgc:112160	0.763038493	**efhd1**	0.606719199
cd81b	0.739742372		

Table 3: Differentially expressed genes in the astroglial cells with DEPe exposure.

Figure 8: Astroglial cluster marker expression data, GSEA and DGE analysis results

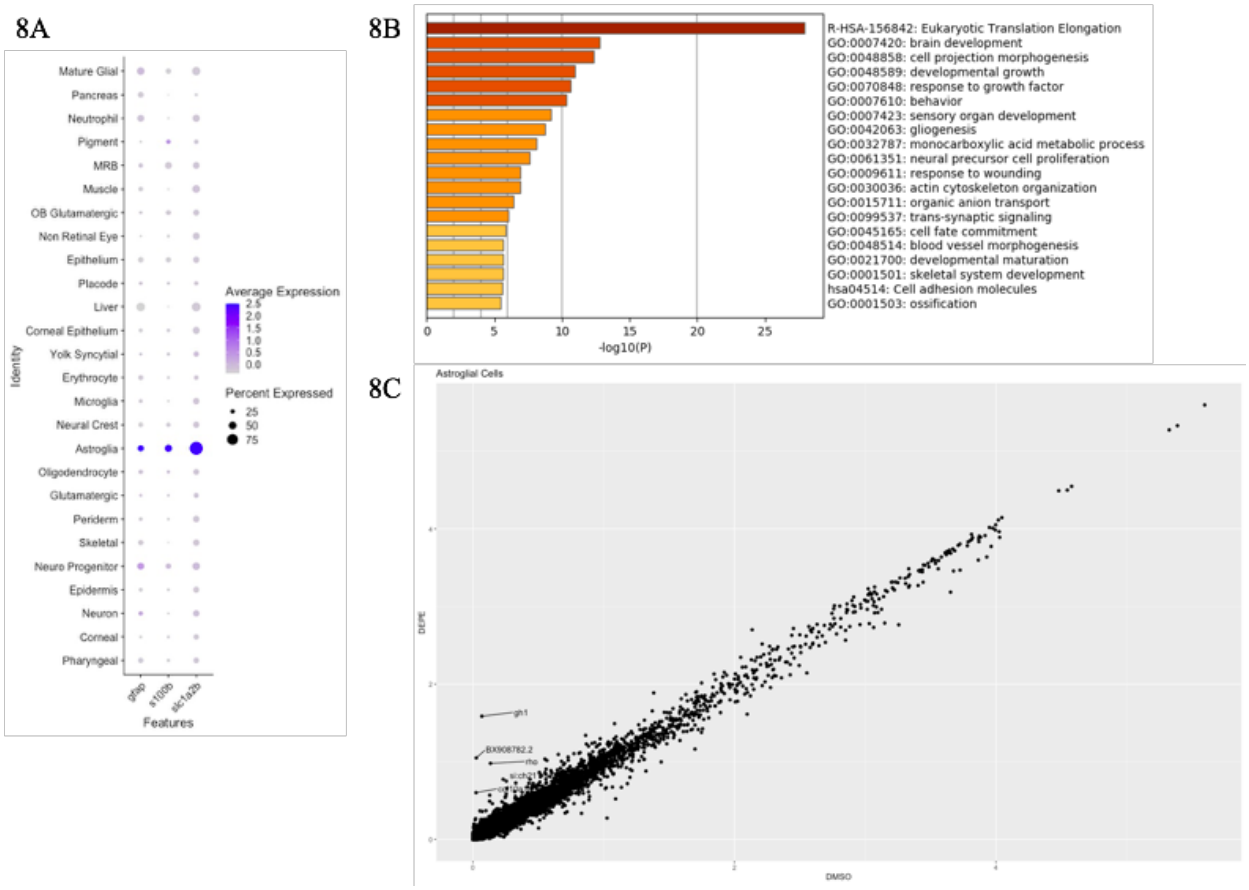

Figure 8: Astroglia were identified with highly upregulated marker genes, gene set enrichment analysis revealed most enriched biological processes, and differentially expressed genes were identified. 7A: The astroglial markers gfap, s100b, and slc1a2b were highly and uniquely expressed in the astroglial cells compared to other cell clusters. 7B: Gene set enrichment analysis gives us an overall look at the most enriched biological processes given the gene expression data from the astroglial cluster. The top enriched biological processes, such as brain development, cell projection morphogenesis, developmental growth, gliogenesis, and monocarboxylic acid metabolis process are known functions of astroglia. 7C: Scatter plot featuring and labeling some of the most differentially expressed genes in astroglia that exhibit a dramatic response to DEPe exposure.

Microglial IPA Comparison Analysis

After filtering all canonical pathways represented by the IPA analysis for those that have a Z-score > 2 (defined in Methods) and $p < 0.05$ in either DMSO or DEPe condition, the pathways were visualized side-by-side using IPA Comparison Analysis. This analysis provided us with direct insight into the pathways that were most changed with DEPe exposure in the two cell types of interest. Selected pathways that exhibited the greatest changes were interpreted (Fig. 9A, 9B).

In microglia, Integrin Signaling was more active with DEPe exposure. Integrins are the major adhesion molecule of the cell, and are involved in cell-to-cell and cell-to-ECM interactions, cell migration, phagocytosis, cytoskeleton reorganization, and proliferation (Kim et al., 2014). The integrins of platelets and leukocytes have been the best characterized, but integrin is present in many cell types. Interestingly, integrins may have important roles in neurodegenerative diseases through interactions with various disease-linked proteins. For example, amyloid beta and α-syn have been observed to interact with integrins (Kim et al., 2014) and have led to microglial activation and neuronal cell death. Familial PD-linked mutant and wild-type α-syn induced αM-integrin activation via NADPH oxidase has been observed in microglia. Pro-inflammatory cytokines TNF and IFN promote microglial activation, and have been shown to increase expression of various integrins (Milner & Campbell, 2003). The activation of Integrin Signaling indicates that DEPe exposure may increase integrin signaling in microglia, leading to changes in microglial cytoskeleton structure, proliferation, migration, and its overall activation state. Interestingly, this supports the observations made in Chapter 1 and 2, where DEPe exposure has been observed to activate microglia structurally and functionally. In addition, in microglia, Paxillin Signaling was active with DEPe exposure. With DMSO, Paxillin

Signaling was not conclusively active or inhibited according to this analysis. Integrins have been observed to promote the activation of paxillins (Gitik, Kleinhaus, Hadas, Reichert, & Rotshenker, 2014), which aligns with the finding above regarding Integrin Signaling. Paxillin is a multi-domain adaptor protein that is found at the interface between the plasma membrane and the actin cytoskeleton in many cell types, including microglia (Gitik et al., 2014). Adhesion and growth factor-related signals are integrated and processed with the help of paxillin (L. M. Stuart et al., 2007). When paxillin protein expression is increased due to stimulation by molecules such as TGF-B1, malignant cell attachment and spreading is enhanced (Han et al., 2001). Paxillin is involved in a signaling cascade that promotes microglial activation and recruitment to proteins, such as β-amyloid deposits in the brain (L. M. Stuart et al., 2007). The activation of microglial Paxillin Signaling Pathway suggests that DEPe exposure may increase paxillin signaling, leading to disease associated microglial cell attachment, spreading, and adhesion compared to DMSO. Also, the Fcγ Receptor-Mediated Phagocytosis in Macrophages and Monocytes Pathway was more active with DEPe exposure in the microglial cluster compared to DMSO exposure. Fcγ receptor binding initiates a signaling cascade which leads to expression of several lysosomal genes, including those involved in acidification, which we have observed in microglial cells with DEPe exposure (Gray et al., 2016). Furthermore, in a LPS-induced systemic inflammation model in mice, expression levels of multiple FcγR on microglia were increased in expression not just in the ME7 prion mouse model but also after LPS application (Lunnon et al., 2011). This adds to the evidence that microglia are activated with DEPe exposure. Finally, the Tec Kinase Signaling Pathway was more active with DEPe exposure compared to DMSO. Most Tec Kinases are expressed in hematopoietic cells and modulate their responses to external stimuli. Their expression in microglia is logical, because not only do zebrafish microglia directly develop from

a hematopoietic origin, the rostral blood island (RBI) (Wu et al., 2020), mammalian microglia are known to originate from hematopoietic sites during embryogenesis as well (Ginhoux, Lim, Hoeffel, Low, & Huber, 2013). Burton's Tyrosine Kinase (BTK), a Tec Kinase, is found in cells that have a hematopoietic lineage with the exception of plasma and T-cells, and is indeed found in microglia. It is a regulator of microglial phagocytosis, and siRNA-induced inhibition of BTK has been observed to not only decrease phagocytosis, but also decrease the expression of an Alzheimer's Disease risk factor gene, phospholipase gamma 2 (Keaney, Gasser, Gillet, Scholz, & Kadiu, 2019). In addition, levels of microglial BTK have been observed to be elevated in a 5xFAD mouse model of AD, and post-mortem AD patient brains have exhibited upregulated levels of BTK transcripts (Keaney et al., 2019). Tec is another Tec Kinase expressed and well-studied in microglia. Both BTK and Tec have been observed to accumulate at the base of phagocytic cups, and their inhibition through a pharmacological inhibitor or siRNA has been linked to inhibition of Fcγ Receptor induced phagocytosis (Jongstra-Bilen et al., 2008).

The activation of the Integrin Signaling Pathway, Paxillin Signaling Pathway, Fcγ Receptor Mediated Phagocytosis in Macrophages and Monocytes Pathway, and the Tec Kinase Signaling Pathways all reliably indicate that DEPe treated microglia upregulate pathways that are related to microglial activation, both at the structural and functional level, including aspects of microglial activation such as migration, structural changes, phagocytosis and lysosome production. Therefore, the results from the microglial IPA Comparison Analysis most certainly indicate major aspects of microglial activation are upregulated with DEPe exposure, and this also supports the *in vivo* results from Chapter 1. It is important to keep in mind that the microglia may appear activated and upregulate many pathways that are directly involved in activation, but they most likely still exist in various states that may be elucidated by further studies related to

structure, function, and more specific gene expression, such as subcluster analysis and trajectory inference/pseudotemporal ordering.

Astroglial IPA Comparison Analysis

Astroglial Xenobiotic CAR and PXR signaling pathways were less active with DEPe exposure. The constitutive active/androstane receptor (CAR) and pregnane X receptor (PXR) signaling pathways are two important members of the NR1I nuclear receptor family, and detect endogenous chemicals and toxic byproducts (Timsit & Negishi, 2007). They are involved in the induction of Phase I and II enzymes, such as CYP3A and CYP2B. PXR alone has been shown to be a mediator of the xenobiotic regulation of CYP3A (Timsit & Negishi, 2007). Interestingly, zebrafish do not have the CAR, as the gene for CAR diverged from PXR over the course of vertebrate evolution, and only has PXR, so for the purposes of this project, we focused on interpreting results related to PXR alone. PXR agonists that were originally established in cell-based studies have been shown to induce CYP2A and CYP3A in zebrafish (Kubota et al., 2015). The decrease in activation of the PXR Signaling Pathway suggests that DEPe exposure may decrease the xenobiotic regulation of CYP3A and other Phase I and II metabolic enzyme processes taking place in astroglia of the zebrafish via PXR. The astroglial Xenobiotic Metabolism AHR Signaling Pathway was less active with DEPe exposure as well. The aryl hydrocarbon receptor (AHR) detects xenobiotic chemicals, such as aryl hydrocarbons, and regulates gene expression of CYPs, such as CYP1 (Larigot, Juricek, Dairou, & Coumoul, 2018). AHR has been shown to mediate the anti-inflammatory effects of Type I IFNs. IFN-1 produced in the CNS, and other metabolites from the gut, have been shown to activate AHR in astrocytes, leading to suppression of CNS inflammation. In addition, AHR has been shown to suppress pro-

inflammatory cytokines in astrocytes, as a response to activated microglia transferring signals through the AHR of astrocytes to ultimately inhibit CNS inflammation (Rothhammer et al., 2016). This function has been demonstrated through knockdown of AHR in astrocytes, which exacerbated an EAE model, and increased astrocytic expression of pro-inflammatory cytokines (Bray, 2016). Also, in zebrafish, AHR has been shown to be responsible for dioxin and non-ortho-polychlorinated biphenyl induction of CYP1 family target genes (Kubota et al., 2015). Therefore, a conserved function seems to exist between mammals and zebrafish for the core function of AHR. The decrease in activation of AHR Signaling Pathway suggests that DEPe exposure may decrease the response to xenobiotic chemicals and therefore lead to decreased CYP expression. Also, the ability of AHR to mediate anti-inflammatory effects of type I IFNs, and to respond to activated microglia to inhibit CNS inflammation, may be diminished with DEPe exposure compared to DMSO. In addition, astroglial Paxillin Signaling was active with DEPe exposure. With DMSO, Paxillin Signaling was not conclusively active or inhibited according to this particular IPA analysis. Paxillin has been shown to promote adhesion and rapid spreading of malignant astrocytoma cells to some ligands (Han et al., 2001). In brain lesions, actin-anchoring paxillin has been observed in the astroglia of brain tracts (Kalman & Szabo, 2001). The activation of astroglial Paxillin Signaling Pathway suggests that DEPe exposure may increase paxillin signaling, leading to abnormal astroglial cell attachment, spreading, and adhesion compared to DMSO. Finally, the Adrenomedullin Signaling Pathway was more active with DEPe exposure compared to DMSO. Adrenomedullin itself is a vasodilator peptide hormone present in almost all tissue in mammals, and in zebrafish, its expression patterns have been described at a basic level, such as being observed in 5dpf larval and adult heads. Adrenomedullin is known to act by forming complexes with calcitonin receptor-like receptor and

receptor activity modifying proteins, RAMPs. These RAMPS then allow the calcitonin receptor-like receptor to move to the cell surface and interact with GPCRs (Dackor, Fritz-Six, Smithies, & Caron, 2007). Interestingly, the extracellular presence of inflammatory cytokines, such as TNFa and IL-1B, has been shown in human astrocyte culture to increase the release of adrenomedullin from the astrocytes, in addition to neurons (Takahashi et al., 2000). In addition, interferon-gamma treatment of mouse astrocytes has also been shown to induce their release of adrenomedullin (Kuchinke, Hart, & Jonakait, 1995). Interferon gamma is the only Type II interferon and has been observed to increase lysosome production and antigen presentation activity of macrophages, among other important effects (Hastings & Cresswell, 2011).

These astroglial IPA Comparison Analysis results indicate that pathways less active with DEPe exposure, such as the PXR and AHR signaling pathways, indicate possibly decreased xenobiotic regulation of CYP3A and other Phase I and II metabolic enzyme processes taking place in astroglia and decreased response to xenobiotic chemicals. The increased activity of the Paxillin Signaling Pathway indicates that abnormal astroglial structural and spreading behavior may be associated with DEPe exposure. Finally, increased activation of the Adrenomedullin Signaling Pathway indicates the possible presence of inflammatory cytokines and an activated immune system. Astroglia are a very diverse population of cells that are in various states at any given time. In addition, the information we have on these astrocytes is strictly limited to their gene expression data and associated pathways. Therefore, it is important to continue to study these cells' structure, functions, and interactions *in vivo* to relate them back to these pathway-based characterizations.

Figure 9: IPA Comparison Analysis Results

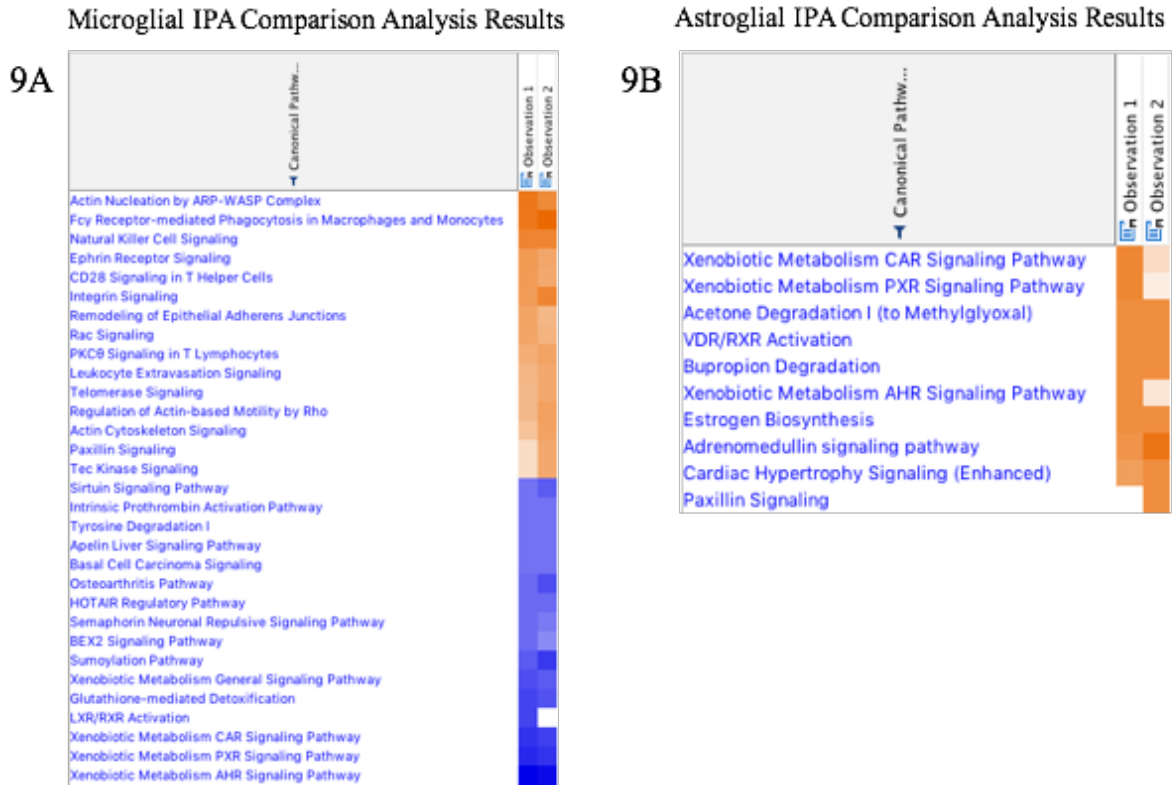

Figure 9: IPA Comparison Analysis was run for the pathways generated from the genes that fit the initial IPA analysis cutoff values. Observation 1 = DMSO, Observation 2 = DEPe. The pathways included in this particular analysis had a Z-score magnitude > 2 (defined in Methods) in at least one of the two Observations and all had $p < 0.05$, with Z-score being the statistical measure of the match between the expected activation state of the pathway in the IPA database and the observed gene expressions of the components of the pathway. Orange means the pathway is being activated, blue means that the pathway is being inhibited, white means conflicting information between activation and inhibition. The pathways that had the greatest visual differences in activation were selected for further interpretation. 9A: Results from microglial IPA Comparison Analysis. Selected pathways for further interpretation were "FCgamma Receptor-mediated Phagocytosis in Macrophages and Monocytes", "Integrin Signaling", "Paxillin Signaling", and "Tec Kinase Signaling". 9B: Results from astroglial IPA Comparison Analysis. Selected pathways for further interpretation were "Xenobiotic Metabolism CAR Signaling Pathway", "Xenobiotic Metabolism PXR Signaling Pathway", "Xenobiotic Metabolism AHR Signaling Pathway", "Adrenomedullin Signaling Pathway", and "Paxillin Signaling".

Subcluster Analysis

We then performed subcluster analysis to further characterize the microglial and astroglial cells, and to begin to identify possible states that these cells may exist in through identification of unique gene expression profiles associated with previously studied states such as disease, activation, and homeostasis. We subclustered the cells using a similar set of commands as the initial clustering technique. We tested multiple values of "resolution", which resulted in 0.5 as the resolution that we believed was most representative of differences in gene expression across subclusters and leading to results that appeared most biologically relevant.

Microglial Subcluster Analysis

Microglial subcluster analysis resulted in the identification of 10 subclusters (Fig. 10A, Table 4). Out of the 10 subclusters, 6 had a large enough number of cells within the subcluster (n > 50) to begin to be characterized. Each subcluster's most differentially expressed genes, compared to the expression of those genes in all other subclusters, were interpreted by referring to instances of its up- or down-regulation in the literature and under what conditions, to begin to characterize the subcluster.

Microglial Subcluster 0 was the largest, and consisted of a comparable number of DMSO and DEPe treated microglia (181 vs. 141, respectively, Fig. 10B). The cells in this subcluster most highly expressed macrophage and immune related genes, such as *lygl1, mfap4,* and *ctsl.1*, as well as myeloid transcription factor genes such as *irf8* and *spi1a*, which altogether confirm their identity as microglia with a myeloid origin (Raj et al., 2018). Also, microglial homeostatic genes were highly expressed, such as *ctss2.2* (Sousa et al., 2018), *c1qa*, and *c1qb* (Walker, 2020). Interestingly, we also observed the high expression of *ccl34b.1*, a marker of phagocytic

microglia in zebrafish (Wu et al., 2020) along with *il1b* (Walker et al., 2006)*, cd63, ctsz (Walker, 2020), s100a10b* (DePaula-Silva et al., 2019), and *lgals2a* (Grubman et al., 2021), (Raj et al., 2018), genes that have been observed to be upregulated in disease-associated and activated microglia. This evidence altogether suggests that the microglia in this subcluster, regardless of treatment type, are in some state of activation, responding to outside stimuli. The cells in Subcluster 1 were a majority DEPe treated (71 vs. 244), and generally appeared to be activated as well. Some of the human orthologs of the top upregulated marker genes observed in the microglia of Subcluster 1 have been observed in activated microglia, such as *ccl20a.*3 (Walker et al., 2006), *hsp70.3*, and *hsp70.2* (Fagone et al., 2012). In addition, the human orthologs of *ccl38a.5* (Banisor, Leist, & Kalman, 2005)*, ccr9a* (Li et al., 2006), and *calm1b* (Sousa et al., 2018) have been upregulated in neurotoxic, activated microglia induced by LPS exposure, and generally contribute to neuroinflammation. Subcluster 2 contained a majority DEPe treated microglia as well (46 vs. 258), but these cells downregulated many disease-associated and activation-associated microglial genes, such as *lgals2a* (Grubman et al., 2021)*, cebpa* (H. C. Pan et al., 2013), *cebpb* (Arneson et al., 2018), *cd63* (Walker, 2020), and although not significantly, *apoeb* (Walker, 2020). In addition, a major phagocytic microglia marker in zebrafish, *ccl34b.*1 (Wu et al., 2020) was downregulated as well. These expression patterns suggest these microglia may be suppressing traditionally observed disease-related processes and greatly contrast from Subcluster 0. Subcluster 3 consisted of a majority DMSO-treated microglial cells (196 vs. 50). Many ribosomal structure-related genes, such as *rpl3, rplp0, rpl7, rpl18a, rpl10, rpl10a, rpl11*, and *rpl12* were highly expressed in the cells of this subcuster, suggesting that these microglia are activated in a similar way to LPS activation, which has been shown to upregulate these ribosomal genes (Y. Yang et al., 2018). *Myca,* observed in human microglia as an oncogene that

regulates cell proliferation upregulated with LPS exposure, was also highly expressed (Pulido-Salgado, Vidal-Taboada, Barriga, Sola, & Saura, 2018). *Rack1*, which has been seen in microglial cell culture to play a protective role against LPS induced inflammation, was highly expressed as well (Yin, Song, & Pan, 2017). Other genes that have been observed to be upregulated in microglia with varying types of stress (ischemia, alcohol, mild chronic stress) are also highly expressed in this subcluster, such as *ahcy* (McDonough et al., 2020)*, arhgdig* (Musaelyan et al., 2020)*, cirbpb* (Rajayer et al., 2013), and *tcp1* (Parakalan et al., 2012). Interestingly, although *tcp1*, a gene enriched in amoeboid microglia was highly upregulated in this subcluster, *ccl34b.1,* a marker for phagocytic microglia in zebrafish (Wu et al., 2020) was significantly downregulated in this subcluster. In addition, *c1qb* (Walker, 2020) and *lgals3bpb* (Rangaraju et al., 2018), (Mathys et al., 2017)commonly observed disease-related genes, were downregulated in this subcluster. This suggests that this subcluster may consist of a state of microglia that responsive to stress similar to LPS exposure, but not necessarily phagocytic or have been established as directly responsive to models of neurodegenerative disease. Subcluster 4 contained only DMSO-treated microglial cells, and the most upregulated gene in this subcluster was *blf,* which is expressed in zebrafish blood precursor cells (Raj et al., 2018). *Rpl39*, another highly upregulated gene in this subcluster, is also expressed in progenitor-like cells (Raj et al., 2018). Interestingly, markers such as *lgals2a* (Grubman et al., 2021) and *cd63* (Walker, 2020) upregulated in disease-associated microglia, were significantly downregulated in this subcluster. In addition, *spi1b (pu1)* was significantly downregulated as well, and downregulation of *spi1b* has been shown to be protective (Pimenova et al., 2021), (Rustenhoven et al., 2018), and reduces the microglial inflammatory and phagocytic response. These expression patterns suggest that the microglial cells in this subcluster, which were all DMSO-treated, are progenitor-like and

aligns with previously described protective behavior. Subcluster 5 consisted of a majority DMSO-treated cells as well (60 vs. 2). These cells exhibited a high expression of *shha, shhb*, and *ntrk2a,* suggesting these microglia are reactive in a protective manner, as the SHH pathway has been observed in mammalian microglia to be activated in reactive glia and drives proliferation in response to neurodegeneration-induced lesions (Pitter et al., 2014), and microglial upregulation of *ntrk2* in mammalian cerebellar cell cultures has been observed to be neuroprotective (Mitrasinovic et al., 2005).

Subcluster 6, 7, 8, and 9 did not consist of enough cells ($n < 50$ for the subclusters) to interpret conclusively. However, they did cluster in interesting ways with expression patterns that may be worth further investigation. For example, Subcluster 6 had a significantly high level of expression of many genes characteristic of disease associated microglia, such as *apoeb* (Walker, 2020), *g0s2* (Walker et al., 2006)*, lgals2a* (Grubman et al., 2021)*, ctsz, cd63, ctsa,* and *cd9b* (Walker, 2020). In addition, an established phagocytic zebrafish microglial marker, *ccl34b.1*, was also highly expressed (Wu et al., 2020). Subcluster 7 highly and uniquely expressing anti-inflammatory cytokines *il4* and *il13*. *Rrbp1b* was also highly expressed, which is a gene significantly upregulated in homeostatic microglia compared to Activated Responsive Microglia (Sierksma et al., 2020). In Subcluster 8, *grn2* was the most highly upregulated gene, and it was also the #1 DEG in our microglial DEG analysis with DEPe exposure. Although the number of cells in this subcluster were much lower than 50, a majority of cells in this subcluster were DEPe treated. In healthy microglia, progranulin is expressed at high levels, and patients with a genetic form of Frontotemporal Dementia (FTD) exhibit granulin haploinsufficiency (Telpoukhovskaia et al., 2020). This haploinsufficiency leads to reduced levels of progranulin and dysregulation in inflammation and lysosomal function. These dysfunctions have been

recapitulated in *grn-/-* mouse microglia. In addition, genes that have been observed to be upregulated in Stage 2 Disease Associated Microglia (DAM), *cd9b* and *cd63* (Walker, 2020) were also highly upregulated in this subcluster's DEPe treated microglial cells. These Stage 2 DAM have been observed to be an altered phenotype, different from pro-inflammatory activation (Stage 1 DAM), that restricts neurodegenerative changes. This suggests that the microglia in this subcluster may be exhibiting a phenotype that is protective to surrounding cells, such as neurons. Finally, Subcluster 9 appeared to be neutrophil-like, due to the high expression of embryonic zebrafish neutrophil markers, such as *npsn, lyz, mmp13a*, and *mpx* (Raj et al., 2018). This suggests that these microglia may be in a less mature state than other microglia in other subclusters, as neutrophils and microglia originate from a common myeloid progenitor. It is also possible that these cells may be contamination of other cell types that were not fully resolved by the clustering technique used in this experiment, and ended up ultimately being clustered in this small subcluster.

Table 4: Microglial Subcluster Data

Subcluster	DMSO	DEPE	Selected marker genes	Characterization
0	181	141	Up: lygl1, mfap4, ctsl.1, ccl34a.4, mhc2a, ctss2.2, irf8, spi1a, c1qa, ccl34b.1	Homeostatic
1	71	244	Up: ccl20a.3, ccl38a.5, ccl36.1, ccr9a, hsp70.3, hsp70.2, ccl34b.1	Activated

2	46	258	Up: tmsb4x, rac2, cebpb Down: lgals2a, cebpa, cebpb, cd63	Protective
3	196	50	Up: myca, ahcy, rps3a, cirbpb, rpl3, rplp0, tcp1, rack1, hsp90ab1, rpl7, rpl18a, rpl10, rpl11, rpl10a, rpl12	Stressed, not phagocytic
4	87	0	Up: blf, fthl1a, prdx2	Progenitor-like
5	60	2	Up: shha, shhb, cfd, vax1	Reactive
6	17	31	Up: apoeb, ccl34b.1, lgals2a, g0s2, ctsz, cd63, ctsa	-
7	8	17	Up: il4, il17, gata2a	-
8	3	20	Up: grn2, cd9b, cd63	-
9	6	17	Up: npsn, lyz, mmp13a, mpx	-

Figure 10: Microglial subclusters and composition of each subcluster by treatment type

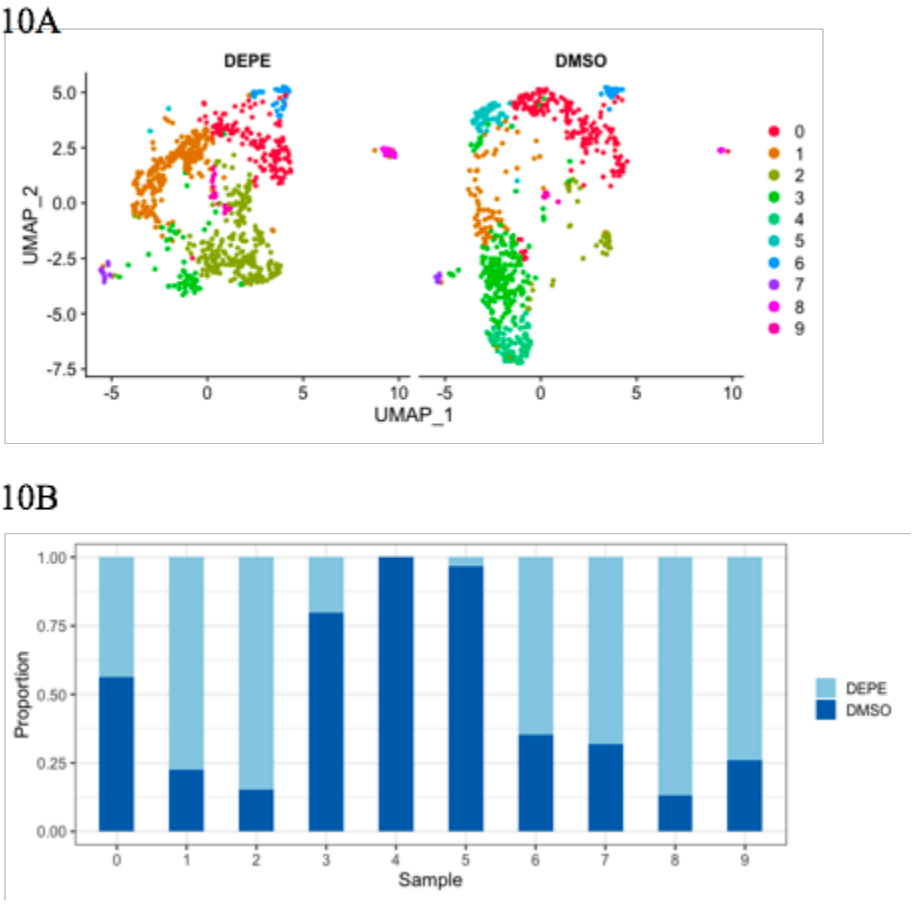

Figure 10: All microglial cells from the integrated scRNA-seq analysis were subsetted and subclustered with a resolution = 0.5. A total of 10 subclusters were identified. The proportion of each subcluster that were DMSO and DEPe treated cells were graphed. 10A: Subclustered microglia were graphed in a UMAP plot with the two treatment types side by side for comparison, although clustering was performed with integrated data. 10B: Bar graph showing the proportion of each subcluster that is made up of DMSO and DEPe treated cells.

Astroglial Subcluster Analysis

Astroglial subcluster analysis resulted in the identification of 12 subclusters (Fig. 11A). These subclusters represent possible states of astroglia that exist in this experiment. Out of the 12 subclusters, 6 had a large enough number of cells within the subcluster (n > 50) to be conclusively characterized. Each subcluster's most differentially expressed genes, compared to

the expression of those genes in all other subclusters, were interpreted to characterize the subcluster (Table 5).

Subcluster 0 was the largest identified subcluster, with around 75% DEPe treated cells compared to DMSO (152 vs. 349). Markers of activated astrocytes, such as*, ptgdsb.1, ptgdsb.2* (D. J. Choi, An, Jou, Park, & Joe, 2019), *eno1b* (You et al., 2020) and *robo4* (Park, Pak, Riew, Shin, & Lee, 2016) were significantly downregulated in this subcluster. Clearly, a large proportion of the DEPe treated astroglial cells in our experiment responded in a manner that is opposite of the behavior that has been traditionally observed in activated astrocytes. This suggests that the astroglia may be suppressing classical activation-related genes and pathways. Subcluster 1 consisted of around the same number of DMSO and DEPe-treated astroglial cells (206 vs. 169). Many of the most highly expressed genes in the cells of this subcluster are upregulated in activated astrocytes and in astrogliosis, such as *aqp1a.1* (McCoy & Sontheimer, 2010)*, ptgdsb.1, ptgdsb.2* (D. J. Choi et al., 2019), *mfge8a* (Cheyuo, Aziz, & Wang, 2019), (X. Xu et al., 2018)*, robo4* (Park et al., 2016)*, cxcl14* (Fang, Han, Hong, Tan, & Tian, 2012)*, cspg5b* (Anderson et al., 2016), and *eno1b* (You et al., 2020). Subcluster 2 had slightly more DEPe-treated astroglia than DMSO-treated (149 vs. 198), but the numbers were comparable. Many highly upregulated genes in this subcluster have been observed as DEG in astrocytes related to neurodegenerative disease, such as *cx43* (Kajiwara et al., 2018)*, glula* (Preman, Alfonso-Triguero, Alberdi, Verkhratsky, & Arranz, 2021) and *mt2* (Michael et al., 2011), (Cesani et al., 2014). In addition, other markers of general astrocyte activation, such as *slc1a2b* (Al-Dalahmah et al., 2020)*, robo4* (Park et al., 2016)*, cspg5b* (Anderson et al., 2016)*, eno1b* (You et al., 2020)*, aqp1a.1* (McCoy & Sontheimer, 2010)*, cxcl14* (Fang et al., 2012)*, cspg5a* (Anderson et al., 2016), and *srgn* (Zamanian et al., 2012) were also significantly upregulated in the cells in this

subcluster, regardless of treatment type. This suggests that the astroglial cells subclustered here may be activated in some way. In Subcluster 3, there was a vast majority of DMSO treated astroglial cells compared to those treated with DEPe (211 vs. 24). Many informative genes were heavily downregulated in the DMSO-treated astroglial cells, such as *fkbp5, srgn* (Zamanian et al., 2012) and *cxcl14* (Fang et al., 2012) which have been observed in mammals to be upregulated in LPS-activated astrocytes. In addition, *mt2* (Michael et al., 2011), (Cesani et al., 2014), *robo4* (Park et al., 2016) and *cx43* (Kajiwara et al., 2018) were significantly downregulated in the DMSO treated cells as well, and this also appears to be protective, as these genes are heavily upregulated in reactive, disease-associated astrocytes. In Subcluster 4, there was a vast majority of DEPe-treated astroglial cells (25 vs. 205). Interestingly, one of the top upregulated genes in this subcluster was *ckmb* (Kuiper et al., 2009) which enhances astrocytic migration and spreading. In addition, *nme2b.2* (Romani, Ignesti, Gargiulo, Hsu, & Cavaliere, 2018) was also highly expressed, and expression of this gene has been observed in mammalian mixed cultures of glia and neurons, and only in physiologically unhealthy conditions. The expression of these genes suggests that the cells in this subcluster are indeed disturbed by and responding to DEPe exposure. However, there were some significantly downregulated genes in the DEPe treated cells of this subcluster that have been associated with disease and reactive astrocytes, such as *midn* (J. Pan, Ma, Yu, Zhang, & Wan, 2020) and *mt2* (Michael et al., 2011), (Cesani et al., 2014). This suggests that these astroglia exist in a state that may be distinct from the previously described, possibly activated astrocytes. In Subcluster 5, there were slightly more DEPe-treated astroglial cells than those treated with DMSO (45 vs. 73). Interestingly, the top most expressed gene was *ifitm1*, which has been observed to be highly expressed in LPS-induced reactive astrocytes (Zamanian et al., 2012), suggesting that these astrocytes may be in a similar

state. *Col1a2*, expressed in astrocytes in response to spinal cord injury (Hara et al., 2017) was also highly expressed. In addition, genes whose upregulation in the brain that have been consistently linked to AD, such as *ms4a17a.11, ms4a17a.9, ms4a17a.7,* and *pmp22a* were highly expressed in this subcluster (Naj et al., 2011), (Seshadri et al., 2010) This suggests that these astroglia, regardless of treatment type, may be in a reactive and disease-relevant state. Subcluster 6 had a majority DEPe-treated astroglial cells (12 vs. 97), and interestingly, the top most expressed gene in both conditions was *prdx1*, which has been observed to be upregulated in samples from various neurodegenerative disease brain tissues (AD, HD and PD) and rodent cell cultures that model neurodegenerative disease (AD, PD) (Szeliga, 2020). It has been suggested that the upregulation of *prdx1* is protective, as it produces an antioxidant protein, and modulates oxidative stress and pathways that are involved in neuroprotection. In addition, markers of disease and astrocyte reactivity, such as *ptgdsb.1* (D. J. Choi et al., 2019)*, apoda.2* (Bhatia, Kim, Shepherd, & Halliday, 2019) and *eno1b* (You et al., 2020) were significantly downregulated in the DEPe-treated astroglia of this cluster. These expression patterns indicate that these astroglial cells may be responding in a protective manner against DEPe exposure.

Subclusters 7-12 did not have a high enough number of cells ($n < 50$) to interpret conclusively. However, they did cluster in interesting ways with expression patterns that may be worth further investigation. For example, in Subcluster 7, both DMSO and DEPe-treated astroglia highly and uniquely expressed *clu* (F. Chen et al., 2021) an astrocyte-derived synaptogenic and anti-amyloid factor, as well as *vim*, an astrocyte marker for reactive gliosis (Liu et al., 2014). In addition, *slc1a2b*, a marker of quiescent astrocytes (Al-Dalahmah et al., 2020), was the most downregulated gene in this subcluster in both treatment types. These expression patterns clearly indicate that these astroglia may be in a reactive, disease-relevant

state. Similarly Subcluster 8 and 9 exhibited high expression of *shha* and *shhb,* which have been observed to be upregulated in activated astrocytes, and is known to be neuroprotective (Allahyari, Clark, Shepard, & Garcia, 2019). In addition, the astroglial cells in Subcluster 9, regardless of DMSO or DEPe treatment type, highly and uniquely expressed *clu*, an astrocyte-derived synaptogenic and anti-amyloid factor (F. Chen et al., 2021). There were not enough cells in Subcluster 10 to identify marker genes given our protocol, as only 2 DMSO-treated cells clustered in that subcluster. Subcluster 11 astroglia highly and significantly upregulated *cd59* in both DMSO and DEPe treated cells. Deficits in *cd59* have been observed to increase the vulnerability of neurons to homologous complement attack (L. B. Yang, Li, Meri, Rogers, & Shen, 2000). In addition, *egr2b* was significantly upregulated, and the increased expression of this gene has been observed in activated glial cells including astrocytes in the inflamed brain cortex (Yan et al., 2013).

Table 5: Astroglial Subcluster Data

Subcluster	DMSO	DEPE	Selected marker genes	Characterization
0	152	349	Down: cd81a, ptgdsb.1, ptgdsb.2, eno1b, robo4, mfge8a	Neuroprotective
1	206	169	Up: aqp1a.1, ptgdsb.1, ptgdsb.2, mfge8a, cd81b, robo4, cxcl14, cspg5b, eno1b	Activated, astrogliosis-related

2	147	198	Up: cx43, glula, mt2, slc1a2b, robo4, cspg5b, eno1b, aqp1a.1, cxcl14, cd81a, cspg5a, srgn	Activated, disease model-associated
3	211	24	Down: fkbp5, srgn, cxcl14, mt2, robo4, cx43	Neuroprotective
4	25	205	Up: nme2b.2 Down: midn, mt2	Activated
5	45	73	Up: ifitm1, col1a2, ms4a17a.11, ms4a17a.9, ms4a17a.7, pmp22a	Activated, disease model-associated
6	12	97	Up: prdx1 Down: ptgdsb.1, apoda.2, and eno1b	Neuroprotective
7	17	29	Up: clu, vim Down: slc1a2b	-
8	19	17	Up: shha, shhb	-
9	10	19	Up: shha, shhb, clu	-
10	2	14	-	-
11	8	17	Up: cd59, egr2b	-

Figure 11: Astroglial subclusters and composition of each subcluster by treatment type

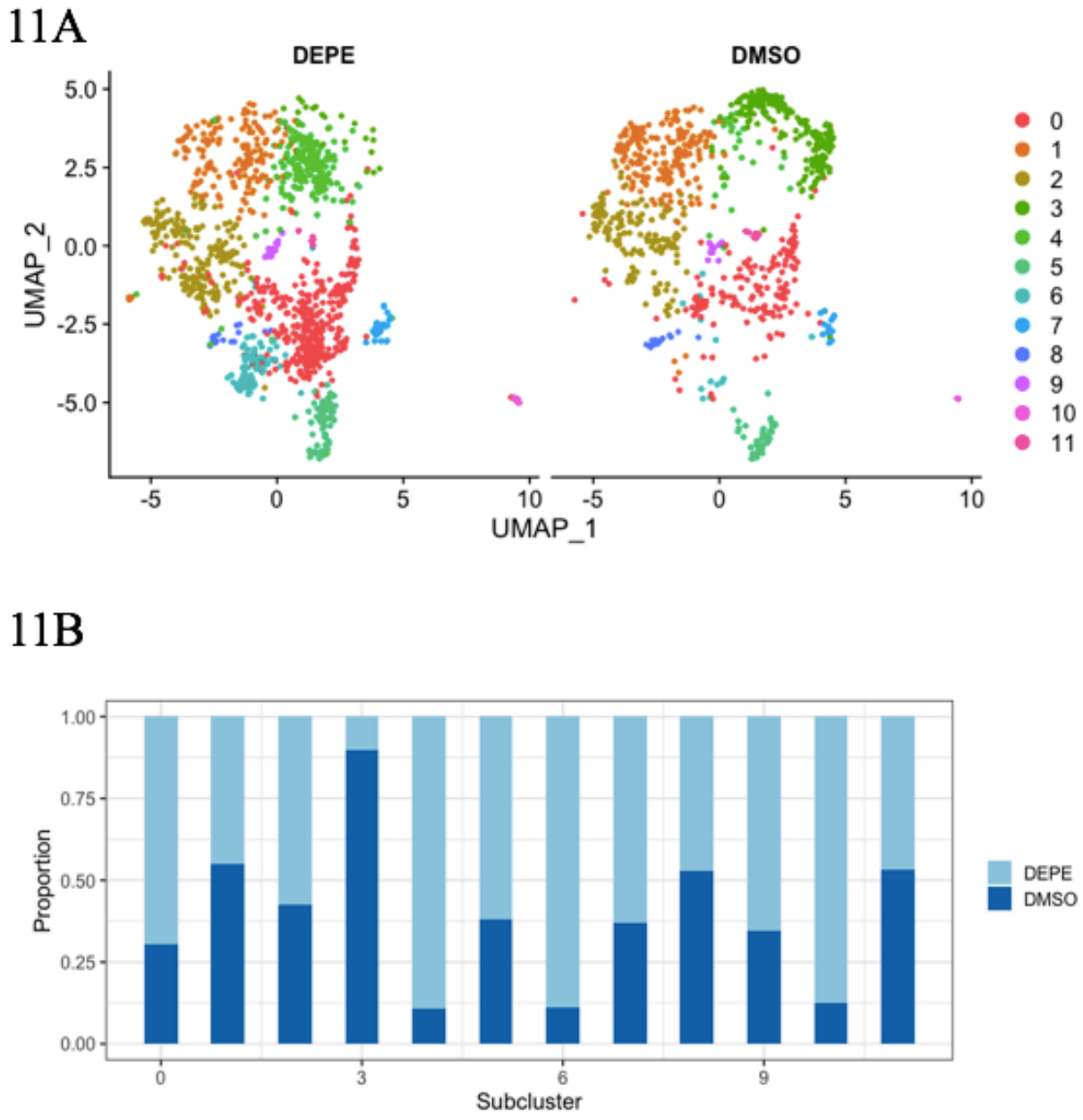

Figure 11: All astroglial cells from the integrated scRNA-seq analysis were subsetted and subclustered with a resolution = 0.5. A total of 12 subclusters were identified. The proportion of each subcluster that were DMSO and DEPe treated cells were graphed. 11A: Subclustered astroglia were graphed in a UMAP plot with the two treatment types side by side for comparison, although clustering was performed with integrated data. 11B: Bar graph showing the proportion of each subcluster that is made up of DMSO and DEPe treated cells.

RNAscope Fluorescent In-Situ Hybridization

RNAscope, an up-and-coming fluorescent in-situ hybridization method, has been validated in mammalian cell cultures and sections, with high potential to be a useful tool to fluorescently image and quantify expression levels of genes of interest directly in sample tissue. Its utility has not been very well-established in ZF larvae, and the current existing literature describing its use in ZF is very limited to younger larvae, around 2 to 3dpf (Gross-Thebing, Paksa, & Raz, 2014), (J. Chen, Poskanzer, Freeman, & Monk, 2020).

In order to validate the DGE results from the scRNA-seq work described above, we developed a 5dpf ZF RNAscope labeling protocol using RNAscope V2. The positive control genes that we selected were *eef1a1l1*, a transcriptional elongation factor that has been established to be expressed in almost all structures of the zebrafish embryo and larvae until at least 90dpf, and *actb1,* a structural constituent of actin cytoskeleton and also expressed in almost all structures of the zebrafish. The two genes labeled very reliably in both at the 3dpf and 5dpf (Fig. 12A) larvae after protocol optimization, regardless of the depth within the larvae that the imaging took place. This establishes for the first time that some very highly and ubiquitously expressed genes are likely to be effectively labeled with RNAscope in 3dpf and 5dpf ZF larvae, and may be a very reliable positive control of labeling efficacy and proper protocol execution.

We then moved on to labeling our cell types of interest, microglia and astroglia, by first selecting a marker gene to identify the cells. We aimed to fulfill the criteria described above in this chapter regarding cell cluster identification: (1) gene must be highly expressed in a large proportion (25% or more) of the cells in that cluster, (2) gene must be lowly expressed in other clusters, (3) Avg. fold change of gene > 1.5, (4) Adjusted p-value < 0.01. We selected *mpeg1.1* for the microglial cell label, because we wanted to be consistent in the label we used to study the

microglia as it has been used in the previous chapters, and *mpeg1.1* was very highly and uniquely expressed in the zebrafish embryo according to past work and our scRNA-seq results, with an average fold change of 1.64. Although only 14% of microglia sampled expressed *mpeg1.1*, which was lower than the 25% threshold of cells that we hoped would express the gene, it was only expressed in 0.03% of all other cells analyzed, which was just above the lowest percentage observed of any of the genes expressed in the microglia, 0.02%, and its p-value was 0, confirming the nature of its unique expression. We selected *s100b* for the astroglial cell label. Some genes, such as *s100b, gfap, her4.1* and *nestin,* are regularly used to label zebrafish radial glial cells or astroglia (Jurisch-Yaksi et al., 2020). However, *gfap*, which is what is most commonly used to label zebrafish radial glial or astroglial cell processes, does not label the cell nuclei as well as *s100b*, and is not suitable for counting (Marz, Schmidt, Rastegar, & Strahle, 2011). In addition, our scRNA-seq data revealed that 24% of all astroglia expressed *s100b* with an average fold change of 2.4 compared to all other cells' expression of the gene, and 0.07% of all other cells analyzed expressed s100b. On the other hand, only 19.8% of astroglia expressed *gfap* with an average fold change of 2.5 comparable to that of *s100b*, and 2.4% of all other cells analyzed expressed gfap, strengthening our reasoning to use s100b as the label for this cell type. For both the microglia and astroglia, there were many other much more highly expressed genes, both in terms of fold change in expression of that gene, as well as the percent of microglial or astroglial cells that express that gene. The information for these genes were used in the initial identification of the cell clusters, but for the purposes of this labeling technique where we wished to quantify the changes in expression of a differentially expressed gene in just the cell types of interest, we selected genes that we determined to be as uniquely expressed as possible in just the cell types of interest, and not just highly expressed in many cell types including our cell type of

interest. Both *mpeg1.1* and *s100b* labeling occurred in the 3dpf and 5dpf (Fig. 12B, 12C) ZF larvae, but the depth of the labeling influenced how many cells were labeled. The deeper labeling was consistently more permanent than the superficial labeling, which tended to be bleached more quickly by the subsequent labeling steps of the genes of interest, described below.

We selected and tested two genes of interest per cell type that were DEG with DEPe exposure for RNAscope labeling and quantification. They were all in the top 10 DEG with DEPe exposure for that cell type. The genes of interest that were labeled for microglia were grn2 and il13 (5.57- and 1.78-fold, respectively). These were selected because out of the top 10 DEG with DEPe exposure, they had a very drastic change in % of microglial cells expressing the gene before and after exposure (5.4% to 23.3% and 3.5% to 43%, respectively), which we believed would increase the likelihood that the change would be dramatic enough to be visible and quantifiable via RNAscope labeling. The genes of interest in the astroglia were gh1 and rho (4.5- and 2.13-fold, respectively). The change in % of astroglial cells expressing gh1 and rho before and after exposure were 1% to 56.6%, and 4.3% to 83.3%, respectively. The efficacy of RNAscope labeling of these genes was similar to the cell ID gene labeling. The deeper tha labeling was, the more likely it was to occur, but superficial labeling was less reliable.

We had difficulty quantifying the change in expression of the DEG in both cell types because the probability that the cells in the particular sample coexpressed the cell ID gene and the DEG were quite low, as explained below, combined with the fact that the Opal dye that was applied first tended to bleach during the application and wash steps for the subsequent dye. Only 14% of microglia expressed the cell ID gene, mpeg1.1, and only 24% of astroglia expressed the cell ID gene, s100b. The percentage of the cell type of interest that expressed the DEG we wished to quantify change in expression of were at most 23.3% or 43% of the microglia in

DEPe-treated larvae and 56.6% or 83% of astroglia in DEPe-treated larvae. This would mean that on average, even at best in the DEPe treated larvae selecting for the DEG that were more highly expressed of the two tested per cell type, only 6% of microglia would co-label and only 20% of the astroglia would co-label even in the most optimized conditions. Considering there are only around 30-35 microglia in the 5dpf ZF larval brain, quantifying change in labeling and fluorescence of DEG in this model proved to be very difficult. Even though there are many more astroglia in the zebrafish brain at 5dpf, the bleaching of the first Opal dye due to the subsequent labeling steps was consistently observed, which prevented us from identifying co-labeled cells effectively.

Figure 12: RNAscope labeling of positive control genes and cell ID genes.

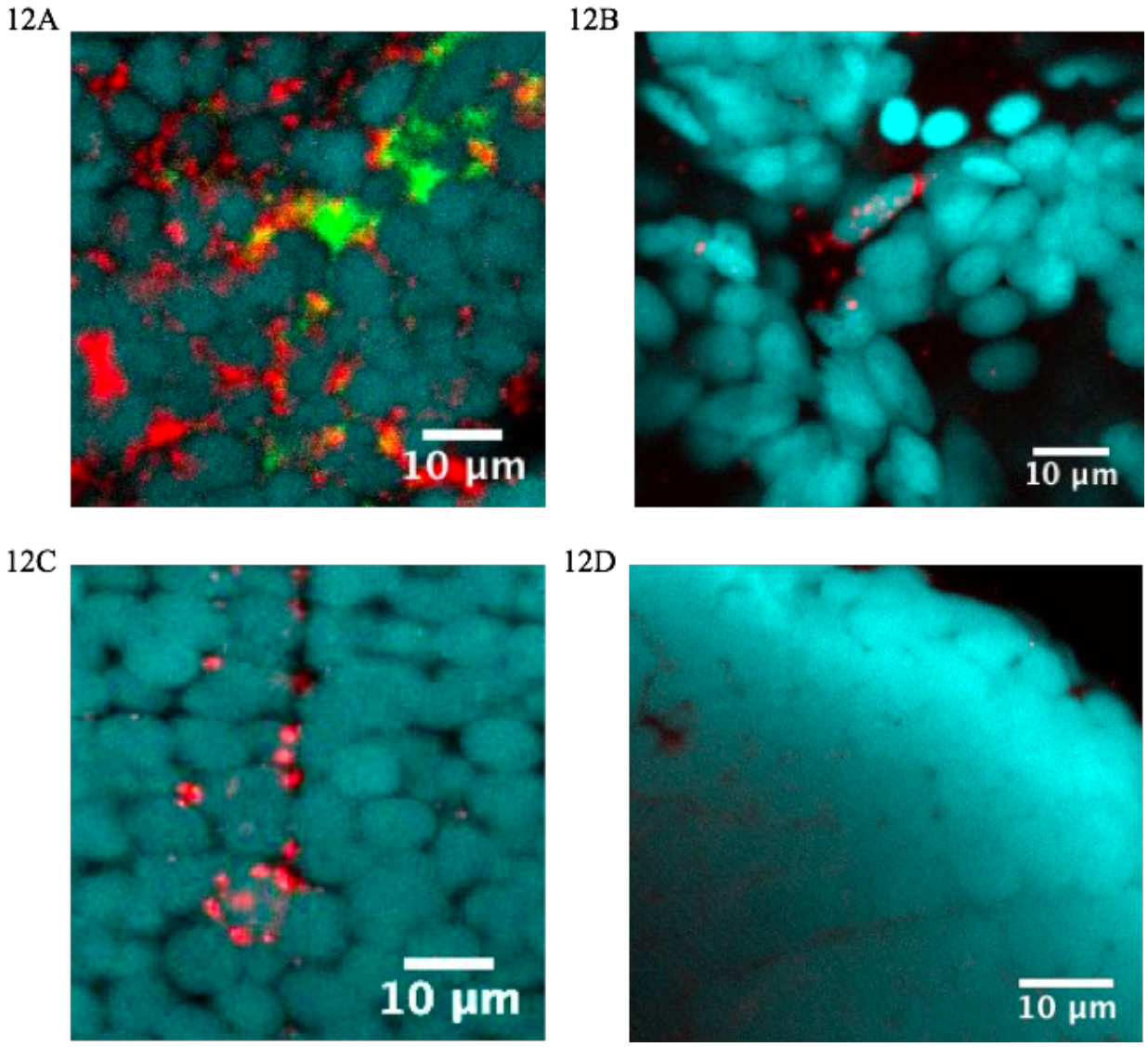

Figure 12: RNAscope V2 labeling in 5dpf larvae with optimized conditions. Cyan labeling in all images is methyl green, a far-red fluorescent nuclear stain. 12A: Positive control genes *eef1a1l1* (green) and *actb1* (red) labeled reliably at 5dpf. 12B: Microglial marker *mpeg1.1* (red) labeling an individual microglial cell, along with the nucleus (cyan). 12C: Astroglial marker *s100b* (red) labeling multiple astroglial cells, along with the nuclei (cyan). 12D: A negative control image, showing the cyan nuclear stain alone. All images are a Z-projection of a tissue slice of 8-10um, imaged at 40x in oil, and the scale bar represents 10um.

Discussion:

In this Chapter, we utilized scRNA-seq to identify and describe potential mechanisms induced in microglial and astroglial cells with DEPe exposure, and how they may contribute to disease. Through scRNA-seq analysis, we obtained evidence of our *in vivo* study results on microglial response to DEPe exposure, through the identification of multiple pathways related to microglial cell activation being more active with DEPe exposure. Importantly, we also identified numerous possible other affected pathways in both of the glial cell types of interest through more specific interpretations of selected IPA Comparison Analysis results. Through the use of an unbiased clustering technique, we identified some possible states in which the microglia and astroglia may exist, revealing the existence of possibly multiple activated states of microglia with different responses to DEPe exposure, as well as a large amount of astroglial states that exhibit very interesting known disease marker gene expression patterns.

It is important to keep in mind that the 5dpf ZF larva is a rapidly developing organism. We recognize that there are developmental changes that are occurring simultaneously with the effects of DEPe exposure over the 5 days of treatment, such as the increased active state of certain pathways or certain DEG over the time course of development, and that ultimately, developmental changes may be influencing our scRNA-seq results. There are a few ways that we have addressed this. Firstly, we used multiple biological replicates of both control and treated cells, which helps increase the power of our study and accuracy of what we identify as changes worthy of further investigation that are likely due to the DEPe exposure. Secondly, we used a basic global scaling normalization technique that makes gene expression data across samples comparable and analyzable. In the future, we plan on performing trajectory analysis/pseudotemporal ordering on certain cell clusters of interest, which takes advantage of

the developmental model that we are using, as it can determine and reveal the progress of a set of cells through a certain process, such as differentiation or maturation. This analysis projects each individual cell onto an axis called pseudotime so they can be visually organized and represented along the progression through the process of interest, such as response to external stimuli (Van den Berge et al., 2020). The goal of this analysis is to add to the initial identification of possible states of microglia and astroglia we established in this study and confirm the populations of cells that are present in each state. In addition, many larval ZF cells have not been as well as human or rodent cell types, and trajectory analysis on the control cell data may reveal novel cell populations or better descriptions of previously identified cell populations at baseline that may be useful for other work. We recognize that for the astroglial cells in particular, we currently only have gene expression data and no *in vivo* results, making any characterization of their behavior and possible states very preliminary. We hope to be able to develop *in vivo* work down the line that identifies these different states through confirmation of function, morphology, and cell movements, that are related to the gene profiles we identified in this work.

The observed cell markers for all 28 identified cell clusters have been well documented in previous single cell research of ZF larvae at various stages (Raj et al., 2018), (Lange et al., 2020). The reported enriched biological processes, established through GSEA, present in all microglial cells conserved across treatment conditions, included cell activation involved in immune response, nervous system development, and regulation of cell adhesion, all of which are known functions of microglia in zebrafish (J. Xu et al., 2016). In the astroglial cells, the most enriched biological processes involved brain development, cell projection morphogenesis, and developmental growth, which suggest that astroglia in zebrafish are closely involved in the development and maintenance of their surrounding tissue (Lange et al., 2020). Although these

results do not directly address our main research goal to describe effects of DEPe exposure, we found them very useful in confirming the cluster identification of microglia and astroglia. In addition, GSEA is a very useful and easy threshold-free technique to quickly gain biological insight into a gene set, which contributes to the available descriptive literature regarding these cell types in the ZF model.

Single-cell analysis gave us insight into the mechanisms that are occurring in response to DEPe exposure. All in all, microglia appeared to be activated through identification of DEG and IPA Comparison Analysis. For the astroglia, the DEG with DEPe exposure suggested a very heterogeneous response of astroglia that did not line up with any one gene expression profile from disease models using astrocytes. The IPA Comparison Analysis identified various interesting pathways related to a possibly decreased xenobiotic response, altered astroglial structure and movement, and response to an inflammatory environment. For both cases, subcluster analysis revealed the high likelihood of the existence of multiple activated states, which require further work, both *in vivo* as well as bioinformatic, to understand. Overall, our studies have begun to identify potential states that the microglia and astroglia may exist. It was important for this study to consider all of the findings together, such as the *in vivo* work with microglial activation, as well as the results from scRNA-seq, because describing cell states and responses requires multiple avenues of observation. Further characterization of these states may reveal therapeutic targets, such as encouraging certain more neuroprotective states to be present during certain parts of the progression of the disease, depending on the patient.

Our efforts to develop an RNAscope V2 labeling protocol for 5dpf ZF larvae and visually confirm the DEG results we obtained in scRNA-seq analysis of DMSO and DEPe treated ZF cells revealed many possible drawbacks to using this technique on ZF larvae, particularly those

older than 2-3 dpf, expressing the genes of interest in just a few cells, and in a large labeling area. We established that labeling highly and ubiquitously expressed genes, such as the positive control genes *eef1a1l1* and *actb1*, is very possible in the 5dpf larvae using V2. We also clearly established that a very useful nuclear stain can be applied at the end of labeling protocols in a simple overnight incubation to image the nucleus, and be an alternative to the more traditionally used Hoescht or DAPI. We concluded that specifying the area in which the labeling is required to consistently occur, and quantifying in just that area, may help increase the usefulness of this technique when attempting to image less abundant targets.

scRNA-seq is extremely useful to discover new gene expression profiles for a cell type of interest, and to identify differentially expressed genes when comparing different exposure conditions or biological states. It is a fast-growing field, and general consensus on the best orthogonal validation methods is still being established. There are currently multiple follow-up techniques that can be employed in the place of RNAscope fluorescent in-situ hybridization (FISH) to validate our scRNA-seq findings. Firstly, imaging is often used to validate single-cell discoveries in a spatial context, and traditional in-situ hybridization (ISH) instead of FISH may prove useful. ISH validation of experimental results has been employed in ZF larvae. There are limitations, however, such as the number of targets that can be imaged in one sample, suitable probe preparation, and colors for imaging. Secondly, flow cytometry is often used to accurately confirm scRNA-seq findings, such as the expression of novel marker genes. It is useful for not only validating expression of novel marker genes along with previously known marker genes, but also for physically isolating that cell population of interest for downstream analysis. Flow cytometry is also slightly limited in the number of targets that can be detected, but flow cytometry technology is quickly improving, allowing for the detection of marker genes as well as

proteins leading to the identification of entire panels of cells of interest. Finally, functional assays are an extremely strong validation of the role of genes in a pathway or biological system of interest. Overexpression, CRISPR knockout, and siRNA knockdown are commonly used methods to validate newly discovered targets. A drawback for these studies is the extensive preparation and development of the assay, as well as possible off-target effects. Orthogonal validation is very important to drawing accurate conclusions from the large-scale data and evidencing their biological implications.

Dissertation Conclusion

Environmental exposures that influence the development of PD have been identified in contexts such as pesticides and some drugs. However, AP in particular still requires mainstream acceptance as a major health risk, not just to the lungs and heart, but to the brain as well. AP is currently the world's leading environmental cause of mortality (Health Effects Institute, 2019). There are a variety of epidemiological studies that link exposure to various components of AP to the development of PD. This opens up a wide avenue of research targets that may inform our understanding of how PD develops and how environmental exposures contribute to it.

This project investigated microglial and astroglial responses to DEPe exposure and identified specific pathways that may be affected with this exposure. We also identified DEG that begin to characterize the microglia as a heterogeneous population, and subclusters that represent many potential states of microglia worth studying further. We identified various pathways involved in xenobiotic response, astroglial morphology and motility, and response to inflammation affected with DEPe exposure in the astroglia, and the DEG reflected this mixed response. Subcluster analysis revealed various subclusters that paralleled gene expression changes that have been observed in disease models using astrocytes.

From the findings reported in this work, we can begin to speculate how DEPe exposure, and therefore air pollution exposure in general, may increase the risk of PD. Firstly, we conclude that exposure to air pollution most certainly changes the states that microglial and astroglial cells exist in, through our direct observation of cell activation and gene expression changes. We established that microglia may not play a direct role in the acute toxicity that DEPe has on neurons, but the long-term effects of the presence of DEPe and the sustained, altered states of microglia may be worth investigating further. Secondly, we are reminded in this work that

pathological accumulation of hα-syn, commonly observed in PD, is enough to activate microglia and prime the brain's immune response. Patients who have a hereditary mutation in their hα-syn gene may be predisposed to responding to air pollution exposure differently than those who do not have the mutation. Thirdly, we have a strong case for the presence of multiple states of glial cells at any given time in the brain, which emphasizes the importance of considering multiple changes that may occur at the same time with air pollution exposure. This may complicate studies regarding environmental exposures and their contributions to the development of PD, but it is a necessary reality. However, follow-up studies involving trajectory analysis and *in vivo* confirmation studies to more explicitly characterize the glial cell states can further elucidate how the cells respond to DEPe exposure, compared to those that were not exposed.

Identifying specific microglial and astroglial responses to DEPe exposure, and their involvement in the development of PD, is very useful not only for understanding the pathophysiology of the disease due to AP exposure, but for the development of potential therapeutics. The neuroinflammatory environment that exists in PD is complex and has many dynamic components. By studying glial cell specific responses to DEPe exposure and identifying specific DEG and pathways most affected, we can focus on cell types, genes, and pathways that may be targets for therapeutics that may halt the trajectory of the development of PD.

References

Al-Dalahmah, O., Sosunov, A. A., Shaik, A., Ofori, K., Liu, Y., Vonsattel, J. P., . . . Goldman, J. E. (2020). Single-nucleus RNA-seq identifies Huntington disease astrocyte states. *Acta Neuropathol Commun, 8*(1), 19. doi:10.1186/s40478-020-0880-6

Allahyari, R. V., Clark, K. L., Shepard, K. A., & Garcia, A. D. R. (2019). Sonic hedgehog signaling is negatively regulated in reactive astrocytes after forebrain stab injury. *Sci Rep, 9*(1), 565. doi:10.1038/s41598-018-37555-x

Anderson, M. A., Burda, J. E., Ren, Y., Ao, Y., O'Shea, T. M., Kawaguchi, R., . . . Sofroniew, M. V. (2016). Astrocyte scar formation aids central nervous system axon regeneration. *Nature, 532*(7598), 195-200. doi:10.1038/nature17623

Arneson, D., Zhang, G., Ying, Z., Zhuang, Y., Byun, H. R., Ahn, I. S., . . . Yang, X. (2018). Single cell molecular alterations reveal target cells and pathways of concussive brain injury. *Nat Commun, 9*(1), 3894. doi:10.1038/s41467-018-06222-0

Banisor, I., Leist, T. P., & Kalman, B. (2005). Involvement of beta-chemokines in the development of inflammatory demyelination. *J Neuroinflammation, 2*(1), 7. doi:10.1186/1742-2094-2-7

Barcia, C. (2013). Glial-mediated inflammation underlying parkinsonism. *Scientifica (Cairo), 2013*, 357805. doi:10.1155/2013/357805

Barnhill, L. M., Khuansuwan, S., Juarez, D., Murata, H., Araujo, J. A., & Bronstein, J. M. (2020). Diesel Exhaust Extract Exposure Induces Neuronal Toxicity by Disrupting Autophagy. *Toxicol Sci, 176*(1), 193-202. doi:10.1093/toxsci/kfaa055

Bhatia, S., Kim, W. S., Shepherd, C. E., & Halliday, G. M. (2019). Apolipoprotein D Upregulation in Alzheimer's Disease but Not Frontotemporal Dementia. *J Mol Neurosci, 67*(1), 125-132. doi:10.1007/s12031-018-1217-9

Block, M. L., Wu, X., Pei, Z., Li, G., Wang, T., Qin, L., . . . Veronesi, B. (2004). Nanometer size diesel exhaust particles are selectively toxic to dopaminergic neurons: the role of microglia, phagocytosis, and NADPH oxidase. *FASEB J, 18*(13), 1618-1620. doi:10.1096/fj.04-1945fje

Booth, H. D. E., Hirst, W. D., & Wade-Martins, R. (2017). The Role of Astrocyte Dysfunction in Parkinson's Disease Pathogenesis. *Trends Neurosci, 40*(6), 358-370. doi:10.1016/j.tins.2017.04.001

Bray, N. (2016). Glia: An astrocytic axis. *Nat Rev Neurosci, 17*(7), 398-399. doi:10.1038/nrn.2016.77

Butovsky, O., & Weiner, H. L. (2018). Microglial signatures and their role in health and disease. *Nat Rev Neurosci, 19*(10), 622-635. doi:10.1038/s41583-018-0057-5

Cannon, J. R., Tapias, V., Na, H. M., Honick, A. S., Drolet, R. E., & Greenamyre, J. T. (2009). A highly reproducible rotenone model of Parkinson's disease. *Neurobiol Dis, 34*(2), 279-290. doi:10.1016/j.nbd.2009.01.016

Cesani, M., Cavalca, E., Macco, R., Leoncini, G., Terreni, M. R., Lorioli, L., . . . Biffi, A. (2014). Metallothioneins as dynamic markers for brain disease in lysosomal disorders. *Ann Neurol, 75*(1), 127-137. doi:10.1002/ana.24053

Chatterjee, B., Chin, A. J., Valdimarsson, G., Finis, C., Sonntag, J. M., Choi, B. Y., . . . Lo, C. W. (2005). Developmental regulation and expression of the zebrafish connexin43 gene. *Dev Dyn, 233*(3), 890-906. doi:10.1002/dvdy.20426

Chen, F., Swartzlander, D. B., Ghosh, A., Fryer, J. D., Wang, B., & Zheng, H. (2021). Clusterin secreted from astrocyte promotes excitatory synaptic transmission and ameliorates Alzheimer's disease neuropathology. *Mol Neurodegener, 16*(1), 5. doi:10.1186/s13024-021-00426-7

Chen, J., Poskanzer, K. E., Freeman, M. R., & Monk, K. R. (2020). Live-imaging of astrocyte morphogenesis and function in zebrafish neural circuits. *Nat Neurosci, 23*(10), 1297-1306. doi:10.1038/s41593-020-0703-x

Cheng, R. K., Jesuthasan, S. J., & Penney, T. B. (2014). Zebrafish forebrain and temporal conditioning. *Philos Trans R Soc Lond B Biol Sci, 369*(1637), 20120462. doi:10.1098/rstb.2012.0462

Cheyuo, C., Aziz, M., & Wang, P. (2019). Neurogenesis in Neurodegenerative Diseases: Role of MFG-E8. *Front Neurosci, 13*, 569. doi:10.3389/fnins.2019.00569

Choi, D. J., An, J., Jou, I., Park, S. M., & Joe, E. H. (2019). A Parkinson's disease gene, DJ-1, regulates anti-inflammatory roles of astrocytes through prostaglandin D2 synthase expression. *Neurobiol Dis, 127*, 482-491. doi:10.1016/j.nbd.2019.04.003

Choi, I., Zhang, Y., Seegobin, S. P., Pruvost, M., Wang, Q., Purtell, K., . . . Yue, Z. (2020). Microglia clear neuron-released alpha-synuclein via selective autophagy and prevent neurodegeneration. *Nat Commun, 11*(1), 1386. doi:10.1038/s41467-020-15119-w

Chou, A. P., Maidment, N., Klintenberg, R., Casida, J. E., Li, S., Fitzmaurice, A. G., . . . Bronstein, J. M. (2008). Ziram causes dopaminergic cell damage by inhibiting E1 ligase of the proteasome. *J Biol Chem, 283*(50), 34696-34703. doi:10.1074/jbc.M802210200

Croisier, E., Moran, L. B., Dexter, D. T., Pearce, R. K., & Graeber, M. B. (2005). Microglial inflammation in the parkinsonian substantia nigra: relationship to alpha-synuclein deposition. *J Neuroinflammation, 2*, 14. doi:10.1186/1742-2094-2-14

Czlonkowska, A., Kohutnicka, M., Kurkowska-Jastrzebska, I., & Czlonkowski, A. (1996). Microglial reaction in MPTP (1-methyl-4-phenyl-1,2,3,6-tetrahydropyridine) induced Parkinson's disease mice model. *Neurodegeneration, 5*(2), 137-143. doi:10.1006/neur.1996.0020

Dackor, R., Fritz-Six, K., Smithies, O., & Caron, K. (2007). Receptor activity-modifying proteins 2 and 3 have distinct physiological functions from embryogenesis to old age. *J Biol Chem, 282*(25), 18094-18099. doi:10.1074/jbc.M703544200

DePaula-Silva, A. B., Gorbea, C., Doty, D. J., Libbey, J. E., Sanchez, J. M. S., Hanak, T. J., . . . Fujinami, R. S. (2019). Differential transcriptional profiles identify microglial- and macrophage-specific gene markers expressed during virus-induced neuroinflammation. *J Neuroinflammation, 16*(1), 152. doi:10.1186/s12974-019-1545-x

Diaz Verdugo, C., Myren-Svelstad, S., Aydin, E., Van Hoeymissen, E., Deneubourg, C., Vanderhaeghe, S., . . . Yaksi, E. (2019). Glia-neuron interactions underlie state transitions to generalized seizures. *Nat Commun, 10*(1), 3830. doi:10.1038/s41467-019-11739-z

Doorn, K. J., Moors, T., Drukarch, B., van de Berg, W., Lucassen, P. J., & van Dam, A. M. (2014). Microglial phenotypes and toll-like receptor 2 in the substantia nigra and hippocampus of incidental Lewy body disease cases and Parkinson's disease patients. *Acta Neuropathol Commun, 2*, 90. doi:10.1186/s40478-014-0090-1

Elbaz, A., Carcaillon, L., Kab, S., & Moisan, F. (2016). Epidemiology of Parkinson's disease. *Rev Neurol (Paris), 172*(1), 14-26. doi:10.1016/j.neurol.2015.09.012

Elmore, M. R., Najafi, A. R., Koike, M. A., Dagher, N. N., Spangenberg, E. E., Rice, R. A., . . . Green, K. N. (2014). Colony-stimulating factor 1 receptor signaling is necessary for microglia viability, unmasking a microglia progenitor cell in the adult brain. *Neuron, 82*(2), 380-397. doi:10.1016/j.neuron.2014.02.040

Fagone, P., Di Rosa, M., Palumbo, M., De Gregorio, C., Nicoletti, F., & Malaguarnera, L. (2012). Modulation of heat shock proteins during macrophage differentiation. *Inflamm Res, 61*(10), 1131-1139. doi:10.1007/s00011-012-0506-y

Fang, J., Han, D., Hong, J., Tan, Q., & Tian, Y. (2012). The chemokine, macrophage inflammatory protein-2gamma, reduces the expression of glutamate transporter-1 on astrocytes and increases neuronal sensitivity to glutamate excitotoxicity. *J Neuroinflammation, 9*, 267. doi:10.1186/1742-2094-9-267

Ferreira, S. A., & Romero-Ramos, M. (2018). Microglia Response During Parkinson's Disease: Alpha-Synuclein Intervention. *Front Cell Neurosci, 12*, 247. doi:10.3389/fncel.2018.00247

Finkelstein, M. M., & Jerrett, M. (2007). A study of the relationships between Parkinson's disease and markers of traffic-derived and environmental manganese air pollution in two Canadian cities. *Environ Res, 104*(3), 420-432. doi:10.1016/j.envres.2007.03.002

Fitzmaurice, A. G., Rhodes, S. L., Lulla, A., Murphy, N. P., Lam, H. A., O'Donnell, K. C., . . . Bronstein, J. M. (2013). Aldehyde dehydrogenase inhibition as a pathogenic mechanism in Parkinson disease. *Proc Natl Acad Sci U S A, 110*(2), 636-641. doi:10.1073/pnas.1220399110

Gao, H. M., & Hong, J. S. (2008). Why neurodegenerative diseases are progressive: uncontrolled inflammation drives disease progression. *Trends Immunol, 29*(8), 357-365. doi:10.1016/j.it.2008.05.002

Gao, L., Yuan, H., Xu, E., & Liu, J. (2020). Toxicology of paraquat and pharmacology of the protective effect of 5-hydroxy-1-methylhydantoin on lung injury caused by paraquat based on metabolomics. *Sci Rep, 10*(1), 1790. doi:10.1038/s41598-020-58599-y

Gerhard, A., Pavese, N., Hotton, G., Turkheimer, F., Es, M., Hammers, A., . . . Brooks, D. J. (2006). In vivo imaging of microglial activation with [11C](R)-PK11195 PET in idiopathic Parkinson's disease. *Neurobiol Dis, 21*(2), 404-412. doi:10.1016/j.nbd.2005.08.002

Ginhoux, F., Lim, S., Hoeffel, G., Low, D., & Huber, T. (2013). Origin and differentiation of microglia. *Front Cell Neurosci, 7*, 45. doi:10.3389/fncel.2013.00045

Gitik, M., Kleinhaus, R., Hadas, S., Reichert, F., & Rotshenker, S. (2014). Phagocytic receptors activate and immune inhibitory receptor SIRPalpha inhibits phagocytosis through paxillin and cofilin. *Front Cell Neurosci, 8*, 104. doi:10.3389/fncel.2014.00104

Goedert, M., & Spillantini, M. G. (2006). Frontotemporal lobar degeneration through loss of progranulin function. *Brain, 129*(Pt 11), 2808-2810. doi:10.1093/brain/awl291

Gray, M. A., Choy, C. H., Dayam, R. M., Ospina-Escobar, E., Somerville, A., Xiao, X., . . . Botelho, R. J. (2016). Phagocytosis Enhances Lysosomal and Bactericidal Properties by Activating the Transcription Factor TFEB. *Curr Biol, 26*(15), 1955-1964. doi:10.1016/j.cub.2016.05.070

Gross-Thebing, T., Paksa, A., & Raz, E. (2014). Simultaneous high-resolution detection of multiple transcripts combined with localization of proteins in whole-mount embryos. *BMC Biol, 12*, 55. doi:10.1186/s12915-014-0055-7

Grubman, A., Choo, X. Y., Chew, G., Ouyang, J. F., Sun, G., Croft, N. P., . . . Polo, J. M. (2021). Transcriptional signature in microglia associated with Abeta plaque phagocytosis. *Nat Commun, 12*(1), 3015. doi:10.1038/s41467-021-23111-1

Grupp, L., Wolburg, H., & Mack, A. F. (2010). Astroglial structures in the zebrafish brain. *J Comp Neurol, 518*(21), 4277-4287. doi:10.1002/cne.22481

Guo, M., Wang, J., Zhao, Y., Feng, Y., Han, S., Dong, Q., . . . Tieu, K. (2020). Microglial exosomes facilitate alpha-synuclein transmission in Parkinson's disease. *Brain, 143*(5), 1476-1497. doi:10.1093/brain/awaa090

Hamilton, L., Astell, K. R., Velikova, G., & Sieger, D. (2016). A Zebrafish Live Imaging Model Reveals Differential Responses of Microglia Toward Glioblastoma Cells In Vivo. *Zebrafish, 13*(6), 523-534. doi:10.1089/zeb.2016.1339

Hammond, L. (2014). Measuring cell fluorescence using ImageJ. Retrieved from https://theolb.readthedocs.io/en/latest/imaging/measuring-cell-fluorescence-using-imagej.html

Hamza, T. H., Zabetian, C. P., Tenesa, A., Laederach, A., Montimurro, J., Yearout, D., . . . Payami, H. (2010). Common genetic variation in the HLA region is associated with late-onset sporadic Parkinson's disease. *Nat Genet, 42*(9), 781-785. doi:10.1038/ng.642

Han, X., Stewart, J. E., Jr., Bellis, S. L., Benveniste, E. N., Ding, Q., Tachibana, K., . . . Gladson, C. L. (2001). TGF-beta1 up-regulates paxillin protein expression in malignant astrocytoma cells: requirement for a fibronectin substrate. *Oncogene, 20*(55), 7976-7986. doi:10.1038/sj.onc.1204996

Hansen, D. V., Hanson, J. E., & Sheng, M. (2018). Microglia in Alzheimer's disease. *J Cell Biol, 217*(2), 459-472. doi:10.1083/jcb.201709069

Hara, M., Kobayakawa, K., Ohkawa, Y., Kumamaru, H., Yokota, K., Saito, T., . . . Okada, S. (2017). Interaction of reactive astrocytes with type I collagen induces astrocytic scar formation through the integrin-N-cadherin pathway after spinal cord injury. *Nat Med, 23*(7), 818-828. doi:10.1038/nm.4354

Hastings, K. T., & Cresswell, P. (2011). Disulfide reduction in the endocytic pathway: immunological functions of gamma-interferon-inducible lysosomal thiol reductase. *Antioxid Redox Signal, 15*(3), 657-668. doi:10.1089/ars.2010.3684

Health Effects Institute. (2019). *State of Global Air 2019: A Special Report*. Retrieved from Boston, MA:

Hoenen, C., Gustin, A., Birck, C., Kirchmeyer, M., Beaume, N., Felten, P., . . . Heurtaux, T. (2016). Alpha-Synuclein Proteins Promote Pro-Inflammatory Cascades in Microglia: Stronger Effects of the A53T Mutant. *PLoS One, 11*(9), e0162717. doi:10.1371/journal.pone.0162717

Howe, K., Clark, M. D., Torroja, C. F., Torrance, J., Berthelot, C., Muffato, M., . . . Stemple, D. L. (2013). The zebrafish reference genome sequence and its relationship to the human genome. *Nature, 496*(7446), 498-503. doi:10.1038/nature12111

Hwang, I. K., Park, J. H., Lee, T. K., Kim, D. W., Yoo, K. Y., Ahn, J. H., . . . Moon, S. M. (2017). CD74-immunoreactive activated M1 microglia are shown late in the gerbil hippocampal CA1 region following transient cerebral ischemia. *Mol Med Rep, 15*(6), 4148-4154. doi:10.3892/mmr.2017.6525

Iannaccone, S., Cerami, C., Alessio, M., Garibotto, V., Panzacchi, A., Olivieri, S., . . . Perani, D. (2013). In vivo microglia activation in very early dementia with Lewy bodies, comparison with Parkinson's disease. *Parkinsonism Relat Disord, 19*(1), 47-52. doi:10.1016/j.parkreldis.2012.07.002

Imamura, K., Hishikawa, N., Sawada, M., Nagatsu, T., Yoshida, M., & Hashizume, Y. (2003). Distribution of major histocompatibility complex class II-positive microglia and cytokine profile of Parkinson's disease brains. *Acta Neuropathol, 106*(6), 518-526. doi:10.1007/s00401-003-0766-2

Jongstra-Bilen, J., Puig Cano, A., Hasija, M., Xiao, H., Smith, C. I., & Cybulsky, M. I. (2008). Dual functions of Bruton's tyrosine kinase and Tec kinase during Fcgamma receptor-induced signaling and phagocytosis. *J Immunol, 181*(1), 288-298. doi:10.4049/jimmunol.181.1.288

Jurisch-Yaksi, N., Yaksi, E., & Kizil, C. (2020). Radial glia in the zebrafish brain: Functional, structural, and physiological comparison with the mammalian glia. *Glia, 68*(12), 2451-2470. doi:10.1002/glia.23849

Kajiwara, Y., Wang, E., Wang, M., Sin, W. C., Brennand, K. J., Schadt, E., . . . Zhang, B. (2018). GJA1 (connexin43) is a key regulator of Alzheimer's disease pathogenesis. *Acta Neuropathol Commun, 6*(1), 144. doi:10.1186/s40478-018-0642-x

Kalman, M., & Szabo, A. (2001). Immunohistochemical investigation of actin-anchoring proteins vinculin, talin and paxillin in rat brain following lesion: a moderate reaction, confined to the astroglia of brain tracts. *Exp Brain Res, 139*(4), 426-434. doi:10.1007/s002210100789

Kastenhuber, E., Kratochwil, C. F., Ryu, S., Schweitzer, J., & Driever, W. (2010). Genetic dissection of dopaminergic and noradrenergic contributions to catecholaminergic tracts in early larval zebrafish. *J Comp Neurol, 518*(4), 439-458. doi:10.1002/cne.22214

Keaney, J., Gasser, J., Gillet, G., Scholz, D., & Kadiu, I. (2019). Inhibition of Bruton's Tyrosine Kinase Modulates Microglial Phagocytosis: Therapeutic Implications for Alzheimer's Disease. *J Neuroimmune Pharmacol, 14*(3), 448-461. doi:10.1007/s11481-019-09839-0

Killoy, K. M., Harlan, B. A., Pehar, M., & Vargas, M. R. (2020). FABP7 upregulation induces a neurotoxic phenotype in astrocytes. *Glia, 68*(12), 2693-2704. doi:10.1002/glia.23879

Kim, C., Cho, E. D., Kim, H. K., You, S., Lee, H. J., Hwang, D., & Lee, S. J. (2014). beta1-integrin-dependent migration of microglia in response to neuron-released alpha-synuclein. *Exp Mol Med, 46*, e91. doi:10.1038/emm.2014.6

Klein, C., & Westenberger, A. (2012). Genetics of Parkinson's disease. *Cold Spring Harb Perspect Med, 2*(1), a008888. doi:10.1101/cshperspect.a008888

Kramer, A., Green, J., Pollard, J., Jr., & Tugendreich, S. (2014). Causal analysis approaches in Ingenuity Pathway Analysis. *Bioinformatics, 30*(4), 523-530. doi:10.1093/bioinformatics/btt703

Kubota, A., Goldstone, J. V., Lemaire, B., Takata, M., Woodin, B. R., & Stegeman, J. J. (2015). Role of pregnane X receptor and aryl hydrocarbon receptor in transcriptional regulation

of pxr, CYP2, and CYP3 genes in developing zebrafish. *Toxicol Sci, 143*(2), 398-407. doi:10.1093/toxsci/kfu240

Kuchinke, W., Hart, R. P., & Jonakait, G. M. (1995). Identification of mRNAs regulated by interferon-gamma in cultured rat astrocytes by PCR differential display. *Neuroimmunomodulation, 2*(6), 347-355. doi:10.1159/000097214

Kuiper, J. W., van Horssen, R., Oerlemans, F., Peters, W., van Dommelen, M. M., te Lindert, M. M., . . . Wieringa, B. (2009). Local ATP generation by brain-type creatine kinase (CK-B) facilitates cell motility. *PLoS One, 4*(3), e5030. doi:10.1371/journal.pone.0005030

Kurkowska-Jastrzebska, I., Wronska, A., Kohutnicka, M., Czlonkowski, A., & Czlonkowska, A. (1999). The inflammatory reaction following 1-methyl-4-phenyl-1,2,3, 6-tetrahydropyridine intoxication in mouse. *Exp Neurol, 156*(1), 50-61. doi:10.1006/exnr.1998.6993

Lam, C. S., Marz, M., & Strahle, U. (2009). gfap and nestin reporter lines reveal characteristics of neural progenitors in the adult zebrafish brain. *Dev Dyn, 238*(2), 475-486. doi:10.1002/dvdy.21853

Lange, C., Rost, F., Machate, A., Reinhardt, S., Lesche, M., Weber, A., . . . Brand, M. (2020). Single cell sequencing of radial glia progeny reveals the diversity of newborn neurons in the adult zebrafish brain. *Development, 147*(1). doi:10.1242/dev.185595

Larigot, L., Juricek, L., Dairou, J., & Coumoul, X. (2018). AhR signaling pathways and regulatory functions. *Biochim Open, 7*, 1-9. doi:10.1016/j.biopen.2018.05.001

Lee, H. J., Suk, J. E., Patrick, C., Bae, E. J., Cho, J. H., Rho, S., . . . Lee, S. J. (2010). Direct transfer of alpha-synuclein from neuron to astroglia causes inflammatory responses in synucleinopathies. *J Biol Chem, 285*(12), 9262-9272. doi:10.1074/jbc.M109.081125

Lee, P. C., Liu, L. L., Sun, Y., Chen, Y. A., Liu, C. C., Li, C. Y., . . . Ritz, B. (2016). Traffic-related air pollution increased the risk of Parkinson's disease in Taiwan: A nationwide study. *Environ Int, 96*, 75-81. doi:10.1016/j.envint.2016.08.017

Lenz, K. M., & Nelson, L. H. (2018). Microglia and Beyond: Innate Immune Cells As Regulators of Brain Development and Behavioral Function. *Front Immunol, 9*, 698. doi:10.3389/fimmu.2018.00698

Levesque, S., Surace, M. J., McDonald, J., & Block, M. L. (2011). Air pollution & the brain: Subchronic diesel exhaust exposure causes neuroinflammation and elevates early markers of neurodegenerative disease. *J Neuroinflammation, 8*, 105. doi:10.1186/1742-2094-8-105

Levesque, S., Taetzsch, T., Lull, M. E., Johnson, J. A., McGraw, C., & Block, M. L. (2013). The role of MAC1 in diesel exhaust particle-induced microglial activation and loss of dopaminergic neuron function. *J Neurochem, 125*(5), 756-765. doi:10.1111/jnc.12231

Levesque, S., Taetzsch, T., Lull, M. E., Kodavanti, U., Stadler, K., Wagner, A., . . . Block, M. L. (2011). Diesel exhaust activates and primes microglia: air pollution, neuroinflammation, and regulation of dopaminergic neurotoxicity. *Environ Health Perspect, 119*(8), 1149-1155. doi:10.1289/ehp.1002986

Li, H., Gang, Z., Yuling, H., Luokun, X., Jie, X., Hao, L., . . . Jinquan, T. (2006). Different neurotropic pathogens elicit neurotoxic CCR9- or neurosupportive CXCR3-expressing microglia. *J Immunol, 177*(6), 3644-3656. doi:10.4049/jimmunol.177.6.3644

Liu, Z., Li, Y., Cui, Y., Roberts, C., Lu, M., Wilhelmsson, U., . . . Chopp, M. (2014). Beneficial effects of gfap/vimentin reactive astrocytes for axonal remodeling and motor behavioral recovery in mice after stroke. *Glia, 62*(12), 2022-2033. doi:10.1002/glia.22723

Lulla, A., Barnhill, L., Bitan, G., Ivanova, M. I., Nguyen, B., O'Donnell, K., . . . Bronstein, J. M. (2016). Neurotoxicity of the Parkinson Disease-Associated Pesticide Ziram Is Synuclein-Dependent in Zebrafish Embryos. *Environ Health Perspect, 124*(11), 1766-1775. doi:10.1289/EHP141

Lunnon, K., Teeling, J. L., Tutt, A. L., Cragg, M. S., Glennie, M. J., & Perry, V. H. (2011). Systemic inflammation modulates Fc receptor expression on microglia during chronic neurodegeneration. *J Immunol, 186*(12), 7215-7224. doi:10.4049/jimmunol.0903833

Lyons, D. A., & Talbot, W. S. (2014). Glial cell development and function in zebrafish. *Cold Spring Harb Perspect Biol, 7*(2), a020586. doi:10.1101/cshperspect.a020586

Madeddu, S., Woods, T. A., Mukherjee, P., Sturdevant, D., Butchi, N. B., & Peterson, K. E. (2015). Identification of Glial Activation Markers by Comparison of Transcriptome Changes between Astrocytes and Microglia following Innate Immune Stimulation. *PLoS One, 10*(7), e0127336. doi:10.1371/journal.pone.0127336

Majumdar, A., Cruz, D., Asamoah, N., Buxbaum, A., Sohar, I., Lobel, P., & Maxfield, F. R. (2007). Activation of microglia acidifies lysosomes and leads to degradation of Alzheimer amyloid fibrils. *Mol Biol Cell, 18*(4), 1490-1496. doi:10.1091/mbc.e06-10-0975

Marz, M., Schmidt, R., Rastegar, S., & Strahle, U. (2011). Regenerative response following stab injury in the adult zebrafish telencephalon. *Dev Dyn, 240*(9), 2221-2231. doi:10.1002/dvdy.22710

Mathys, H., Adaikkan, C., Gao, F., Young, J. Z., Manet, E., Hemberg, M., . . . Tsai, L. H. (2017). Temporal Tracking of Microglia Activation in Neurodegeneration at Single-Cell Resolution. *Cell Rep, 21*(2), 366-380. doi:10.1016/j.celrep.2017.09.039

Mazzolini, J., Le Clerc, S., Morisse, G., Coulonges, C., Kuil, L. E., van Ham, T. J., . . . Sieger, D. (2020). Gene expression profiling reveals a conserved microglia signature in larval zebrafish. *Glia, 68*(2), 298-315. doi:10.1002/glia.23717

Mazzoni, P., Shabbott, B., & Cortes, J. C. (2012). Motor control abnormalities in Parkinson's disease. *Cold Spring Harb Perspect Med, 2*(6), a009282. doi:10.1101/cshperspect.a009282

McCoy, E., & Sontheimer, H. (2010). MAPK induces AQP1 expression in astrocytes following injury. *Glia, 58*(2), 209-217. doi:10.1002/glia.20916

McDonough, A., Noor, S., Lee, R. V., Dodge, R., 3rd, Strosnider, J. S., Shen, J., . . . Weinstein, J. R. (2020). Ischemic preconditioning induces cortical microglial proliferation and a transcriptomic program of robust cell cycle activation. *Glia, 68*(1), 76-94. doi:10.1002/glia.23701

McGeer, P. L., Itagaki, S., Boyes, B. E., & McGeer, E. G. (1988). Reactive microglia are positive for HLA-DR in the substantia nigra of Parkinson's and Alzheimer's disease brains. *Neurology, 38*(8), 1285-1291. doi:10.1212/wnl.38.8.1285

Merry, T. L., Brooks, A. E. S., Masson, S. W., Adams, S. E., Jaiswal, J. K., Jamieson, S. M. F., & Shepherd, P. R. (2020). The CSF1 receptor inhibitor pexidartinib (PLX3397) reduces tissue macrophage levels without affecting glucose homeostasis in mice. *Int J Obes (Lond), 44*(1), 245-253. doi:10.1038/s41366-019-0355-7

Miao, W., Zhao, Y., Huang, Y., Chen, D., Luo, C., Su, W., & Gao, Y. (2020). IL-13 Ameliorates Neuroinflammation and Promotes Functional Recovery after Traumatic Brain Injury. *J Immunol, 204*(6), 1486-1498. doi:10.4049/jimmunol.1900909

Michael, G. J., Esmailzadeh, S., Moran, L. B., Christian, L., Pearce, R. K., & Graeber, M. B. (2011). Up-regulation of metallothionein gene expression in parkinsonian astrocytes. *Neurogenetics, 12*(4), 295-305. doi:10.1007/s10048-011-0294-5

Milner, R., & Campbell, I. L. (2003). The extracellular matrix and cytokines regulate microglial integrin expression and activation. *J Immunol, 170*(7), 3850-3858. doi:10.4049/jimmunol.170.7.3850

Mitrasinovic, O. M., Grattan, A., Robinson, C. C., Lapustea, N. B., Poon, C., Ryan, H., . . . Murphy, G. M., Jr. (2005). Microglia overexpressing the macrophage colony-stimulating factor receptor are neuroprotective in a microglial-hippocampal organotypic coculture system. *J Neurosci, 25*(17), 4442-4451. doi:10.1523/JNEUROSCI.0514-05.2005

Morales, I., Sanchez, A., Rodriguez-Sabate, C., & Rodriguez, M. (2017). Striatal astrocytes engulf dopaminergic debris in Parkinson's disease: A study in an animal model. *PLoS One, 12*(10), e0185989. doi:10.1371/journal.pone.0185989

Morrison, H. W., & Filosa, J. A. (2013). A quantitative spatiotemporal analysis of microglia morphology during ischemic stroke and reperfusion. *J Neuroinflammation, 10*, 4. doi:10.1186/1742-2094-10-4

Mu, Y., Bennett, D. V., Rubinov, M., Narayan, S., Yang, C. T., Tanimoto, M., . . . Ahrens, M. B. (2019). Glia Accumulate Evidence that Actions Are Futile and Suppress Unsuccessful Behavior. *Cell, 178*(1), 27-43 e19. doi:10.1016/j.cell.2019.05.050

Mudunuri, U., Che, A., Yi, M., & Stephens, R. M. (2009). bioDBnet: the biological database network. *Bioinformatics, 25*(4), 555-556. doi:10.1093/bioinformatics/btn654

Musaelyan, K., Yildizoglu, S., Bozeman, J., Du Preez, A., Egeland, M., Zunszain, P. A., . . . Thuret, S. (2020). Chronic stress induces significant gene expression changes in the prefrontal cortex alongside alterations in adult hippocampal neurogenesis. *Brain Commun, 2*(2), fcaa153. doi:10.1093/braincomms/fcaa153

Naj, A. C., Jun, G., Beecham, G. W., Wang, L. S., Vardarajan, B. N., Buros, J., . . . Schellenberg, G. D. (2011). Common variants at MS4A4/MS4A6E, CD2AP, CD33 and EPHA1 are associated with late-onset Alzheimer's disease. *Nat Genet, 43*(5), 436-441. doi:10.1038/ng.801

Neo, S. H., & Tang, B. L. (2017). Collagen 1 signaling at the central nervous system injury site and astrogliosis. *Neural Regen Res, 12*(10), 1600-1601. doi:10.4103/1673-5374.217323

Ni, W., Rajkumar, K., Nagy, J. I., & Murphy, L. J. (1997). Impaired brain development and reduced astrocyte response to injury in transgenic mice expressing IGF binding protein-1. *Brain Res, 769*(1), 97-107. doi:10.1016/s0006-8993(97)00676-8

Niklaus, S., Cadetti, L., Vom Berg-Maurer, C. M., Lehnherr, A., Hotz, A. L., Forster, I. C., . . . Neuhauss, S. C. F. (2017). Shaping of Signal Transmission at the Photoreceptor Synapse by EAAT2 Glutamate Transporters. *eNeuro, 4*(3). doi:10.1523/ENEURO.0339-16.2017

Oosterhof, N., Holtman, I. R., Kuil, L. E., van der Linde, H. C., Boddeke, E. W., Eggen, B. J., & van Ham, T. J. (2017). Identification of a conserved and acute neurodegeneration-specific microglial transcriptome in the zebrafish. *Glia, 65*(1), 138-149. doi:10.1002/glia.23083

Ouchi, Y., Yoshikawa, E., Sekine, Y., Futatsubashi, M., Kanno, T., Ogusu, T., & Torizuka, T. (2005). Microglial activation and dopamine terminal loss in early Parkinson's disease. *Ann Neurol, 57*(2), 168-175. doi:10.1002/ana.20338

Palacios, N., Fitzgerald, K., Roberts, A. L., Hart, J. E., Weisskopf, M. G., Schwarzschild, M. A., . . . Laden, F. (2014). A prospective analysis of airborne metal exposures and risk of Parkinson disease in the nurses' health study cohort. *Environ Health Perspect, 122*(9), 933-938. doi:10.1289/ehp.1307218

Pan, H. C., Yang, C. N., Hung, Y. W., Lee, W. J., Tien, H. R., Shen, C. C., . . . Sheu, M. L. (2013). Reciprocal modulation of C/EBP-alpha and C/EBP-beta by IL-13 in activated microglia prevents neuronal death. *Eur J Immunol, 43*(11), 2854-2865. doi:10.1002/eji.201343301

Pan, J., Ma, N., Yu, B., Zhang, W., & Wan, J. (2020). Transcriptomic profiling of microglia and astrocytes throughout aging. *J Neuroinflammation, 17*(1), 97. doi:10.1186/s12974-020-01774-9

Parakalan, R., Jiang, B., Nimmi, B., Janani, M., Jayapal, M., Lu, J., . . . Dheen, S. T. (2012). Transcriptome analysis of amoeboid and ramified microglia isolated from the corpus callosum of rat brain. *BMC Neurosci, 13*, 64. doi:10.1186/1471-2202-13-64

Park, J. H., Pak, H. J., Riew, T. R., Shin, Y. J., & Lee, M. Y. (2016). Increased expression of Slit2 and its receptors Robo1 and Robo4 in reactive astrocytes of the rat hippocampus after transient forebrain ischemia. *Brain Res, 1634*, 45-56. doi:10.1016/j.brainres.2015.12.056

Pastor-Belda, M., Campillo, N., Arroyo-Manzanares, N., Torres, C., Perez-Carceles, M. D., Hernandez-Cordoba, M., & Vinas, P. (2019). Bioaccumulation of Polycyclic Aromatic Hydrocarbons for Forensic Assessment Using Gas Chromatography-Mass Spectrometry. *Chem Res Toxicol, 32*(8), 1680-1688. doi:10.1021/acs.chemrestox.9b00213

Paul, K. C., Chuang, Y. H., Cockburn, M., Bronstein, J. M., Horvath, S., & Ritz, B. (2018). Organophosphate pesticide exposure and differential genome-wide DNA methylation. *Sci Total Environ, 645*, 1135-1143. doi:10.1016/j.scitotenv.2018.07.143

Peri, F., & Nusslein-Volhard, C. (2008). Live imaging of neuronal degradation by microglia reveals a role for v0-ATPase a1 in phagosomal fusion in vivo. *Cell, 133*(5), 916-927. doi:10.1016/j.cell.2008.04.037

Pimenova, A. A., Herbinet, M., Gupta, I., Machlovi, S. I., Bowles, K. R., Marcora, E., & Goate, A. M. (2021). Alzheimer's-associated PU.1 expression levels regulate microglial inflammatory response. *Neurobiol Dis, 148*, 105217. doi:10.1016/j.nbd.2020.105217

Pitter, K. L., Tamagno, I., Feng, X., Ghosal, K., Amankulor, N., Holland, E. C., & Hambardzumyan, D. (2014). The SHH/Gli pathway is reactivated in reactive glia and drives proliferation in response to neurodegeneration-induced lesions. *Glia, 62*(10), 1595-1607. doi:10.1002/glia.22702

Preman, P., Alfonso-Triguero, M., Alberdi, E., Verkhratsky, A., & Arranz, A. M. (2021). Astrocytes in Alzheimer's Disease: Pathological Significance and Molecular Pathways. *Cells, 10*(3). doi:10.3390/cells10030540

Pulido-Salgado, M., Vidal-Taboada, J. M., Barriga, G. G., Sola, C., & Saura, J. (2018). RNA-Seq transcriptomic profiling of primary murine microglia treated with LPS or LPS + IFNgamma. *Sci Rep, 8*(1), 16096. doi:10.1038/s41598-018-34412-9

Qin, L., Wu, X., Block, M. L., Liu, Y., Breese, G. R., Hong, J. S., . . . Crews, F. T. (2007). Systemic LPS causes chronic neuroinflammation and progressive neurodegeneration. *Glia, 55*(5), 453-462. doi:10.1002/glia.20467

Raj, B., Wagner, D. E., McKenna, A., Pandey, S., Klein, A. M., Shendure, J., . . . Schier, A. F. (2018). Simultaneous single-cell profiling of lineages and cell types in the vertebrate brain. *Nat Biotechnol, 36*(5), 442-450. doi:10.1038/nbt.4103

Rajayer, S. R., Jacob, A., Yang, W. L., Zhou, M., Chaung, W., & Wang, P. (2013). Cold-inducible RNA-binding protein is an important mediator of alcohol-induced brain inflammation. *PLoS One, 8*(11), e79430. doi:10.1371/journal.pone.0079430

Rangaraju, S., Dammer, E. B., Raza, S. A., Rathakrishnan, P., Xiao, H., Gao, T., . . . Levey, A. I. (2018). Identification and therapeutic modulation of a pro-inflammatory subset of disease-associated-microglia in Alzheimer's disease. *Mol Neurodegener, 13*(1), 24. doi:10.1186/s13024-018-0254-8

Ritz, B., Lee, P. C., Hansen, J., Lassen, C. F., Ketzel, M., Sorensen, M., & Raaschou-Nielsen, O. (2016). Traffic-Related Air Pollution and Parkinson's Disease in Denmark: A Case-Control Study. *Environ Health Perspect, 124*(3), 351-356. doi:10.1289/ehp.1409313

Romani, P., Ignesti, M., Gargiulo, G., Hsu, T., & Cavaliere, V. (2018). Extracellular NME proteins: a player or a bystander? *Lab Invest, 98*(2), 248-257. doi:10.1038/labinvest.2017.102

Rothhammer, V., Mascanfroni, I. D., Bunse, L., Takenaka, M. C., Kenison, J. E., Mayo, L., . . . Quintana, F. J. (2016). Type I interferons and microbial metabolites of tryptophan modulate astrocyte activity and central nervous system inflammation via the aryl hydrocarbon receptor. *Nat Med, 22*(6), 586-597. doi:10.1038/nm.4106

Rustenhoven, J., Smith, A. M., Smyth, L. C., Jansson, D., Scotter, E. L., Swanson, M. E. V., . . . Dragunow, M. (2018). PU.1 regulates Alzheimer's disease-associated genes in primary human microglia. *Mol Neurodegener, 13*(1), 44. doi:10.1186/s13024-018-0277-1

Saleem, S., & Kannan, R. R. (2018). Zebrafish: an emerging real-time model system to study Alzheimer's disease and neurospecific drug discovery. *Cell Death Discov, 4*, 45. doi:10.1038/s41420-018-0109-7

Samii, A., Etminan, M., Wiens, M. O., & Jafari, S. (2009). NSAID use and the risk of Parkinson's disease: systematic review and meta-analysis of observational studies. *Drugs Aging, 26*(9), 769-779. doi:10.2165/11316780-000000000-00000

Sanchez-Guajardo, V., Febbraro, F., Kirik, D., & Romero-Ramos, M. (2010). Microglia acquire distinct activation profiles depending on the degree of alpha-synuclein neuropathology in a rAAV based model of Parkinson's disease. *PLoS One, 5*(1), e8784. doi:10.1371/journal.pone.0008784

Seshadri, S., Fitzpatrick, A. L., Ikram, M. A., DeStefano, A. L., Gudnason, V., Boada, M., . . . Consortium, E. (2010). Genome-wide analysis of genetic loci associated with Alzheimer disease. *JAMA, 303*(18), 1832-1840. doi:10.1001/jama.2010.574

Shiau, C. E., Kaufman, Z., Meireles, A. M., & Talbot, W. S. (2015). Differential requirement for irf8 in formation of embryonic and adult macrophages in zebrafish. *PLoS One, 10*(1), e0117513. doi:10.1371/journal.pone.0117513

Shin, W. H., Lee, D. Y., Park, K. W., Kim, S. U., Yang, M. S., Joe, E. H., & Jin, B. K. (2004). Microglia expressing interleukin-13 undergo cell death and contribute to neuronal survival in vivo. *Glia, 46*(2), 142-152. doi:10.1002/glia.10357

Siddiqui, I. J., Pervaiz, N., & Abbasi, A. A. (2016). The Parkinson Disease gene SNCA: Evolutionary and structural insights with pathological implication. *Sci Rep, 6*, 24475. doi:10.1038/srep24475

Sierksma, A., Lu, A., Mancuso, R., Fattorelli, N., Thrupp, N., Salta, E., . . . Fiers, M. (2020). Novel Alzheimer risk genes determine the microglia response to amyloid-beta but not to TAU pathology. *EMBO Mol Med, 12*(3), e10606. doi:10.15252/emmm.201910606

Simpson, D. S. A., & Oliver, P. L. (2020). ROS Generation in Microglia: Understanding Oxidative Stress and Inflammation in Neurodegenerative Disease. *Antioxidants (Basel), 9*(8). doi:10.3390/antiox9080743

Smith, J. A., Das, A., Ray, S. K., & Banik, N. L. (2012). Role of pro-inflammatory cytokines released from microglia in neurodegenerative diseases. *Brain Res Bull, 87*(1), 10-20. doi:10.1016/j.brainresbull.2011.10.004

Sousa, C., Golebiewska, A., Poovathingal, S. K., Kaoma, T., Pires-Afonso, Y., Martina, S., . . . Michelucci, A. (2018). Single-cell transcriptomics reveals distinct inflammation-induced microglia signatures. *EMBO Rep, 19*(11). doi:10.15252/embr.201846171

Stefanis, L. (2012). alpha-Synuclein in Parkinson's disease. *Cold Spring Harb Perspect Med, 2*(2), a009399. doi:10.1101/cshperspect.a009399

Steiner, S., Bisig, C., Petri-Fink, A., & Rothen-Rutishauser, B. (2016). Diesel exhaust: current knowledge of adverse effects and underlying cellular mechanisms. *Arch Toxicol, 90*(7), 1541-1553. doi:10.1007/s00204-016-1736-5

Stokholm, M. G., Iranzo, A., Ostergaard, K., Serradell, M., Otto, M., Svendsen, K. B., . . . Pavese, N. (2017). Assessment of neuroinflammation in patients with idiopathic rapid-eye-movement sleep behaviour disorder: a case-control study. *Lancet Neurol, 16*(10), 789-796. doi:10.1016/S1474-4422(17)30173-4

Stuart, L. M., Bell, S. A., Stewart, C. R., Silver, J. M., Richard, J., Goss, J. L., . . . Moore, K. J. (2007). CD36 signals to the actin cytoskeleton and regulates microglial migration via a p130Cas complex. *J Biol Chem, 282*(37), 27392-27401. doi:10.1074/jbc.M702887200

Stuart, T., Butler, A., Hoffman, P., Hafemeister, C., Papalexi, E., Mauck, W. M., 3rd, . . . Satija, R. (2019). Comprehensive Integration of Single-Cell Data. *Cell, 177*(7), 1888-1902 e1821. doi:10.1016/j.cell.2019.05.031

Sulzer, D., Alcalay, R. N., Garretti, F., Cote, L., Kanter, E., Agin-Liebes, J., . . . Sette, A. (2017). T cells from patients with Parkinson's disease recognize alpha-synuclein peptides. *Nature, 546*(7660), 656-661. doi:10.1038/nature22815

Svahn, A. J., Graeber, M. B., Ellett, F., Lieschke, G. J., Rinkwitz, S., Bennett, M. R., & Becker, T. S. (2013). Development of ramified microglia from early macrophages in the zebrafish optic tectum. *Dev Neurobiol, 73*(1), 60-71. doi:10.1002/dneu.22039

Szeliga, M. (2020). Peroxiredoxins in Neurodegenerative Diseases. *Antioxidants (Basel), 9*(12). doi:10.3390/antiox9121203

Takahashi, K., Nakayama, M., Totsune, K., Murakami, O., Sone, M., Kitamuro, T., . . . Shibahara, S. (2000). Increased secretion of adrenomedullin from cultured human astrocytes by cytokines. *J Neurochem, 74*(1), 99-103. doi:10.1046/j.1471-4159.2000.0740099.x

Tanner, C. M., Kamel, F., Ross, G. W., Hoppin, J. A., Goldman, S. M., Korell, M., . . . Langston, J. W. (2011). Rotenone, paraquat, and Parkinson's disease. *Environ Health Perspect, 119*(6), 866-872. doi:10.1289/ehp.1002839

Telpoukhovskaia, M. A., Liu, K., Sayed, F. A., Etchegaray, J. I., Xie, M., Zhan, L., . . . Gan, L. (2020). Discovery of small molecules that normalize the transcriptome and enhance cysteine cathepsin activity in progranulin-deficient microglia. *Sci Rep, 10*(1), 13688. doi:10.1038/s41598-020-70534-9

Timsit, Y. E., & Negishi, M. (2007). CAR and PXR: the xenobiotic-sensing receptors. *Steroids, 72*(3), 231-246. doi:10.1016/j.steroids.2006.12.006

Tompkins, M. M., & Hill, W. D. (1997). Contribution of somal Lewy bodies to neuronal death. *Brain Res, 775*(1-2), 24-29. doi:10.1016/s0006-8993(97)00874-3

Van den Berge, K., Roux de Bezieux, H., Street, K., Saelens, W., Cannoodt, R., Saeys, Y., . . . Clement, L. (2020). Trajectory-based differential expression analysis for single-cell sequencing data. *Nat Commun, 11*(1), 1201. doi:10.1038/s41467-020-14766-3

Var, S. R., & Byrd-Jacobs, C. A. (2020). Role of Macrophages and Microglia in Zebrafish Regeneration. *Int J Mol Sci, 21*(13). doi:10.3390/ijms21134768

von Maydell, D., & Jorfi, M. (2019). The interplay between microglial states and major risk factors in Alzheimer's disease through the eyes of single-cell RNA-sequencing: beyond black and white. *J Neurophysiol, 122*(4), 1291-1296. doi:10.1152/jn.00395.2019

Walker, D. G. (2020). Defining activation states of microglia in human brain tissue: an unresolved issue for Alzheimer’s disease. *Neuroimmunol Neuroinflammation, 7*, 194-124. Retrieved from https://nnjournal.net/article/view/3552

Walker, D. G., Link, J., Lue, L. F., Dalsing-Hernandez, J. E., & Boyes, B. E. (2006). Gene expression changes by amyloid beta peptide-stimulated human postmortem brain

microglia identify activation of multiple inflammatory processes. *J Leukoc Biol, 79*(3), 596-610. doi:10.1189/jlb.0705377

Wang, A., Cockburn, M., Ly, T. T., Bronstein, J. M., & Ritz, B. (2014). The association between ambient exposure to organophosphates and Parkinson's disease risk. *Occup Environ Med, 71*(4), 275-281. doi:10.1136/oemed-2013-101394

Wang, A., Costello, S., Cockburn, M., Zhang, X., Bronstein, J., & Ritz, B. (2011). Parkinson's disease risk from ambient exposure to pesticides. *Eur J Epidemiol, 26*(7), 547-555. doi:10.1007/s10654-011-9574-5

Wang, Q., Liu, Y., & Zhou, J. (2015). Neuroinflammation in Parkinson's disease and its potential as therapeutic target. *Transl Neurodegener, 4*, 19. doi:10.1186/s40035-015-0042-0

Wu, S., Nguyen, L. T. M., Pan, H., Hassan, S., Dai, Y., Xu, J., & Wen, Z. (2020). Two phenotypically and functionally distinct microglial populations in adult zebrafish. *Sci Adv, 6*(47). doi:10.1126/sciadv.abd1160

Xu, J., Wang, T., Wu, Y., Jin, W., & Wen, Z. (2016). Microglia Colonization of Developing Zebrafish Midbrain Is Promoted by Apoptotic Neuron and Lysophosphatidylcholine. *Dev Cell, 38*(2), 214-222. doi:10.1016/j.devcel.2016.06.018

Xu, X., Zhang, A., Zhu, Y., He, W., Di, W., Fang, Y., & Shi, X. (2018). MFG-E8 reverses microglial-induced neurotoxic astrocyte (A1) via NF-kappaB and PI3K-Akt pathways. *J Cell Physiol, 234*(1), 904-914. doi:10.1002/jcp.26918

Yan, Y., Tan, X., Wu, X., Shao, B., Wu, X., Cao, J., . . . Cui, G. (2013). Involvement of early growth response-2 (Egr-2) in lipopolysaccharide-induced neuroinflammation. *J Mol Histol, 44*(3), 249-257. doi:10.1007/s10735-013-9482-y

Yang, L. B., Li, R., Meri, S., Rogers, J., & Shen, Y. (2000). Deficiency of complement defense protein CD59 may contribute to neurodegeneration in Alzheimer's disease. *J Neurosci, 20*(20), 7505-7509. Retrieved from https://www.ncbi.nlm.nih.gov/pubmed/11027207

Yang, Y., Boza-Serrano, A., Dunning, C. J. R., Clausen, B. H., Lambertsen, K. L., & Deierborg, T. (2018). Inflammation leads to distinct populations of extracellular vesicles from microglia. *J Neuroinflammation, 15*(1), 168. doi:10.1186/s12974-018-1204-7

Yin, H., Song, S., & Pan, X. (2017). Knockdown of miR-155 protects microglia against LPS-induced inflammatory injury via targeting RACK1: a novel research for intracranial infection. *J Inflamm (Lond), 14*, 17. doi:10.1186/s12950-017-0162-7

You, Y., Borgmann, K., Edara, V. V., Stacy, S., Ghorpade, A., & Ikezu, T. (2020). Activated human astrocyte-derived extracellular vesicles modulate neuronal uptake, differentiation and firing. *J Extracell Vesicles, 9*(1), 1706801. doi:10.1080/20013078.2019.1706801

Zamanian, J. L., Xu, L., Foo, L. C., Nouri, N., Zhou, L., Giffard, R. G., & Barres, B. A. (2012). Genomic analysis of reactive astrogliosis. *J Neurosci, 32*(18), 6391-6410. doi:10.1523/JNEUROSCI.6221-11.2012

Zambusi, A., Pelin Burhan, O., Di Giaimo, R., Schmid, B., & Ninkovic, J. (2020). Granulins Regulate Aging Kinetics in the Adult Zebrafish Telencephalon. *Cells, 9*(2). doi:10.3390/cells9020350

Zhang, W., Dallas, S., Zhang, D., Guo, J. P., Pang, H., Wilson, B., . . . Zhang, J. (2007). Microglial PHOX and Mac-1 are essential to the enhanced dopaminergic neurodegeneration elicited by A30P and A53T mutant alpha-synuclein. *Glia, 55*(11), 1178-1188. doi:10.1002/glia.20532